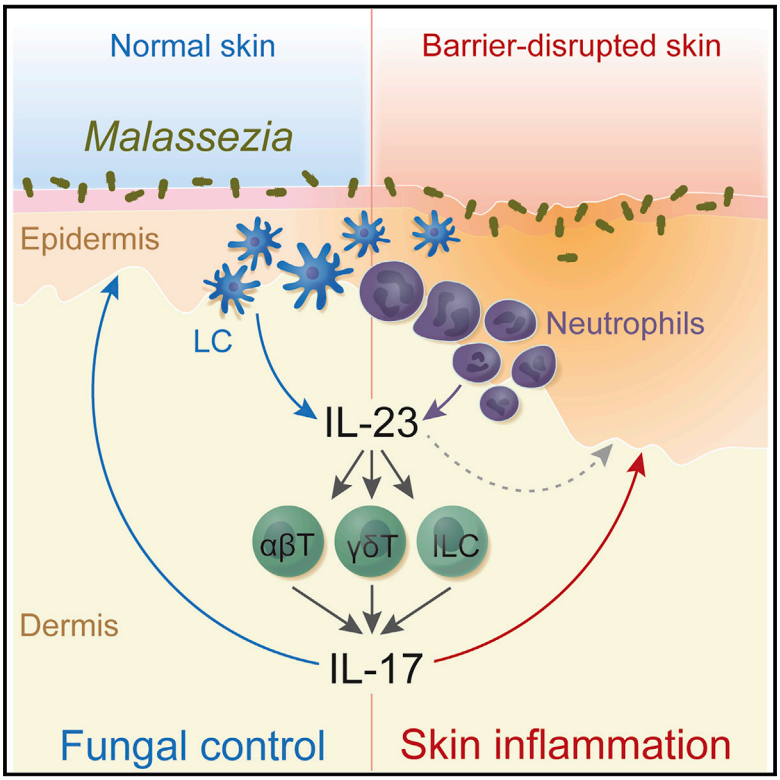
Article

Cell Host & Microbe

The Skin Commensal Yeast *Malassezia* Triggers a Type 17 Response that Coordinates Anti-fungal Immunity and Exacerbates Skin Inflammation

Graphical Abstract



Authors

Florian Sparber, Corinne De Gregorio, Simone Steckholzer, ..., Martin Glatz, Federica Sallusto, Salomé LeibundGut-Landmann

Correspondence

salome.leibundgut-landmann@uzh.ch

In Brief

The skin commensal yeast *Malassezia* is associated with common skin disorders like atopic dermatitis, but how the mammalian host responds to *Malassezia* remains unclear. Using an epicutaneous infection model in mice, Sparber et al. demonstrate that the IL-23-IL-17 pathway controls fungal colonization and also drives *Malassezia*-induced inflammation in atopy-like skin.

Highlights

- The skin commensal yeast *Malassezia* drives type 17 immunity in the skin
- *Malassezia*-specific human memory T cells display a Th17 phenotype
- Mice deficient in IL-17AF or IL-23 show uncontrolled *Malassezia* growth on the skin
- In the disrupted skin, IL-23 and IL-17AF promote *Malassezia*-induced inflammation

Sparber et al., 2019, Cell Host & Microbe *25*, 389–403
March 13, 2019 © 2019 Elsevier Inc.
https://doi.org/10.1016/j.chom.2019.02.002

CellPress

Cell Host & Microbe
Article

The Skin Commensal Yeast *Malassezia* Triggers a Type 17 Response that Coordinates Anti-fungal Immunity and Exacerbates Skin Inflammation

Florian Sparber,[1] Corinne De Gregorio,[2] Simone Steckholzer,[1] Filipa M. Ferreira,[3] Tamas Dolowschiak,[4] Fiorella Ruchti,[1] Florian R. Kirchner,[1] Sarah Mertens,[1] Immo Prinz,[5] Nicole Joller,[4] Thorsten Buch,[3] Martin Glatz,[6] Federica Sallusto,[2,7] and Salomé LeibundGut-Landmann[1,8,*]

[1]Section of Immunology, Vetsuisse Faculty, University of Zürich, Zürich 8057, Switzerland
[2]Institute for Research in Biomedicine, Università della Svizzera Italiana, Bellinzona 6500, Switzerland
[3]Institute of Laboratory Animal Science, University of Zürich, Schlieren 8952, Switzerland
[4]Institute of Experimental Immunology, University of Zürich, Zürich 8057, Switzerland
[5]Institute of Immunology, Hannover Medical School, Hannover 30625, Germany
[6]Department of Dermatology, University and University Hospital of Zürich, Zürich 8091, Switzerland
[7]Institute of Microbiology, ETH Zürich, Zürich 8093, Switzerland
[8]Lead Contact
*Correspondence: salome.leibundgut-landmann@uzh.ch
https://doi.org/10.1016/j.chom.2019.02.002

SUMMARY

Commensal fungi of the mammalian skin, such as those of the genus *Malassezia*, are associated with atopic dermatitis and other common inflammatory skin disorders. Understanding of the causative relationship between fungal commensalism and disease manifestation remains incomplete. By developing a murine epicutaneous infection model, we found *Malassezia* spp. selectively induce IL-17 and related cytokines. This response is key in preventing fungal overgrowth on the skin, as disruption of the IL-23-IL-17 axis compromises *Malassezia*-specific cutaneous immunity. Under conditions of impaired skin integrity, mimicking a hallmark of atopic dermatitis, the presence of *Malassezia* dramatically aggravates cutaneous inflammation, which again was IL-23 and IL-17 dependent. Consistently, we found a CCR6$^+$ Th17 subset of memory T cells to be *Malassezia* specific in both healthy individuals and atopic dermatitis patients, whereby the latter showed enhanced frequency of these cells. Thus, the *Malassezia*-induced type 17 response is pivotal in orchestrating antifungal immunity and in actively promoting skin inflammation.

INTRODUCTION

Microbes coexist with mammalian organisms and create complex ecosystems on body surfaces, which contribute to health and disease. The constant exposure of the host to microbes shapes the immune reactivity of the host locally and at distant sites and even influences seemingly unrelated processes ranging from digestion to behavior (Belkaid and Tamoutounour, 2016). Perturbations that disrupt the equilibrium of the microbial ecosystem may lead to the overgrowth of species with pathogenic potential and in turn to the development of disease (Williams and Gallo, 2015). Fungi are increasingly being recognized as common members of the microbiota on nearly all surfaces, including the skin (Findley et al., 2013), and recent examples revealed that—similar to their bacterial counterparts—commensal fungi might have an important role in host physiology and immunity (Iliev and Leonardi, 2017).

Among the fungal communities on the mammalian skin, *Malassezia* species are by far the most abundant members, with >90% of all commensal fungi belonging to this genus (Findley et al., 2013; Gemmer et al., 2002). 17 species of *Malassezia* are currently known, 10 of which have been identified on human skin sites (Cabañes, 2014). *M. sympodialis* is among the most frequently identified and in turn best studied species, while *M. furfur* on the other hand is found enriched on diseased skin in humans (Prohic et al., 2016). *M. pachydermatis* is the most frequent species found in dogs and other homoeothermic animals (Cabañes, 2014). *Malassezia* spp. are well adapted to thrive in the temperate and sebaceous microenvironment of the skin. They are lipophilic, explaining their predilection for seborrheic skin sites such as the scalp and the trunk. They lack a fatty acid synthase and thus rely on exogenous fatty acid sources for their nutritive requirements (Wu et al., 2015).

Because of the constant presence of *Malassezia* on the host, the immune system is continuously exposed to the fungus, which is reflected by *Malassezia*-responsive T cells and antibodies in the blood of healthy individuals (Ashbee and Bond, 2010). Despite its high abundance on the mammalian skin, the mechanisms of immune surveillance of *Malassezia* remain unknown.

Besides their commensal lifestyle, *Malassezia* spp. have also been associated with several common skin disorders including pityriasis versicolor, seborrheic dermatitis, and more severe inflammatory skin pathologies such as atopic dermatitis (AD) in humans (Sugita et al., 2010) and dermatitis and otitis externa in dogs (Bond et al., 2010). The role of *Malassezia* in skin disease pathogenesis is not well understood. A causative link between *Malassezia* and disease development has been made only for

dandruff and pityriasis versicolor, while its role in AD remains correlative and not well defined (Casagrande et al., 2006; Johansson et al., 2002, 2004). It is generally believed that *Malassezia* actively promotes disease symptoms in predisposed atopic individuals, albeit firm evidence for this causal link is missing and the mechanistic basis has not been established. Alternatively, *Malassezia* may also exert a protective role in AD (Li et al., 2018).

AD is one of the most common allergies, affecting up to 30% of children and 10% of adults in developed countries (Weidinger and Novak, 2016). The incidence of AD has dramatically increased over the last three decades presumably in consequence of stringent hygiene and reduced exposure to microbes in early life (Flohr and Yeo, 2011). AD is characterized clinically by periodic flares of dry, red, itchy skin lesions that can severely affect the quality of life of those affected. A hallmark of AD is skin barrier defects (Cabanillas and Novak, 2016) that increase the likelihood of environmental factors and irritants to penetrate the skin and promote inflammation. *Malassezia* itself may contribute to barrier disruption through the production of free fatty acids that can damage the integrity of the skin and thereby contribute to irritation and inflammation (Saunders et al., 2012). The immune response to *Malassezia* may also enhance inflammation in the atopic skin (Glatz et al., 2015).

The interaction of *Malassezia* with the mammalian immune system, both during homeostasis and disease, is not well understood. The mechanisms of fungal recognition and the immune pathways that maintain commensalism and/or promote pathology remain to be defined. Most of what we know today about the host-fungal interplay is based on experiments with isolated host cells *in vitro* (Sparber and LeibundGut-Landmann, 2017). A suitable experimental model to study the interaction between *Malassezia* spp. and the host *in vivo* in the complex environment of the mammalian skin has not been available so far. To fill this gap, we developed an experimental model of *Malassezia* skin colonization in mice. This allowed us to identify cellular and molecular players of the host response to *Malassezia* that maintain homeostasis during commensalism and at the same time promote pathology under inflamed conditions.

RESULTS

Malassezia spp. Colonization of the Mouse Skin

To study the interaction of *Malassezia* spp. with the mammalian skin *in vivo*, we established an infection model in C57BL/6 mice. The yeast was not detectable in our colony of specific pathogen-free (SPF) mice under steady-state conditions. Epicutaneous application of *Malassezia* ssp. onto the dorsal ear skin resulted in robust colonization of the skin on day 2 post infection (p.i.), while no fungal counts were detected in mock-infected control mice. The colonization efficiency was comparable between *M. sympodialis*, *M. furfur*, and *M. pachydermatis* (Figure 1A), with yeast cells localizing exclusively to the keratinized layer of the epidermis (Figure 1B). Disrupting the barrier integrity of the skin by mild tape stripping prior to infection (Holzmann et al., 2004) did not alter the capacity of *Malassezia* spp. to colonize the *stratum corneum* (Figures 1C–1E). The fungal load remained high for up to a week and declined thereafter with some variations between the different species (Figure S1). The skin of *Malassezia*-free mice can thus readily be colonized by various species of *Malassezia*.

Malassezia spp. Trigger Infiltration of Myeloid Cells into the Colonized Skin

Given the robust colonization of the mouse skin with *Malassezia* spp., we were interested in understanding the immune response to the yeast. *M. pachydermatis* colonization of the epidermis in the mouse skin was accompanied by infiltration of leukocytes, in particular $CD11b^+$ myeloid cells, to the site of infection (Figure 2A). Detailed characterization of these infiltrates by flow cytometry revealed low numbers of cells in the *Malassezia*-negative skin but a sharp increase in $CD11b^+Ly6G^+$ neutrophils, $CD11b^+Ly6G^-Ly6C^{hi}$ monocytes, and $CD11b^+Ly6G^-Ly6C^{low}$Siglec-F^+ eosinophils upon encounter of *M. pachydermatis*, both in percentages and absolute numbers (Figures 2B and 2C). Consistent with the massive infiltration of neutrophils and monocytes, we detected a strong rise in the local expression of neutrophil- and monocyte-recruiting chemokines and growth factors in the *Malassezia*-exposed skin (Figure 2D). The remaining population of $Ly6G^-Ly6C^{low}$Siglec-F^- myeloid cells consisted mostly of $CD11c^+$MHC-II^+ mononuclear phagocytes (MNPs) including dendritic cells and macrophages. In contrast to the infiltrating neutrophils and monocytes, this population did not change or even declined upon *Malassezia* exposure (Figure 2C).

The recruitment of myeloid cell infiltrates to the epithelium in response to *Malassezia* was independent of the barrier integrity of the ear skin and occurred similarly under conditions with or without tape stripping (Figures 2C and S2A). Moreover, the response was not restricted to *M. pachydermatis*; it was also observed in response to *M. sympodialis* and *M. furfur* (Figure S2B). Of note, barrier disruption on its own stimulated only a very limited myeloid response in the skin compared to completely untreated conditions (Figures 2C and S2). Together, these results indicate that *Malassezia* triggers a robust response in the host upon contact with the mammalian skin.

Exposure of the Skin to *Malassezia* spp. Results in a Selective Activation of the IL-17 Pathway

Next, we explored the cytokine response to the fungus in the *Malassezia*-exposed skin. In particular, we were interested in interleukin (IL)-17 and related cytokines given their important function in barrier tissue immunity in response to other fungi. IL-17A and IL-17F, two closely related members of the IL-17 cytokine family, are essential for immunosurveillance of *Candida albicans* at mucosal surfaces as evidenced by studies of primary immunodeficiency patients suffering from chronic mucocutaneous candidiasis (Li et al., 2017) and by experimental infections in mice (Conti et al., 2009; Gladiator et al., 2013).

When analyzing cytokine expression in the *Malassezia*-exposed skin, we observed a pronounced and rapid induction of IL-17A and IL-22 transcripts in response to *M. pachydermatis* (Figure 3A), while transcripts encoding interferon (IFN)-γ and the type-2-associated cytokines IL-5, IL-13, and thymic stromal lymphopoietin (TSLP) remained unchanged or were even downregulated in the *M. pachydermatis*-colonized skin (Figure S3A). Consistent with our previous results, the local and selective induction of type 17 cytokines was independent of skin barrier integrity, and it was conserved across all three *Malassezia*

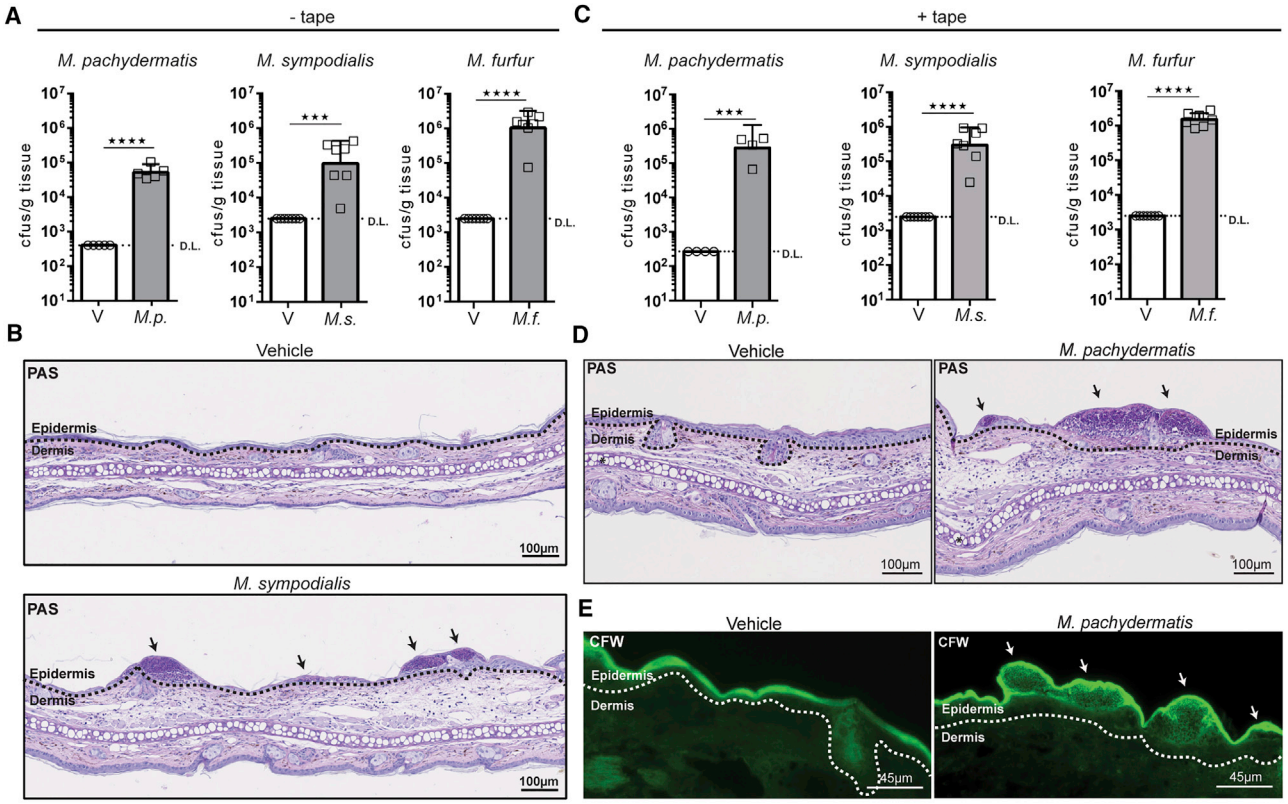


Figure 1. Experimental Colonization of Mice with *Malassezia* spp. *M. pachydermatis*, *M. sympodialis* or *M. furfur* in Olive Oil or Olive Oil Alone (Vehicle) Applied to the Dorsal Ear Skin of WT Mice

The skin was left untreated (A and B) or mildly tape-stripped (C–E) prior to infection. Fungal burden on day 2 p.i. (A and C). Histology of ear sections on day 2 p.i. stained with periodic acid-Schiff (PAS) (B and D) or calcofluor white (CFW) (E). D.L., detection limit; dotted line, basal membrane; arrows, accumulations of yeast cells; V, vehicle).

In (A) and (C), each symbol represents one animal. Graphs show pooled data from two independent experiments. The geomean and 95% confidence intervals are shown. Statistics were calculated using unpaired Student's t test. ***p<0.001, ****p<0.0001.

See also Figure S1.

species tested (Figure S3B). In line with the polarization of the *Malassezia*-induced cytokine response toward a type 17 profile, the expression of the key IL-17A- and IL-22-instructing factors IL-23, IL-1β, and IL-6 and the IL-17 target molecule β-defensin-3 were up-regulated in the *Malassezia*-exposed compared to the uninfected skin (Figures 3B and 3C).

To identify the cells involved in the local type-17 immune response, we applied a flow cytometry approach. Intracellular staining of IL-17A in lymphocytes that were freshly isolated from the skin of day-2-infected wild-type (WT) mice revealed dermal γδ T cells and αβ T cells as rapid producers of this cytokine (Figures 3D, 3E, S3C, and S3D). T cell receptor (TCR)-negative innate lymphocytes (ILCs) also expressed the cytokine, especially at a slightly later time point after infection, as revealed when analyzing *Il17a*^{Cre}*R26R*^{eYFP} reporter mice (Figures S3E and S3F). These data were further confirmed by *Il17a* expression analysis of sorted skin cell populations (Figures 3F and S4A). The response of γδ T cells, αβ T cells, and ILCs to *M. pachydermatis* skin exposure manifested also by expansion of the populations within the first 5 days p.i. (Figure S3F). In contrast, dendritic epidermal T cells (DETCs) neither expanded nor contributed considerably to IL-17A production in response to *M. pachydermatis* (Figures 3D–3F, S3E, and S3F). The tripartite cellular source of IL-17A in the *Malassezia*-exposed skin was reminiscent of the situation in the oral mucosa during experimental oropharyngeal candidiasis (Sparber et al., 2018).

Next, we set out to identify the cell type(s) producing the IL-17-instructing cytokine IL-23 in the infected skin. For this, we fluorescence-activated cell sorting (FACS)-sorted various myeloid skin cell subsets on day 2 p.i., including Ly6G^{+} neutrophils, Ly6C^{hi} monocytes, EpCam^{-} MNPs, and EpCam^{+} MNPs, the latter representing epidermal Langerhans cells (Figure S4). Of those, neutrophils and Langerhans cells were found to express the highest levels of *Il23a* transcripts (Figure 3G).

Finally, we asked the question of whether complementary to the local cytokine response, which we observed as early as 2 days after infection, *Malassezia* spp. would also activate the adaptive immune system in our experimental setting. Indeed, we found a strong induction of *Malassezia*-specific CD4^{+} T cells in the skin-draining lymph nodes that were polarized toward IL-17A-secreting Th17 effector cells (Figures 3H and 3I), while no concurrent induction of Th1 or Th2 cells was detected (Figure S5A). The selective Th17 response to the fungus was observed irrespectively of whether the skin was barrier disrupted or not prior to

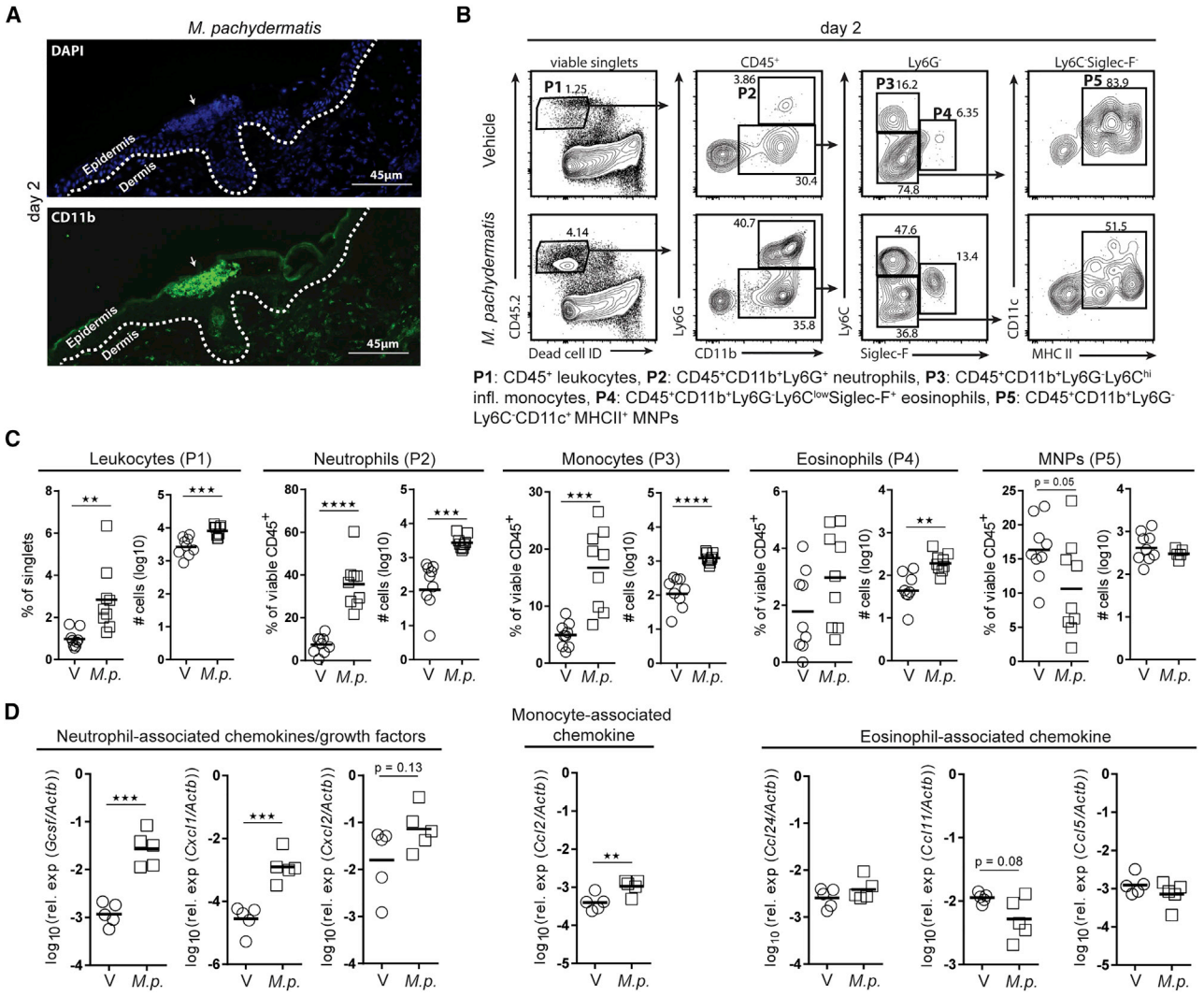


Figure 2. *Malassezia* Triggers a Rapid Infiltration of Myeloid Cells into the Infected Tissue

WT mice infected with *M. pachydermatis* (*M.p.*) or vehicle treated (V) after mild tape stripping of the dorsal ear skin and analyzed on day 2 p.i.

(A) Ear sections stained with DAPI and anti-CD11b. Dotted line, basal membrane; arrow, micro abscesses.

(B and C) FACS gating strategy for neutrophils (P2), inflammatory monocytes (P3), eosinophils (P4), and mononuclear phagocytes (MNPs, comprising DC and macrophages) (P5) in the ear skin (B) and summary graphs with the percentage and absolute number of cells per ½ ear (C). Numbers in (B) indicate the % of cells in each gate.

(D) Chemokine expression in the ear skin.

In (C) and (D), each symbol represents one animal. Graphs show pooled data from three (C) or two (D) independent experiments. The mean of each group is indicated. Statistics were calculated using unpaired Student's t test. **p<0.01, ***p<0.001, ****p<0.0001.

See also Figure S2.

infection (Figures 3H, 3I, S5B, and S5C). *M. sympodialis* displayed a similar capacity as *M. pachydermatis* to instruct IL-17A production by CD4+ T cells, while *M. furfur* was an even stronger inducer of Th17 immunity, both in the barrier-disrupted as well as in the unperturbed skin (Figures S5D and S5E). In summary, we revealed a very robust and selective activation of the IL-17 pathway by *Malassezia* spp., both via innate and adaptive immunity.

The IL-17 Pathway Is Critical for Preventing Uncontrolled Fungal Growth

Given the strong and selective induction of type 17 immunity in response to *Malassezia* skin exposure, we aimed at determining the role of this pathway in fungal control. For this, we assessed Rag1-deficient animals and animals with a selective defect in the T cell compartment, and we used *M. pachydermatis* as a representative fungal species. Rag1- and TCRβδ-deficient mice displayed very high skin colonization levels on day 12 p.i., a time point when WT mice had almost completely cleared the fungus from the skin (Figures 4A and S1). Compared with WT control animals, TCRδ-deficient mice lacking γδ but not αβ T cells also had a significantly higher fungal burden, indicating a crucial contribution of γδ T cells to fungal control (Figure 4B). Consistently, mice lacking a functional IL-17 pathway owing to a genetic defect in the IL-17A- and IL-17F- or in

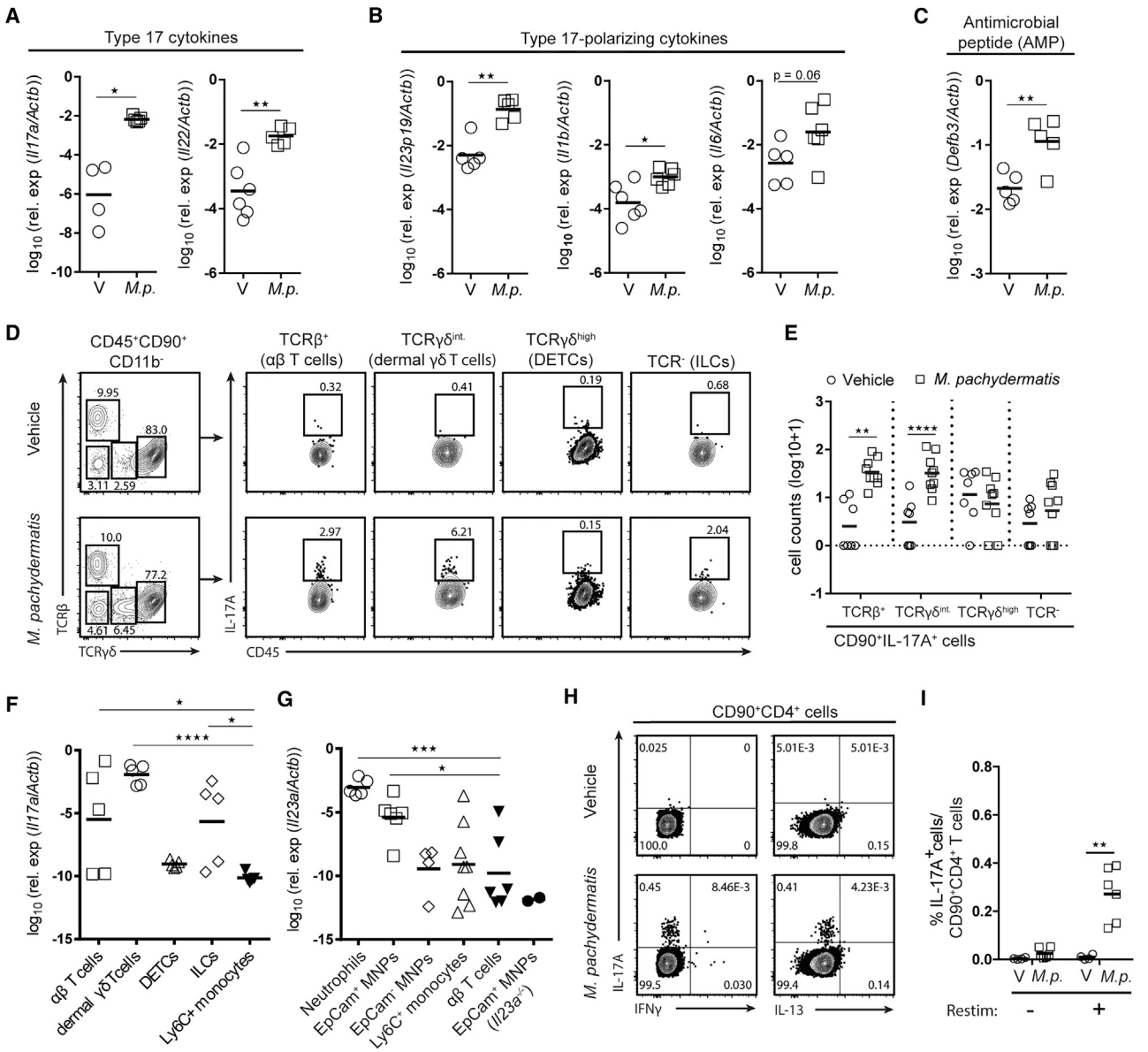


Figure 3. *Malassezia* Exposure of the Skin Results in a Selective Activation of the IL-17 Pathway

WT mice infected with *M. pachydermatis* (*M.p.*) or vehicle treated (V) after mild tape stripping of the dorsal ear skin.

(A–C) Expression of type 17 cytokine transcripts (A), type-17-polarizing cytokine transcripts (B), and antimicrobial peptide transcripts (C) in the ear skin on day 2 p.i.

(D and E) FACS gating strategy for αβ T cells, innate lymphoid cells (ILCs), dermal γδ T cells, and epidermal γδ T cells (DETCs) in the ear skin (D) and summary graph with absolute numbers of IL-17A$^+$ subsets per ear on day 2 p.i. (E). Plots in (D) represent concatenated samples from two ears each; numbers indicate the % of cells in each gate.

(F and G) *Il17a* (F) and *Il23a* transcripts (G) in the indicated cell populations sorted from the ear skin on day 2 p.i.

(H and I) IL-17A production by CD90$^+$CD4$^+$ T cells in the auricular lymph nodes on day 12 p.i.

Numbers in (H) indicate the % of cells in each quadrant.

In (A–C), (E–G), and (I), each symbol represents one animal. Graphs show pooled data from two to three independent experiments. The mean of each group is shown. Statistics were calculated using Student's t test or one-way ANOVA as appropriate. *p<0.05, **p<0.01, ***p<0.001, ****p<0.0001.

See also Figures S3, S4, and S5A–S5E.

IL-23-encoding genes, respectively, were unable to clear the fungus (Figure 4C). In contrast, IL-22, which is functionally related to IL-17A and IL-17F and which was also strongly induced in the *M. pachydermatis*-exposed skin (Figure 3A), was not required for the control of fungal colonization (Figure 4D). The defect in fungal control in the absence of a functional IL-17 pathway was underlined by the reduced expression of antimicrobial peptides, many of which were bearing antifungal activity

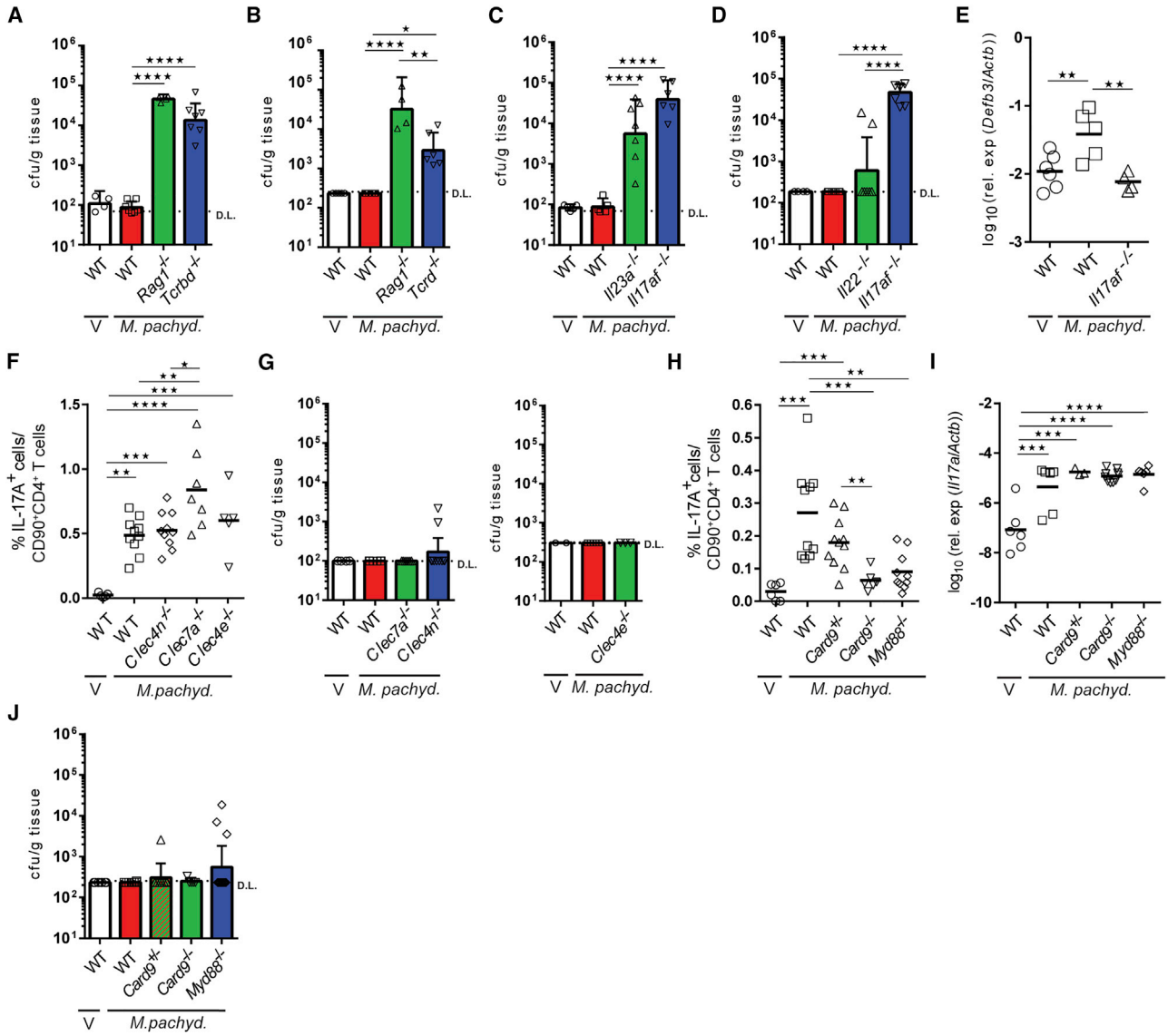


Figure 4. The IL-17 Pathway Is Critical for Preventing Uncontrolled Fungal Growth

(A–E) WT, *Rag1*$^{-/-}$ and *Tcrbd*$^{-/-}$ mice (A), WT, *Rag1*$^{-/-}$ and *Tcrd*$^{-/-}$ mice (B), WT, *Il23a*$^{-/-}$ and *Il17af*$^{-/-}$ mice (C), WT, *Il22*$^{-/-}$ and *Il17af*$^{-/-}$ mice (D) or WT and *Il17af*$^{-/-}$ mice (E) mildly tape stripped on the dorsal ear skin and infected with *M. pachydermatis* or vehicle treated (V). Fungal burden in the ear skin on day 12 p.i. (A–D). *Defb3* mRNA expression in the ear skin on day 2 p.i. (E).

(F–J) WT, *Clec7a*$^{-/-}$, *Clec4n*$^{-/-}$ and *Clec4e*$^{-/-}$, mice (F, G) or *Card9*$^{-/-}$, *Myd88*$^{-/-}$, and *Card9*$^{+/-}$ littermate control mice (H–J) mildly tape stripped on the dorsal ear skin and infected with *M. pachydermatis* or vehicle treated. IL-17A-production by CD90^{+}CD4^{+} T cells in the auricular lymph nodes on day 12 p.i. (F and H). Skin fungal burden on day 12 p.i. (G and J). *Il17a* mRNA expression in the ear skin on day 2 p.i. (I).

Each symbol represents one animal. In (E), (F), (H), and (I), the mean of each group is indicated. Graphs in (A–D), (G), and (J) show the geomean and 95% confidence interval. D.L., detection limit. All graphs show pooled data from two to three independent experiments. Statistics were calculated using one-way ANOVA. *p<0.05, **p<0.01, ***p<0.001, ****p<0.0001.

(Swidergall and Ernst, 2014), in the *Malassezia*-exposed skin of IL-17AF-deficient animals (Figure 4E). Together, these results demonstrate a critical role of the IL-23-IL-17 axis in cutaneous immunity against *Malassezia*.

The Role of C-type Lectin Receptor Signaling in the Host Response to *Malassezia* in the Mammalian Skin

C-type lectin receptor (CLR) family members are specialized in sensing fungal microbes and linking fungal recognition to the initiation of T cell responses, in particular those of the Th17 type (LeibundGut-Landmann et al., 2007). Mincle and Dectin-2 as well as the downstream signaling kinase Syk have previously been implicated in *Malassezia*-induced immune activation (Ishikawa et al., 2013; Kistowska et al., 2014; Yamasaki et al., 2009). However, mice lacking Mincle (*Clec4e*$^{-/-}$), Dectin-2 (*Clec4n*$^{-/-}$), or the prototypic CLR Dectin-1 (*Clec7a*$^{-/-}$) mice mounted a normal or even enhanced Th17 response to *M. pachydermatis* skin colonization if compared to their WT counterparts (Figure 4F). Likewise, fungal

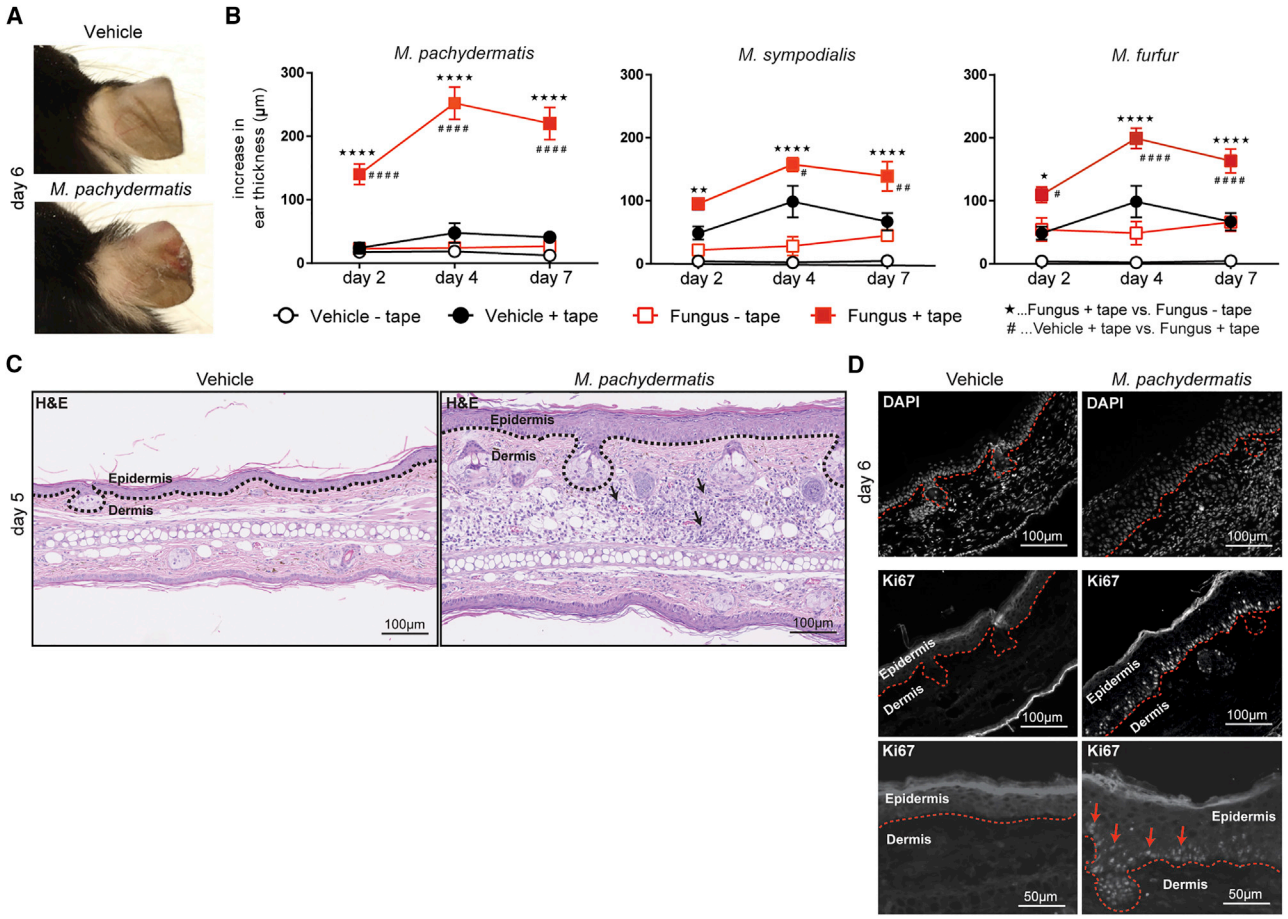


Figure 5. Epicutaneous Application of *Malassezia* spp. Promotes Inflammation in the Barrier-Disrupted Skin

WT mice mildly tape stripped on the dorsal ear skin and/or infected with *M. pachydermatis*, *M. sympodialis*, or *M. furfur* or vehicle treated (V).

(A) Macroscopic images of the dorsal ear on day 6 p.i.

(B) Increase in ear thickness over time. Graphs shows mean +/– SEM of two independent experiments with at least 3 mice per group each.

(C) Histology of ear sections stained with H&E on day 5 p.i. Arrows, leukocyte infiltrates; dotted line: basal membrane.

(D) Ear sections stained with DAPI or anti-Ki67 antibody as indicated on day 6 p.i. Bottom panels: increased magnification of anti-Ki67-stained sections. Arrows: $Ki67^{+}$ keratinocytes; dotted line: basal membrane.

Statistics were calculated using one-way ANOVA. Stars indicate the comparison of tape-stripped versus non-tape stripped groups; hashes indicate the comparison between vehicle-treated and *Malassezia* spp.-infected groups. $^{*/\#}p<0.05$, $^{**/\#\#}p<0.01$, $^{****/\#\#\#\#}p<0.0001$.

control was not impaired in any of the three receptor-deficient mouse lines (Figure 4G), indicating that none of the three CLRs on its own was essential for driving type 17 immunity and fungal control of *Malassezia* in the skin. Redundancy may however mask a partial contribution of individual receptors. Indeed, a broader abrogation of CLR signaling by genetic deletion of the common adaptor Card9 resulted in a severely impaired Th17 response to *Malassezia* (Figure 4H). In addition, the TLR-IL-1R signaling pathway also contributed critically to the induction of the antifungal Th17 response (Figure 4H). Interestingly and in contrast to the adaptive response, early IL-17 expression on day 2 p.i. was independent of Card9 and MyD88 in the *Malassezia*-exposed skin (Figure 4I) and consequently, fungal control was not compromised in the absence of Card9 or MyD88 (Figure 4J). Together, these results indicate a critical role of both the CLR and MyD88 pathway in the regulation of adaptive immunity to *Malassezia*.

Epicutaneous Application of *Malassezia* spp. Promotes Inflammation in the Barrier-Disrupted Skin

After having established the host protective principles that regulate *Malassezia* colonization in the skin, we aspired to explore the potential of the fungus to promote inflammation in our experimental system under AD-like conditions, which we mimicked by tape stripping of the skin prior to epicutaneous application of the fungus. While barrier disruption on its own induced only a mild inflammatory response, the addition of *Malassezia* strongly enhanced inflammation both macroscopically and microscopically (Figures 5A–5C). The ear skin of the barrier-disrupted mice was massively thickened upon exposure of any of the three tested *Malassezia* species if compared to the uninfected tape-stripped skin (Figures 5B and 5C) and was characterized by edema, inflammatory infiltrates throughout the ear tissue, and strong epithelial hyperplasia (Figures 5C and 5D). The increase in epithelial cell proliferation was confirmed by

Ki67 staining of keratinocytes in the *stratum basale* of the ear skin of *M. pachydermatis*-infected and tape-stripped animals (Figure 5D). The overall response peaked between day 4 and day 7 p.i. and thereby followed the kinetics of the fungal load in the skin, which had its maximum on days 2 to 4 p.i. and declined thereafter (Figure S1). This temporal discordance supported the idea that the inflammatory phenotype was secondary to the presence of the fungus and the antifungal response in the skin. Together, these results provide evidence that *Malassezia* spp. actively drive skin inflammation in the barrier-disrupted skin, promoting pathological features that resemble lesions in human AD.

Malassezia-Induced Skin Inflammation Is Driven by the Type 17 Pathway

Given the prominent induction of IL-17 and related cytokines by *Malassezia* spp., we hypothesized that the antifungal response might actively contribute to the inflammatory phenotype in the barrier-disrupted skin of colonized animals. Indeed, IL-17AF-deficiency curtailed the increase in skin thickening upon the application of *M. pachydermatis* to the barrier-disrupted skin (Figure 6A). The phenotype was even more strongly impaired in *Il23a*$^{-/-}$ compared to *Il17af*$^{-/-}$ mice (Figure 6A), suggesting that other IL-23-dependent factors may partially compensate for the lack of IL-17 in *Il17af*$^{-/-}$ mice. IL-22 was linked to AD before (Cavani et al., 2012; Gittler et al., 2012), and in our system, IL-22 was strongly induced in the *Malassezia*-exposed skin, irrespective of the presence or absence of IL-17A and IL-17F (Figure 6B). However, IL-22-deficient mice did not display a phenotype in our experimental system (Figure 6C). We therefore concluded that, in contrast to IL-17AF, IL-22 was not responsible for driving inflammation in the *Malassezia*-exposed, barrier-disrupted skin, although redundancy between IL-17AF and IL-22 cannot be excluded. In line with a lymphocytic source of IL-17 cytokines in the *Malassezia*-exposed skin, the lack of T cells, and in particular γδ T cells, also abolished *Malassezia*-induced skin inflammation (Figures 6D and 6E). In summary, our results indicate that the IL-23-IL-17 axis and γδ T cells play a central role in stimulating an aggravated inflammatory response and enhanced skin thickening in response to *Malassezia*.

Finally, we aimed at evaluating the impact of pre-existing T cell memory to *Malassezia*, as it exists in humans and dogs that are naturally colonized with the yeast, on promoting skin inflammation in our model. To generate a population of *Malassezia*-specific memory T cells, we applied *M. pachydermatis* onto the dorsal ear skin as described before. 5 weeks later, a time point at which the fungus was no longer detectable, we re-challenged the animals with the fungus via the same route. The presence of *Malassezia*-specific memory Th17 cells in the primed mice was evidenced by the rapid production of IL-17A by CD90^{+}CD4^{+} T cells following challenge infection, while during a primary infection, the response was not apparent earlier than 6 days p.i. (Figure 6F). Again, no IL-13 or IFN-γ production could be evidenced under these experimental conditions (Figure S5F). Importantly, the presence of *Malassezia*-specific memory T cells accelerated the kinetics of the inflammatory reaction to the fungus in the barrier-disrupted mouse skin (Figure 6G). Together, these data indicate that *Malassezia*-specific Th17 cells can promote the pathological skin inflammation under AD-like conditions.

Human *Malassezia*-Specific Memory T Cells from Healthy and Atopic Individuals Display a Th17 Phenotype

To corroborate the findings obtained in mice on the relevance of the IL-17 pathway in *Malassezia* immunity and *Malassezia*-driven skin inflammation, we turned to analyze the T cell response to the commensal yeast in humans. As a consequence of the continuous exposure of the barrier tissues to commensal microbes, the circulating pool of lymphocytes in humans comprises memory T helper cell populations with specificities toward these organisms (Acosta-Rodriguez et al., 2007). We initially analyzed the memory T cell compartment in healthy non-atopic individuals by sorting CD4^{+}CCR6^{+} and CD4^{+}CCR6^{-} memory T cells (containing Th17 and an untypical subset of Th1 cells termed Th1*, or Th1 and Th2 subsets, respectively [Sallusto, 2016]), CFSE-labeling and re-stimulating them with autologous monocytes that were pulsed with various species of *Malassezia*. Analysis of cell division by means of carboxyfluorescein succinimidyl ester (CFSE) dilution revealed proliferation of both CCR6^{+} and CCR6^{-} memory T cells in response to *Malassezia* spp., whereby the CCR6^{+} subset responded somewhat stronger under all conditions tested (Figures 7A and 7B). We then analyzed the cytokine production by *Malassezia*-responsive T cells by Luminex. The CCR6^{+} subset produced high amounts of IL-17A and IL-22 when stimulated with any of the three *Malassezia* species tested (Figure 7C). In addition, we detected IFN-γ and IL-5 secretion by the CCR6^{-} subset (Figure 7C). Re-stimulation of T cells with monocytes that were not pulsed with Ag or pulsed with heat-killed *C. albicans* served as negative and reference control, respectively (Figures S6A and S6B). A similar result was also obtained when analyzing cytokine production by intracellular cytokine staining and flow cytometry (Figure S7).

Next, we compared the T cell polarization profile of memory T cells from healthy individuals with that of AD patients. The frequency and cytokine response of *Malassezia*-responsive memory CD4^{+} T cells were increased in AD patients compared to non-atopic donors (Figure 7D). Consistent with the literature (Johansson et al., 2009; Valli et al., 2010), we found production of type 2 cytokines, which were derived predominantly from CCR6^{-} memory T cells (Figure 7E). Strikingly, the *Malassezia*-specific production of IL-17 and IL-22 was also increased in the memory T cell compartment from AD patients compared to healthy controls (Figure 7E). As expected, the IL-17 and IL-22 response was most pronounced in the CCR6^{+} subset. The increase in cytokine concentration appeared to be the result of an increase in the expansion of the overall *Malassezia*-specific T cell compartment (Figure 7D) as cytokine production on a per-cell basis was not altered in AD patients compared to healthy donors when cytokine-production was quantified by flow cytometry (Figure S7). Together, these data revealed a so far unrecognized contribution of IL-17 and related cytokines to the overall T cell response to *Malassezia* spp. in humans, both in healthy subjects and in AD patients, and thereby underpin the relevance of our findings from our experimental model of *Malassezia* colonization.

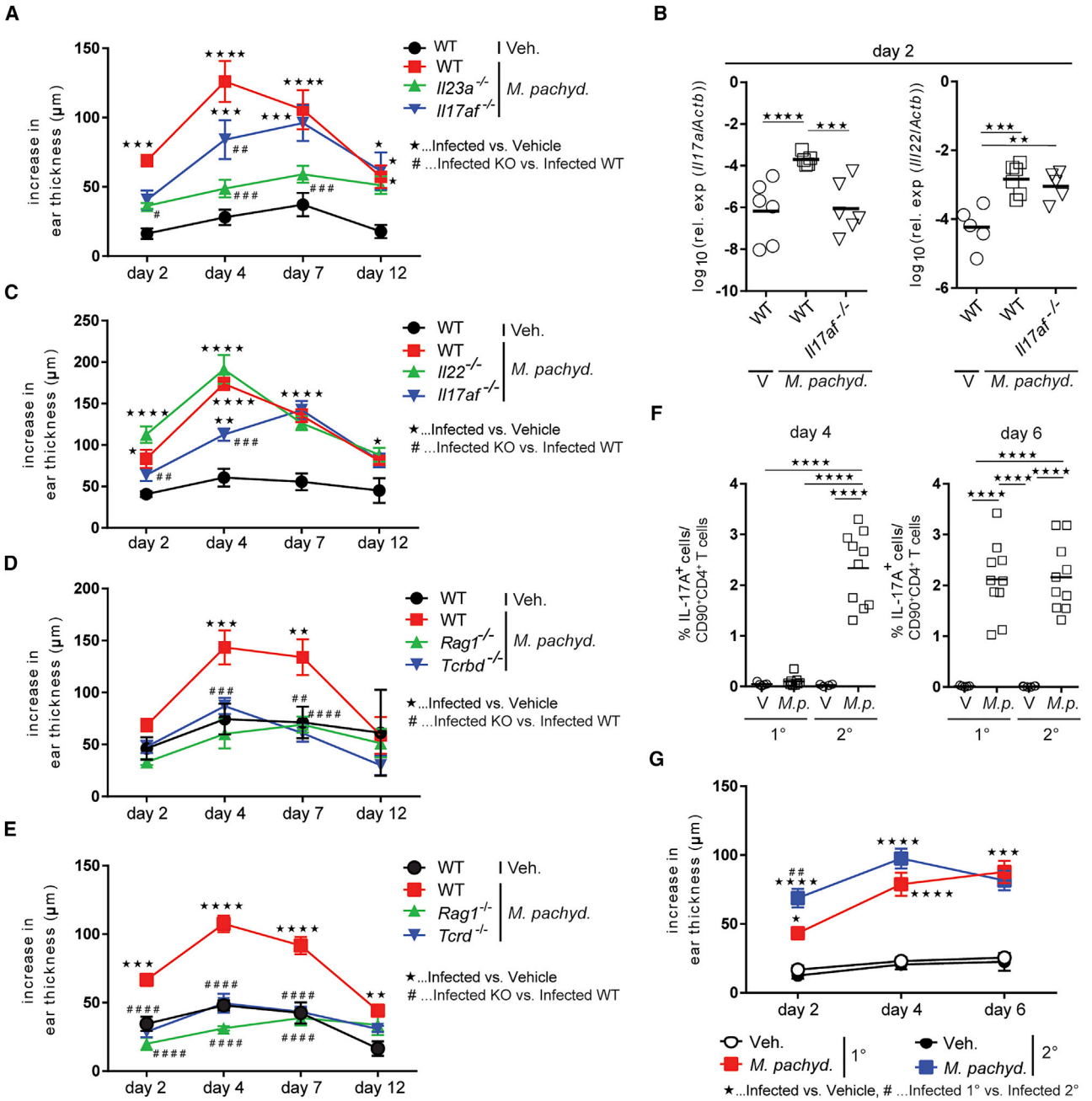


Figure 6. The IL-23-IL-17 Immune Axis Plays a Critical Role in Promoting Excessive Skin Inflammation

(A–E) WT, *Il23a*$^{-/-}$, and *Il17af*$^{-/-}$ mice (A, B), WT, *Il17af*$^{-/-}$, and *Il22*$^{-/-}$ mice (C), WT, *Rag1*$^{-/-}$, and *Tcrbd*$^{-/-}$ mice (D), or WT, *Rag1*$^{-/-}$, and *Tcrd*$^{-/-}$ mice (E) mildly tape stripped and infected with *M. pachydermatis* or vehicle treated (V). Increase in ear thickness over time (A, C, D, and E) and *Il17a* and *Il22* mRNA expression in the skin on day 2 p.i. (B).

(F and G) WT mice were primed with *M. pachydermatis* (2°) or left uninfected (1°) 6 weeks prior to (re-)infection. The ear skin was pretreated by tape stripping in all conditions. IL-17A production by CD90^{+}CD4^{+} T cells in the auricular lymph nodes 4 and 6 days after (re-)infection (F) and increase in ear thickness on days 2, 4, and 6 after (re-)infection (G).

In (B) and (F), each symbol represents one animal. Graphs show pooled data from two independent experiments; the mean of each group is indicated. Graphs in (A), (C–E), and (G) show the mean +/– SEM of each group with pooled data from 2 to 3 independent experiments with 4–5 mice per group. Statistics were calculated using one-way ANOVA. In (A) and (C–E), stars indicate the comparison of vehicle-treated and *M. pachydermatis*-infected groups; hashes indicate the comparison between infected knockout (KO) and infected WT groups. In (G), stars indicate the comparison of vehicle-treated and *M. pachydermatis*-infected groups; hashes indicate the comparison between 1° and 2° infected groups. $^{*/\#}p<0.05$, $^{**/\#\#}p<0.01$, $^{***/\#\#\#}p<0.001$, $^{****/\#\#\#\#}p<0.0001$.

See also Figure S5F.

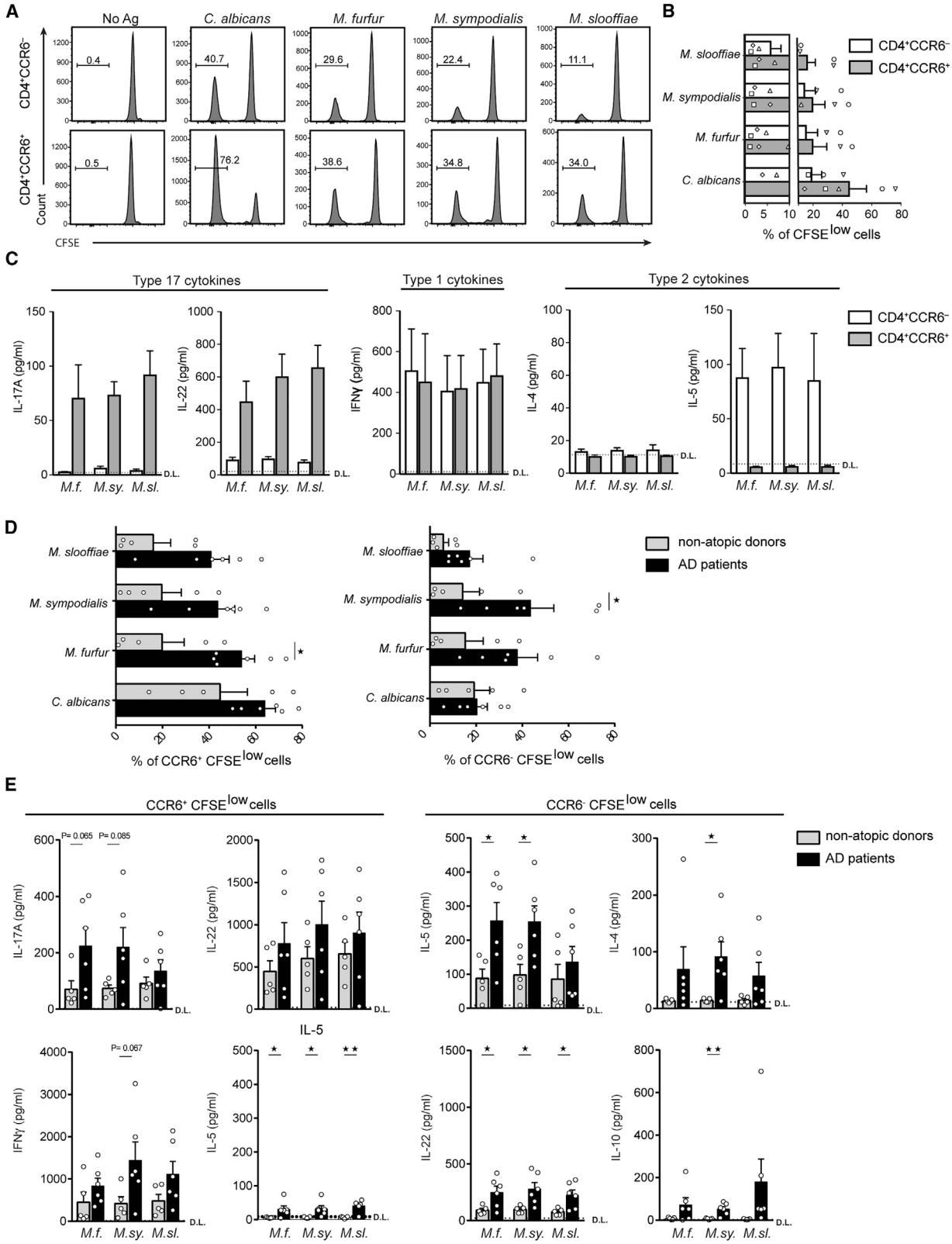


Figure 7. Human *Malassezia*-Specific Memory T Cells Display a Strong Th17 Signature

(A–C) CCR6$^+$ and CCR6$^-$ human memory CD4$^+$ T cells sorted from the peripheral blood of non-atopic individuals and co-cultured for 5 days with autologous monocytes that were pulsed with heat-killed *Malassezia* spp. Unpulsed monocytes and monocytes pulsed with heat-killed *C. albicans* served as controls.

(legend continued on next page)

DISCUSSION

Malassezia is by far the most abundant fungal commensal on the mammalian skin. Besides its commensal lifestyle, *Malassezia* can also mediate common skin diseases (Velegraki et al., 2015) and, beyond that, may be implicated in extracutaneous pathologies (Sokol et al., 2017). Despite its prevalence and clinical relevance, the yeast obtained little attention in the past, and it remains largely unknown how it contributes to immune homeostasis and disease. *Malassezia* continuously interacts with the host, but the complex interplay with the skin immune system is not well understood (Sparber and LeibundGut-Landmann, 2017). Our experimental model allowed us to study these aspects *in vivo* in the complex environment of the mammalian skin. We thereby revealed a distinct polarization of the *Malassezia*-specific immune response toward a type 17 profile, which was central for preventing uncontrolled fungal growth in the skin. Moreover, the IL-23-IL-17 axis promoted the inflammatory response in the barrier-disrupted skin, which mimics AD-like conditions. Consistent with the key role of the IL-17 pathway in the interaction of the skin immune system with *Malassezia*, we also identified a strong Th17 signature in human *Malassezia*-specific T cells.

Type 17 immunity is well known for its host-protective effects against fungal infections in barrier tissues, in particular those caused by *C. albicans*. This is evidenced most strikingly by inborn errors in genes involved in IL-17 signaling or IL-17 induction that lead to increased susceptibility to chronic mucocutaneous candidiasis. The IL-17 pathway is also associated with immunity against other fungal diseases, at least in preclinical settings including dermatophytosis (Burstein et al., 2018), pulmonary infections with dimorphic fungi (Wüthrich et al., 2011), and ocular mold infections (Taylor et al., 2014). Our findings highlight the relevance of type 17 immunity to the abundant mammalian skin commensal yeast *Malassezia*. Upon primary exposure of the murine skin to *Malassezia*, we observed a rapid induction of IL-17 expression. Reminiscent of what is known from other experimental models of fungal infection in mice (Conti et al., 2014; Gladiator et al., 2013; Hernández-Santos et al., 2018; Kagami et al., 2010; Kashem et al., 2015; Sparber et al., 2018), the initial peak of IL-17 expression by innate immune cells, in particular $\gamma\delta$ T cells, appears long before the adaptive immune system is fully activated. The swift activation of the innate immune system in our experimental model results in fungal elimination within $\sim$2 weeks p.i. Despite this important difference to the situation in naturally colonized hosts, the model allows delineating the key pathways that regulate the crosstalk between *Malassezia* spp. and the host.

Whether the IL-17 pathway also regulates fungal homeostasis in the human skin remains to be determined. The hypothesis is supported by a prominent population of Th17 cells within the *Malassezia*-specific memory T cell pool. So far, *Malassezia* overgrowth has not been reported in individuals bearing genetic defects in the IL-17 pathway. However, these individuals are very rare, and changes in *Malassezia* colonization density on the human skin may not become readily apparent if fungal loads are not determined in a quantitative manner. Moreover, increased fungal loads may not be directly associated with the emergence of disease symptoms. Changes in *Malassezia* colonization levels were correlated with the manifestation of AD in dogs (Cafarchia et al., 2005), but such a link remains uncertain in human AD (Chng et al., 2016; Darabi et al., 2009; Sandström Falk et al., 2005).

Our study revealed a dual role of IL-17 in the host response to *Malassezia*. Beyond its antifungal effect, IL-17 promotes inflammatory pathology in the *Malassezia*-colonized barrier-disrupted skin, and *Malassezia*-specific Th17 cells constitute a prominent subset among the overall *Malassezia*-specific T cell population in human AD patients. Previous studies analyzing the polarization of *Malassezia*-specific T cells in atopic individuals focused on type 2 immunity (Glatz et al., 2015), as allergic diseases have generally been regarded as Th2 driven. Consistent with Balaji et al. (2011), our results from humans and mice suggest the contribution of type 17 immunity to AD.

The potential of IL-17 in driving pathology in the skin is best understood in psoriasis, and targeting IL-17 in psoriatic patients has produced spectacular outcomes (Hawkes et al., 2017). The relevance of type 17 immunity in the pathogenesis of allergic diseases has been recognized more recently and appears to be of particular importance in some subtypes of AD (Cosmi et al., 2016; Esaki et al., 2016; Koga et al., 2008; Leonardi et al., 2015). The contribution of *Malassezia*-induced IL-17 to the manifestation of inflammatory skin pathology that we observed in our experimental model is reminiscent of the recently reported role of IL-17 in driving skin inflammation in response to *Staphylococcus aureus* (Liu et al., 2017; Nakagawa et al., 2017). *S. aureus* is the most well-known bacterial microbe associated with AD, and the prevalence rate of *S. aureus* colonization correlates with disease severity (Geoghegan et al., 2018). *S. aureus* toxins can trigger the production of IL-17 cytokines in experimentally infected mice, which in turn promotes cutaneous inflammation (Liu et al., 2017; Nakagawa et al., 2017). In contrast to the situation reported here with *Malassezia*, IL-17A and IL-17F were however not implicated in bacterial control (Nakagawa et al., 2017). Mechanistically, *S. aureus*-induced IL-17 production in the murine skin was shown to be initiated by keratinocyte-derived IL-1 and IL-36. Whether similar mechanisms regulate the IL-17 response to *Malassezia* remains to be determined. Factors beyond IL-17 cytokines also contribute to *Malassezia*-driven inflammation as indicated by our observation that the skin

Representative FACS plots (A) and summary graph (B) show the percentages of proliferating ($CFSE^{low}$) $CD4^+CCR6^-$ (upper row, gray bars) and $CD4^+CCR6^+$ T cells (lower row, white bars). (C) Type 17 (IL-17A and IL-22), type 1 (IFN-γ), and type 2 cytokines (IL-4 and IL-5) by $CD4^+CCR6^-$ (white bars) and $CD4^+CCR6^+$ T cells (gray bars). The mean + SEM of each group is indicated.

(D and E) Comparison of proliferation (D) and cytokine production (E) by *Malassezia* spp.-responsive $CCR6^+$ and $CCR6^-$ memory T cells from atopic patients (black bars) with those from non-atopic individuals (from A–C, gray bars). Each symbol represents one donor. Graphs show pooled data from 3 independent experiments with 5 donors per group. The mean + SEM of each group is indicated. Statistics were calculated using one-way ANOVA or unpaired Student's t test, as appropriate. *$p<0.05$, **$p<0.01$.

See also Figures S6 and S7.

phenotype was more severely curtailed in *Il23a*$^{-/-}$ animals than in *Il17af*$^{-/-}$ animals.

In humans, T cell dysregulation and a prevalent type 2 profile dominate the allergic response, and as such, *Malassezia*-specific Th2 cells are abundant in atopic individuals (Glatz et al., 2015). What initiates the transition from a Th17 response in healthy individuals to a mixed Th17-Th2 response in AD patients remains unknown. *Malassezia*-specific Th2 cells may emerge as a result of T cell plasticity, or they may be generated *de novo* in diseased individuals. Alternatively, the large pool of Th2 cells in AD patients may arise from selective expansion of *Malassezia*-specific Th2 cells that exist in small numbers in non-atopic individuals. The detailed analysis of the T cell repertoire in healthy individuals and in AD patients during flares and remission phases might provide valuable insights (Becattini et al., 2015).

Malassezia research was hampered in the past by the lack of adequate experimental systems. The establishment of an animal model represents a major advancement in the field. It opens the door for future explorations of fundamental principles of fungal-host interactions that contribute to homeostasis in the mammalian skin and of the mechanistic processes that control the balance between protective immunity and allergic inflammation, both in the intact skin and under conditions of barrier deficiency or Th2 polarization (Moosbrugger-Martinz et al., 2017), both of which represent key hallmarks of AD. Recent reports on the assembly and annotation of several *Malassezia* genomes (Gioti et al., 2013; Wu et al., 2015; Zhu et al., 2017) and the development of insertional and targeted mutagenesis in *Malassezia* (Ianiri et al., 2016, 2017) make the identification of fungal determinants that govern the interaction of the fungus with the host tangible. Our experimental model will facilitate the functional validation of such factors under diverse host conditions and thereby further promotes a comprehensive understanding of the *Malassezia*-host interplay.

STAR★METHODS

Detailed methods are provided in the online version of this paper and include the following:

- KEY RESOURCES TABLE
- CONTACT FOR REAGENT AND RESOURCE SHARING
- EXPERIMENTAL MODEL AND SUBJECT DETAILS
  - Ethic Statement
  - Animals
  - Fungal Strains
  - Experimental Model
  - Atopic Patients and Healthy Controls
- METHOD DETAILS
  - Isolation of Skin and Lymph Node Cells
  - *Ex Vivo* Murine T Cell Stimulation, Surface and Intracellular Staining
  - Flow Cytometry and Cell Sorting
  - RNA Isolation and Quantitative RT-PCR
  - Histochemistry and Immunofluorescence
  - Human Cell Sorting
  - *Ex Vivo* Human T Cell Stimulation, Surface and Intracellular Staining
- QUANTIFICATION AND STATISTICAL ANALYSIS
- DATA AND SOFTWARE AVAILABILITY

SUPPLEMENTAL INFORMATION

Supplemental Information can be found online at https://doi.org/10.1016/j.chom.2019.02.002.

ACKNOWLEDGMENTS

The authors would like to thank AD patients and healthy donors for blood donation; G.D. Brown, Y. Iwakura, J.-C. Reneault, C. Wells, B. Marsland, D. Sancho, and B. Becher for mice; J. Heitman and T. Boekhout for *Malassezia* strains; the staff of the Laboratory Animal Service Center of University of Zurich for animal husbandry; the Laboratory for Animal Model Pathology of University of Zurich and the Flow Cytometry Facility of University of Zurich for support; and members of the LeibundGut-lab for helpful advice and discussions. This work was supported by the University of Zürich and in part by the European Research Council (# 323183 PREDICT to F. Sallusto). F. Sallusto and the Institute for Research in Biomedicine are supported by the Helmut Horten Foundation. T.D. was funded by the Forschungskredit of the University of Zurich (# FK-17-044). The work in N.J.'s lab is supported by the Swiss National Science Foundation (# PP00P3_150663 to N.J.) and the European Research Council (# 677200 Immune Regulation to N.J.). The work in T.B.'s lab is supported by the Swiss Multiple Sclerosis Society and the Hertie Foundation (# P1150013).

AUTHOR CONTRIBUTIONS

Conceptualization, F. Sparber, F. Sallusto, and S.L.-L.; Methodology, F. Sparber, C.D.G., and T.D.; Investigation, F. Sparber, C.D.G., F.R.K., S.S., T.D., F.R., S.M., and S.L.-L.; Formal Analysis, F. Sparber and C.D.G.; Validation, F. Sparber and S.L.-L.; Resources, F.M.F., T.B., and I.P.; Visualization, F. Sparber; Project Administration, M.G. and S.L.-L.; Funding Acquisition, F. Sparber and S.L.-L.; Supervision, S.L.-L.; Writing – Original Draft, F. Sparber and S.L.-L.; Writing – Review & Editing, C.D.G., F. Sallusto, I.P., N.J., T.B., and M.G.

DECLARATION OF INTERESTS

The authors declare no competing interests.

Received: July 25, 2018
Revised: November 28, 2018
Accepted: February 5, 2019
Published: March 13, 2019

REFERENCES

Acosta-Rodriguez, E.V., Rivino, L., Geginat, J., Jarrossay, D., Gattorno, M., Lanzavecchia, A., Sallusto, F., and Napolitani, G. (2007). Surface phenotype and antigenic specificity of human interleukin 17-producing T helper memory cells. Nat. Immunol. *8*, 639–646.

Adachi, O., Kawai, T., Takeda, K., Matsumoto, M., Tsutsui, H., Sakagami, M., Nakanishi, K., and Akira, S. (1998). Targeted disruption of the MyD88 gene results in loss of IL-1- and IL-18-mediated function. Immunity *9*, 143–150.

Ashbee, H.R., and Bond, R. (2010). Malassezia species and immunity: host-pathogen interactions. In Malassezia and the Skin, Science., Clinical Practice, T. Boekhout, P. Mayser, E. Guého-Kellermann, and A. Velegraki, eds. (Springer), pp. 139–173.

Balaji, H., Heratizadeh, A., Wichmann, K., Niebuhr, M., Crameri, R., Scheynius, A., and Werfel, T. (2011). Malassezia sympodialis thioredoxin-specific T cells are highly cross-reactive to human thioredoxin in atopic dermatitis. J. Allergy Clin. Immunol. *128*, 92–99.e4.

Becattini, S., Latorre, D., Mele, F., Foglierini, M., De Gregorio, C., Cassotta, A., Fernandez, B., Kelderman, S., Schumacher, T.N., Corti, D., et al. (2015). T cell immunity. Functional heterogeneity of human memory CD4^{+} T cell clones primed by pathogens or vaccines. Science *347*, 400–406.

Becker, C., Dornhoff, H., Neufert, C., Fantini, M.C., Wirtz, S., Huebner, S., Nikolaev, A., Lehr, H.A., Murphy, A.J., Valenzuela, D.M., et al. (2006). Cutting edge: il-23 cross-regulates IL-12 production in T cell-dependent experimental colitis. J. Immunol. *177*, 2760–2764.

Belkaid, Y., and Tamoutounour, S. (2016). The influence of skin microorganisms on cutaneous immunity. Nat. Rev. Immunol. *16*, 353–366.

Bond, R., Guillot, J., and Cabañes, F.J. (2010). Malassezia yeasts in animal disease. In Malassezia and the Skin: Science and Clinical Practice, T. Boekhout, P. Mayser, E. Guého-Kellermann, and A. Velegraki, eds. (Springer), pp. 271–299.

Burstein, V.L., Guasconi, L., Beccacece, I., Theumer, M.G., Mena, C., Prinz, I., Cervi, L., Herrero, M., Masih, D.T., and Chiapello, L.S. (2018). IL-17-mediated immunity controls skin infection and T Helper 1 response during experimental Microsporum canis dermatophytosis. J. Invest. Dermatol. *138*, 1744–1753.

Cabañes, F.J. (2014). Malassezia yeasts: how many species infect humans and animals? PLoS Pathog. *10*, e1003892.

Cabanillas, B., and Novak, N. (2016). Atopic dermatitis and filaggrin. Curr. Opin. Immunol. *42*, 1–8.

Cafarchia, C., Gallo, S., Romito, D., Capelli, G., Chermette, R., Guillot, J., and Otranto, D. (2005). Frequency, body distribution, and population size of Malassezia species in healthy dogs and in dogs with localized cutaneous lesions. J. Vet. Diagn. Invest. *17*, 316–322.

Casagrande, B.F., Flückiger, S., Linder, M.T., Johansson, C., Scheynius, A., Crameri, R., and Schmid-Grendelmeier, P. (2006). Sensitization to the yeast Malassezia sympodialis is specific for extrinsic and intrinsic atopic eczema. J. Invest. Dermatol. *126*, 2414–2421.

Cavani, A., Pennino, D., and Eyerich, K. (2012). Th17 and Th22 in skin allergy. Chem. Immunol. Allergy *96*, 39–44.

Chng, K.R., Tay, A.S., Li, C., Ng, A.H., Wang, J., Suri, B.K., Matta, S.A., McGovern, N., Janela, B., Wong, X.F., et al. (2016). Whole metagenome profiling reveals skin microbiome-dependent susceptibility to atopic dermatitis flare. Nat. Microbiol. *1*, 16106.

Ciardo, D.E., Schär, G., Böttger, E.C., Altwegg, M., and Bosshard, P.P. (2006). Internal transcribed spacer sequencing versus biochemical profiling for identification of medically important yeasts. J. Clin. Microbiol. *44*, 77–84.

Conti, H.R., Peterson, A.C., Brane, L., Huppler, A.R., Hernández-Santos, N., Whibley, N., Garg, A.V., Simpson-Abelson, M.R., Gibson, G.A., Mamo, A.J., et al. (2014). Oral-resident natural Th17 cells and γδ T cells control opportunistic Candida albicans infections. J. Exp. Med. *211*, 2075–2084.

Conti, H.R., Shen, F., Nayyar, N., Stocum, E., Sun, J.N., Lindemann, M.J., Ho, A.W., Hai, J.H., Yu, J.J., Jung, J.W., et al. (2009). Th17 cells and IL-17 receptor signaling are essential for mucosal host defense against oral candidiasis. J. Exp. Med. *206*, 299–311.

Cosmi, L., Liotta, F., and Annunziato, F. (2016). Th17 regulating lower airway disease. Curr. Opin. Allergy Clin. Immunol. *16*, 1–6.

Cossarizza, A., Chang, H.D., Radbruch, A., Akdis, M., Andrä, I., Annunziato, F., Bacher, P., Barnaba, V., Battistini, L., Bauer, W.M., et al. (2017). Guidelines for the use of flow cytometry and cell sorting in immunological studies. Eur. J. Immunol. *47*, 1584–1797.

Darabi, K., Hostetler, S.G., Bechtel, M.A., and Zirwas, M. (2009). The role of Malassezia in atopic dermatitis affecting the head and neck of adults. J. Am. Acad. Dermatol. *60*, 125–136.

Esaki, H., Brunner, P.M., Renert-Yuval, Y., Czarnowicki, T., Huynh, T., Tran, G., Lyon, S., Rodriguez, G., Immaneni, S., Johnson, D.B., et al. (2016). Early-onset pediatric atopic dermatitis is TH2 but also TH17 polarized in skin. J. Allergy Clin. Immunol. *138*, 1639–1651.

Findley, K., Oh, J., Yang, J., Conlan, S., Deming, C., Meyer, J.A., Schoenfeld, D., Nomicos, E., Park, M., et al.; NIH Intramural Sequencing Center Comparative Sequencing Program (2013). Topographic diversity of fungal and bacterial communities in human skin. Nature *498*, 367–370.

Flohr, C., and Yeo, L. (2011). Atopic dermatitis and the hygiene hypothesis revisited. Curr. Probl. Dermatol. *41*, 1–34.

Fuertes Marraco, S.A., Grosjean, F., Duval, A., Rosa, M., Lavanchy, C., Ashok, D., Haller, S., Otten, L.A., Steiner, Q.G., Descombes, P., et al. (2012). Novel murine dendritic cell lines: a powerful auxiliary tool for dendritic cell research. Front. Immunol. *3*, 331.

Gemmer, C.M., DeAngelis, Y.M., Theelen, B., Boekhout, T., and Dawson, T.L., Jr. (2002). Fast, noninvasive method for molecular detection and differentiation of Malassezia yeast species on human skin and application of the method to dandruff microbiology. J. Clin. Microbiol. *40*, 3350–3357.

Geoghegan, J.A., Irvine, A.D., and Foster, T.J. (2018). Staphylococcus aureus and atopic dermatitis: a complex and evolving relationship. Trends Microbiol. *26*, 484–497.

Gioti, A., Nystedt, B., Li, W., Xu, J., Andersson, A., Averette, A.F., Münch, K., Wang, X., Kappauf, C., Kingsbury, J.M., et al. (2013). Genomic insights into the atopic eczema-associated skin commensal yeast Malassezia sympodialis. mBio *4*, e00572–12.

Gittler, J.K., Shemer, A., Suárez-Fariñas, M., Fuentes-Duculan, J., Gulewicz, K.J., Wang, C.Q., Mitsui, H., Cardinale, I., de Guzman Strong, C., Krueger, J.G., et al. (2012). Progressive activation of T(H)2/T(H)22 cytokines and selective epidermal proteins characterizes acute and chronic atopic dermatitis. J. Allergy Clin. Immunol. *130*, 1344–1354.

Gladiator, A., Wangler, N., Trautwein-Weidner, K., and LeibundGut-Landmann, S. (2013). Cutting edge: il-17-secreting innate lymphoid cells are essential for host defense against fungal infection. J. Immunol. *190*, 521–525.

Glatz, M., Bosshard, P.P., Hoetzenecker, W., and Schmid-Grendelmeier, P. (2015). The role of Malassezia spp. in atopic dermatitis. J. Clin. Med. *4*, 1217–1228.

Gueho, E., Simmons, R.B., Pruitt, W.R., Meyer, S.A., and Ahearn, D.G. (1987). Association of Malassezia pachydermatis with systemic infections of humans. J. Clin. Microbiol. *25*, 1789–1790.

Guillot, J., and Guého, E. (1995). The diversity of Malassezia yeasts confirmed by rRNA sequence and nuclear DNA comparisons. Antonie Leeuwenhoek *67*, 297–314.

Haas, J.D., Ravens, S., Düber, S., Sandrock, I., Oberdörfer, L., Kashani, E., Chennupati, V., Föhse, L., Naumann, R., Weiss, S., et al. (2012). Development of interleukin-17-producing γδ T cells is restricted to a functional embryonic wave. Immunity *37*, 48–59.

Hawkes, J.E., Chan, T.C., and Krueger, J.G. (2017). Psoriasis pathogenesis and the development of novel targeted immune therapies. J. Allergy Clin. Immunol. *140*, 645–653.

Hernández-Santos, N., Wiesner, D.L., Fites, J.S., McDermott, A.J., Warner, T., Wüthrich, M., and Klein, B.S. (2018). Lung epithelial cells coordinate innate lymphocytes and immunity against pulmonary fungal infection. Cell Host Microbe *23*, 511–522.e5.

Holzmann, S., Tripp, C.H., Schmuth, M., Janke, K., Koch, F., Saeland, S., Stoitzner, P., and Romani, N. (2004). A model system using tape stripping for characterization of Langerhans cell-precursors in vivo. J. Invest. Dermatol. *122*, 1165–1174.

Ianiri, G., Applen Clancey, S., Lee, S.C., and Heitman, J. (2017). FKBP12-dependent inhibition of calcineurin mediates immunosuppressive antifungal drug action in Malassezia. MBio *8*.

Ianiri, G., Averette, A.F., Kingsbury, J.M., Heitman, J., and Idnurm, A. (2016). Gene function analysis in the ubiquitous human commensal and pathogen Malassezia genus. MBio *7*.

Iliev, I.D., and Leonardi, I. (2017). Fungal dysbiosis: immunity and interactions at mucosal barriers. Nat. Rev. Immunol. *17*, 635–646.

Ishikawa, T., Itoh, F., Yoshida, S., Saijo, S., Matsuzawa, T., Gonoi, T., Saito, T., Okawa, Y., Shibata, N., Miyamoto, T., et al. (2013). Identification of distinct ligands for the C-type lectin receptors Mincle and Dectin-2 in the pathogenic fungus Malassezia. Cell Host Microbe *13*, 477–488.

Itohara, S., Mombaerts, P., Lafaille, J., Iacomini, J., Nelson, A., Clarke, A.R., Hooper, M.L., Farr, A., and Tonegawa, S. (1993). T cell receptor delta gene mutant mice: independent generation of alpha beta T cells and programmed rearrangements of gamma delta TCR genes. Cell *72*, 337–348.

Johansson, C., Ahlborg, N., Andersson, A., Lundeberg, L., Karlsson, M.A., Scheynius, A., and Tengvall Linder, M. (2009). Elevated peripheral allergen-

specific T cell response is crucial for a positive atopy patch test reaction. Int. Arch. Allergy Immunol. *150*, 51–58.

Johansson, C., Eshaghi, H., Linder, M.T., Jakobson, E., and Scheynius, A. (2002). Positive atopy patch test reaction to Malassezia furfur in atopic dermatitis correlates with a T helper 2-like peripheral blood mononuclear cells response. J. Invest. Dermatol. *118*, 1044–1051.

Johansson, C., Tengvall Linder, M., Aalberse, R.C., and Scheynius, A. (2004). Elevated levels of IgG and IgG4 to Malassezia allergens in atopic eczema patients with IgE reactivity to Malassezia. Int. Arch. Allergy Immunol. *135*, 93–100.

Kagami, S., Rizzo, H.L., Kurtz, S.E., Miller, L.S., and Blauvelt, A. (2010). IL-23 and IL-17A, but not IL-12 and IL-22, are required for optimal skin host defense against Candida albicans. J. Immunol. *185*, 5453–5462.

Kashem, S.W., Riedl, M.S., Yao, C., Honda, C.N., Vulchanova, L., and Kaplan, D.H. (2015). Nociceptive sensory fibers drive interleukin-23 production from CD301b+ dermal dendritic cells and drive protective cutaneous immunity. Immunity *43*, 515–526.

Kistowska, M., Fenini, G., Jankovic, D., Feldmeyer, L., Kerl, K., Bosshard, P., Contassot, E., and French, L.E. (2014). Malassezia yeasts activate the NLRP3 inflammasome in antigen-presenting cells via Syk-kinase signalling. Exp. Dermatol. *23*, 884–889.

Koga, C., Kabashima, K., Shiraishi, N., Kobayashi, M., and Tokura, Y. (2008). Possible pathogenic role of Th17 cells for atopic dermatitis. J. Invest. Dermatol. *128*, 2625–2630.

Kreymborg, K., Etzensperger, R., Dumoutier, L., Haak, S., Rebollo, A., Buch, T., Heppner, F.L., Renauld, J.C., and Becher, B. (2007). IL-22 is expressed by Th17 cells in an IL-23-dependent fashion, but not required for the development of autoimmune encephalomyelitis. J. Immunol. *179*, 8098–8104.

LeibundGut-Landmann, S., Gross, O., Robinson, M.J., Osorio, F., Slack, E.C., Tsoni, S.V., Schweighoffer, E., Tybulewicz, V., Brown, G.D., Ruland, J., et al. (2007). Syk- and CARD9-dependent coupling of innate immunity to the induction of T helper cells that produce interleukin 17. Nat. Immunol. *8*, 630–638.

Leonardi, S., Cuppari, C., Manti, S., Filippelli, M., Parisi, G.F., Borgia, F., Briuglia, S., Cannavò, P., Salpietro, A., Arrigo, T., et al. (2015). Serum interleukin 17, interleukin 23, and interleukin 10 values in children with atopic eczema/dermatitis syndrome (AEDS): association with clinical severity and phenotype. Allergy Asthma Proc. *36*, 74–81.

Li, H., Goh, B.N., Teh, W.K., Jiang, Z., Goh, J.P.Z., Goh, A., Wu, G., Hoon, S.S., Raida, M., Camattari, A., et al. (2018). Skin commensal Malassezia globosa secreted protease attenuates Staphylococcus aureus biofilm formation. J. Invest. Dermatol. *138*, 1137–1145.

Li, J., Vinh, D.C., Casanova, J.L., and Puel, A. (2017). Inborn errors of immunity underlying fungal diseases in otherwise healthy individuals. Curr. Opin. Microbiol. *40*, 46–57.

Liu, H., Archer, N.K., Dillen, C.A., Wang, Y., Ashbaugh, A.G., Ortines, R.V., Kao, T., Lee, S.K., Cai, S.S., Miller, R.J., et al. (2017). Staphylococcus aureus epicutaneous exposure drives skin inflammation via IL-36-Mediated T cell responses. Cell Host Microbe *22*, 653–666.e5.

Mombaerts, P., Clarke, A.R., Rudnicki, M.A., Iacomini, J., Itohara, S., Lafaille, J.J., Wang, L., Ichikawa, Y., Jaenisch, R., and Hooper, M.L. (1992a). Mutations in T-cell antigen receptor genes alpha and beta block thymocyte development at different stages. Nature *360*, 225–231.

Mombaerts, P., Iacomini, J., Johnson, R.S., Herrup, K., Tonegawa, S., and Papaioannou, V.E. (1992b). RAG-1-deficient mice have no mature B and T lymphocytes. Cell *68*, 869–877.

Moosbrugger-Martinz, V., Schmuth, M., and Dubrac, S. (2017). A mouse model for atopic dermatitis using topical application of vitamin D3 or of its analog MC903. Methods Mol. Biol. *1559*, 91–106.

Nakagawa, S., Matsumoto, M., Katayama, Y., Oguma, R., Wakabayashi, S., Nygaard, T., Saijo, S., Inohara, N., Otto, M., Matsue, H., et al. (2017). Staphylococcus aureus Virulent PSMalpha peptides induce keratinocyte Alarmin release to orchestrate IL-17-dependent skin inflammation. Cell Host Microbe *22*, 667–677.e5.

Odds, F.C., Brown, A.J., and Gow, N.A. (2004). Candida albicans genome sequence: a platform for genomics in the absence of genetics. Genome Biol. *5*, 230.

Picelli, S., Faridani, O.R., Björklund, A.K., Winberg, G., Sagasser, S., and Sandberg, R. (2014). Full-length RNA-seq from single cells using Smart-seq2. Nat. Protoc. *9*, 171–181.

Prohic, A., Jovovic Sadikovic, T., Krupalija-Fazlic, M., and Kuskunovic-Vlahovljak, S. (2016). Malassezia species in healthy skin and in dermatological conditions. Int. J. Dermatol. *55*, 494–504.

Russel, W.M.S., and Burch, R.L. (1959). The Principles of Humane Experimental Technique (Methuen & Co.).

Saijo, S., Ikeda, S., Yamabe, K., Kakuta, S., Ishigame, H., Akitsu, A., Fujikado, N., Kusaka, T., Kubo, S., Chung, S.H., et al. (2010). Dectin-2 recognition of alpha-mannans and induction of Th17 cell differentiation is essential for host defense against Candida albicans. Immunity *32*, 681–691.

Sallusto, F. (2016). Heterogeneity of human CD4(+) T cells against microbes. Annu. Rev. Immunol. *34*, 317–334.

Sandström Falk, M.H., Tengvall Linder, M., Johansson, C., Bartosik, J., Bäck, O., Särnhult, T., Wahlgren, C.F., Scheynius, A., and Faergemann, J. (2005). The prevalence of Malassezia yeasts in patients with atopic dermatitis, seborrhoeic dermatitis and healthy controls. Acta Derm. Venereol. *85*, 17–23.

Saunders, C.W., Scheynius, A., and Heitman, J. (2012). Malassezia fungi are specialized to live on skin and associated with dandruff, eczema, and other skin diseases. PLoS Pathog. *8*, e1002701.

Sokol, H., Leducq, V., Aschard, H., Pham, H.P., Jegou, S., Landman, C., Cohen, D., Liguori, G., Bourrier, A., Nion-Larmurier, I., et al. (2017). Fungal microbiota dysbiosis in IBD. Gut *66*, 1039–1048.

Sparber, F., Dolowschiak, T., Mertens, S., Lauener, L., Clausen, B.E., Joller, N., Stoitzner, P., Tussiwand, R., and LeibundGut-Landmann, S. (2018). Langerin+ DCs regulate innate IL-17 production in the oral mucosa during Candida albicans-mediated infection. PLoS Pathog. *14*, e1007069.

Sparber, F., and LeibundGut-Landmann, S. (2017). Host responses to Malassezia spp. in the mammalian skin. Front. Immunol. *8*, 1614.

Sugita, T., Boekhout, T., Velegraki, A., Guillot, J., Hadina, S., and Cabanes, F.J. (2010). Epidemiology of Malassezia-related skin diseases. In Malassezia and the Skin, T. Boekhout, E. Guého, P. Mayser, and A. Velegraki, eds. (Springer-Verlag), pp. 65–119.

Swidergall, M., and Ernst, J.F. (2014). Interplay between Candida albicans and the antimicrobial peptide armory. Eukaryot. Cell *13*, 950–957.

Taylor, P.R., Leal, S.M., Jr., Sun, Y., and Pearlman, E. (2014). Aspergillus and Fusarium corneal infections are regulated by Th17 cells and IL-17-producing neutrophils. J. Immunol. *192*, 3319–3327.

Taylor, P.R., Tsoni, S.V., Willment, J.A., Dennehy, K.M., Rosas, M., Findon, H., Haynes, K., Steele, C., Botto, M., Gordon, S., et al. (2007). Dectin-1 is required for beta-glucan recognition and control of fungal infection. Nat. Immunol. *8*, 31–38.

Valli, J.L., Williamson, A., Sharif, S., Rice, J., and Shewen, P.E. (2010). In vitro cytokine responses of peripheral blood mononuclear cells from healthy dogs to distemper virus, Malassezia and Toxocara. Vet. Immunol. Immunopathol. *134*, 218–229.

Velegraki, A., Cafarchia, C., Gaitanis, G., Iatta, R., and Boekhout, T. (2015). Malassezia infections in humans and animals: pathophysiology, detection, and treatment. PLoS Pathog. *11*, e1004523.

Weidinger, S., and Novak, N. (2016). Atopic dermatitis. Lancet *387*, 1109–1122.

Wells, C.A., Salvage-Jones, J.A., Li, X., Hitchens, K., Butcher, S., Murray, R.Z., Beckhouse, A.G., Lo, Y.L., Manzanero, S., Cobbold, C., et al. (2008). The macrophage-inducible C-type lectin, mincle, is an essential component of the innate immune response to Candida albicans. J. Immunol. *180*, 7404–7413.

Williams, M.R., and Gallo, R.L. (2015). The role of the skin microbiome in atopic dermatitis. Curr. Allergy Asthma Rep. *15*, 65.

Wu, G., Zhao, H., Li, C., Rajapakse, M.P., Wong, W.C., Xu, J., Saunders, C.W., Reeder, N.L., Reilman, R.A., Scheynius, A., et al. (2015). Genus-wide

comparative genomics of Malassezia delineates its phylogeny, physiology, and niche adaptation on human skin. PLoS Genet. *11*, e1005614.

Wüthrich, M., Gern, B., Hung, C.Y., Ersland, K., Rocco, N., Pick-Jacobs, J., Galles, K., Filutowicz, H., Warner, T., Evans, M., et al. (2011). Vaccine-induced protection against 3 systemic mycoses endemic to North America requires Th17 cells in mice. J. Clin. Invest. *121*, 554–568.

Yamasaki, S., Matsumoto, M., Takeuchi, O., Matsuzawa, T., Ishikawa, E., Sakuma, M., Tateno, H., Uno, J., Hirabayashi, J., Mikami, Y., et al. (2009). C-type lectin Mincle is an activating receptor for pathogenic fungus, Malassezia. Proc. Natl. Acad. Sci. U S A *106*, 1897–1902.

Zhu, Y., Engström, P.G., Tellgren-Roth, C., Baudo, C.D., Kennell, J.C., Sun, S., Billmyre, R.B., Schröder, M.S., Andersson, A., Holm, T., et al. (2017). Proteogenomics produces comprehensive and highly accurate protein-coding gene annotation in a complete genome assembly of Malassezia sympodialis. Nucleic Acids Res. *45*, 2629–2643.

STAR★METHODS

KEY RESOURCES TABLE

REAGENT or RESOURCE	SOURCE	IDENTIFIER
Antibodies		
Alexa Fluor 700 Anti-mCD45.2 (104)	Biolegend	Cat# 109821, RRID: AB_493730
PeCy7 Anti-mCD11b (M1/70)	Thermo Fisher	Cat# 25-0112-81, RRID: AB_469587
APC Anti-mCD11c (N418)	Biolegend	Cat# 117309, RRID: AB_313778
Pacific Blue Anti-mMHCII (M5/114.15.2)	Biolegend	Cat# 107619, RRID: AB_493528
BV510 Anti-mLy6C (HK1.4)	Biolegend	Cat# 128033, RRID: AB_2562351
FITC Anti-mLy6G (1A8)	Biolegend	Cat# 127605, RRID: AB_1236488
PE Anti-mSiglecF (E50-2440)	BD Bioscience	Cat# 552126, RRID: AB_394341
FITC Anti-mCD3 (145-2C11)	Biolegend	Cat# 100305, RRID: AB_312670
Pacific Blue Anti-mCD4 (RM4-5)	Biolegend	Cat# 100534, RRID: AB_493375
PeCy7 Anti-mIL-17A (TC11-18H10.1)	Biolegend	Cat# 506921, RRID: AB_2125011
APC Anti-mIFNγ (XMG1.2)	Biolegend	Cat# 505809, RRID: AB_315403
eFluor 610 Anti-mIL-13 (eBio13A)	Thermo Fisher	Cat# 61-7133-82, RRID: AB_2574654
Alexa Fluor 488 Anti-mKi67 (16A8)	Biolegend	Cat# 652417, RRID: AB_256423
Alexa Fluor 488 Anti-mCD11b (M1/70)	Biolegend	Cat# 101219, RRID: AB_493545
BV570 Anti-mCD90 (30-H12)	Biolegend	Cat# 105329, RRID: AB_10917055
PeCy7 Anti-mTCRγδ (GL3)	Biolegend	Cat# 118123, RRID: AB_11203530
APC Anti-mTCRβ (H57-597)	Biolegend	Cat# 109211, RRID: AB_313434
Alexa fluor 647 Anti-mLangerin (929F3.01)	Dendritics	Cat# DDX0362A647-100, RRID: AB_1148741
Qdot 655 Anti-hCD45RA (MEM-56)	Thermo Fisher	Cat# Q10069, RRID: AB_2556451
PE Texas Red Anti-hCD4 (S3.5)	Thermo Fisher	Cat# MHCD0417, RRID: AB_10371766
PECy5 Anti-hCD8 (B9.11)	Beckman Coulter	Cat# A07758, RRID: AB_2713928
PECy5 Anti-hCD14 (RMO52)	Beckman Coulter	Cat# A07765, RRID: AB_2621824
PECy5 Anti-hCD16 (3G8)	Beckman Coulter	Cat# A07767
PECy5 Anti-hCD19 (J3-119)	Beckman Coulter	Cat# A07771
PECy5 Anti-hCD25 (B1.49.9)	Beckman Coulter	Cat# IM2646, RRID: AB_131142
PECy5 Anti-hCD56 (N901)	Beckman Coulter	Cat# A07789, RRID: AB_1575976
PE Anti-hCCR6 (11A9)	BD Bioscience	Cat# 561019, RRID: AB_10565962
BV421 Anti-hCCR7 (G043H7)	Biolegend	Cat# 353207, RRID: AB_10915137
Pacific Blue Anti-hICOS (C398.4A)	Biolegend	Cat# 313521, RRID: AB_10895762
BV785 Anti-hCD25 (BC96)	Biolegend	Cat# 302637, RRID: AB_11219197
PECy7 Anti-hIL-10 (JES3-9D7)	Biolegend	Cat# 501419, RRID: AB_2280292
PE Anti-hIL-9 (MH9A4)	Biolegend	Cat# 507604, RRID: AB_315486
BV650 Anti-hIFN-γ (4S.B3)	Biolegend	Cat# 502537, RRID: AB_11126140
BV605 Anti-hIL-17A (BL168)	Biolegend	Cat# 512325, RRID: AB_11218595
APC Anti-hIL-4 (MP4-25D2)	BD Bioscience	Cat# 554486, RRID: AB_398562
Percp-eFluor 710 Anti-hIL-22 (22URTI)	Thermo Fisher	Cat# 46-7229-42, RRID: AB_10596639
hCD4 magnetic microbeads	Milteny	Cat# 130-045-101
hCD14 magnetic microbeads	Milteny	Cat# 130-050-201
Biological Samples		
Human peripheral blood samples from healthy donors	Department of Dermatology, University Hospital Zurich	N/A
Human peripheral blood samples from atopic patients	Department of Dermatology, University Hospital Zurich	N/A
Human Serum (5%)	Swiss Red Cross	N/A

(*Continued on next page*)

Continued

REAGENT or RESOURCE	SOURCE	IDENTIFIER
Fetal Calve Serum	Bioconcept	Cat# 2-01F10-I
Chemicals, Peptides, and Recombinant Proteins		
Phosphate Buffered Salt Solutions (PBS, 1x)	Amimed/Bioconcept	Cat# 3-05F39
RPMI 1640	Life Technologies	Cat# 21875034
2-Mercaptoethanol	Life Technologies	Cat# 31350-010
EDTA (0.5M, pH 8)	Life Technologies	Cat# AM9260G
Hanks Buffered Salt Solution (HBSS, 1x)	Life Technologies	Cat# 14175-053
Brefeldin A	Sigma-Aldrich	Cat# B6542-25MG
DNAse I	Sigma-Aldrich	Cat# DN25-100MG
Collagenase I	Life Technologies	Cat# 17100017
Liberase TM	Roche	Cat# 05401119001
TRI Reagent	Sigma-Aldrich	Cat# T9424-100ML
SYBR Green	Roche	Cat# 04913914001
Revert Aid Transcriptase	Thermo Fisher	Cat# EP0451
SuperScript II Reverse Transcriptase Kit	Thermo Fisher	Cat# 18064014
LIVE/DEAD Near IR Dead cell Stain Kit	Thermo Fisher	Cat# L10119
LIVE/DEAD Aqua Dead Cell Stain Kit	Thermo Fisher	Cat# L34957
BD Cytofix/Cytoperm reagent	BD Bioscience	Cat# 554714
Paraformaldehyde	Sigma-Aldrich	Cat# P6148-500G
Ficoll-Plaque PLUS	GE Healthcare	Cat# 17144002
L-Glutamine	Thermo Fisher	Cat# X0550-100
Penicillin/Streptomycin	Amimed/Bioconcept	Cat# 4-01F00-H
Phorbol 12-myristate 13-acetate (PMA)	Sigma-Aldrich	Cat# P8139
Ionomycin	Sigma-Aldrich	Cat# I0634-1MG
O.C.T. compound	Tissue-TEK	Cat# 4583
Methanol	Merck	Cat# 1.06009.2500
Nonidet P40	Axonlab	Cat# A1694,0250
Malt extract	Sigma-Aldrich	Cat# 70167-500G
Glycerol (99%)	Honeywell	Cat# 10314830
Ox-bile	Sigma-Aldrich	Cat# 70168-100G
Tween-40	Sigma-Aldrich	Cat# P1504-100ML
Peptone	Oxoid	Cat# LP0037
Oleic Acid	Sigma-Aldrich	Cat#75090-5ML
Native Olive Oil	Commerc. available	N/A
Agar	Sigma-Aldrich	Cat# A1296-1KG
Ketasol	Graeub AG	Lot# 6680416
Rompun (2%)	Bayer	Lot# KP0BFHR
Calcofluor White	Sigma-Aldrich	Cat# 18909-100ML-F
Deposited Data		
Raw and analyzed data	This paper	Zenodo: https://doi.org/10.5281/zenodo.2577503
Experimental Models: Cell Lines		
MutuDC1940 cells	Hans Acha-Orbea, University of Lausanne (Fuertes Marraco et al., 2012)	N/A
Experimental Models: Organisms/Strains		
Mouse: WT: C57BL/6JRj	Janvier Elevage	C57BL/6JRj
Mouse: *Rag1*$^{-/-}$: B6.129S7-Rag1^{tm1Mom}/J	Swiss Immunological Mouse Repository (SwImMR) hosted by the University of Zurich, (Mombaerts et al., 1992b)	MGI: 1857241

(*Continued on next page*)

Continued

REAGENT or RESOURCE	SOURCE	IDENTIFIER
Mouse: *TCRd*$^{-/-}$: B6;129P2- TCRd^{tm1Mom}	Burkhard Becher, University of Zurich, (Itohara et al., 1993)	MGI: 1857257
Mouse: *TCRbd*$^{-/-}$: B6;129P2-TCRb^{tm1Mom} x TCRd^{tm1Mom}	Swiss Immunological Mouse Repository (SwImMR) hosted by the University of Zurich, (Itohara et al., 1993; Mombaerts et al., 1992a)	MGI: 1857256, MGI: 1857257
Mouse: *Il23a*$^{-/-}$: B6.129-IL23^{tm1Gdy}	Burkhard Becher, University of Zurich, (Becker et al., 2006)	MGI: 3625894
Mouse: *Il17af*$^{-/-}$: C57BL/6.Il17a/Il17f$^{tm1.1Impr}$	Hannover Medical School (Haas et al., 2012)	MGI: 5438791, MGI: 5438793
Mouse: *Il22*$^{-/-}$: C57BL/6.Il22^{tm1Jcrd}	Burkard Becher, University of Zurich, (Kreymborg et al., 2007)	MGI: 4453827
Mouse: *Clec4e*$^{-/-}$: C57BL/6.Clec4e$^{tm1.1Cfg}$	David Sancho (CNIC), (Wells et al., 2008)	MGI: 5052164
Mouse: *Clec4n*$^{-/-}$: C57BL/6.Clec4n^{tm1Yiw}	Benjamin Marsland, University of Lausanne, (Saijo et al., 2010)	MGI: 4459637
Mouse: *Clec7a*$^{-/-}$: C57BL/6.Clec7a^{tmGdb}	Benjamin Marsland, University of Lausanne, (Taylor et al., 2007)	MGI: 3695710
Mouse: *Myd88*$^{-/-}$: C57BL/6.Myd88^{tm1Ak}	Swiss Immunological Mouse Repository (SwImMR) hosted by the University of Zurich, (Adachi et al., 1998)	MGI: 2385681
Mouse: *Card9*$^{-/-}$: C57BL/6-Card9^{em1ThBu}	Thorsten Buch University of Zurich (unpublished data)	N/A
M. pachydermatis: strain ATCC 14522	ATCC (Guillot and Guého, 1995)	ATCC 14522, CBS 1879
M. sympodialis: strain ATCC 42132	Joseph Heitman, Duke University (Gueho et al., 1987)	ATCC 42132, M1154/77
M. furfur: strain JPLK23	Joseph Heitman, Duke University (Guillot and Guého, 1995)	JPLK23
M. sympodialis: clinical isolate	this report	N/A
M. slooffiae: clinical isolate	this report	N/A
C. albicans: strain SC5314	(Odds et al., 2004)	SC5314
Oligonucleotides		
See Table S1		N/A
Software and Algorithms		
GraphPad Prism V6	GraphPad	www.graphpad.com
NDP.view2.	Hamamatsu	U12388-01, www.hamamatsu.com
FlowJo V10	FlowJo LLC	www.flowjo.com
Other		
Gallios Flow Cytometer	Beckman Coulter	www.beckmancoulter.com
FACS Aria III	BD Bioscience	www.bdbiosciences.com
FlexMAP 3D	Luminex	www.luminexcorp.com
NanoZoomer 2.0-HT	Hamamatsu	www.hamamatsu.com
Transpore Hypoallergic Tape	3M	Cat# 1527-1
Oditest 0-5mm measurement device	KROEPLIN	Cat# S0247
BD Calibrite Beads	BD Bioscience	Cat# 349502

CONTACT FOR REAGENT AND RESOURCE SHARING

Further information and requests for resources and reagents should be directed to and will be fulfilled by the Lead Contact, Salomé LeibundGut-Landmann (salome.leibundgut-landmann@uzh.ch). *Il17af*$^{-/-}$ (Hannover Medical School), *Il22*$^{-/}$ (Ludwig Cancer Research Brussels), *Clec4n*$^{-/-}$ (The Tokyo University of Science) and *Clec4e*$^{-/-}$ (The University of Melbourne) mice as well as the DC^{1940} cell line (University of Lausanne) were obtained via an MTA between the University of Zurich and the respective entities.

EXPERIMENTAL MODEL AND SUBJECT DETAILS

Ethic Statement

All mouse experiments in this study were conducted in strict accordance with the guidelines of the Swiss Animals Protection Law and were performed under the protocols approved by the Veterinary office of the Canton Zurich, Switzerland (license number 183/2015). All efforts were made to minimize suffering and ensure the highest ethical and humane standards according to the 3R principles (Russel and Burch, 1959). Samples from humans comprised blood samples and skin swabs. Those samples were collected from volunteers after informed consent. Sampling of humans was approved by the ethics committee of the Canton Zurich (ID 2016-00301).

Animals

WT C57BL/6j mice were purchased by Janvier Elevage. *Rag1*$^{-/-}$ (Mombaerts et al., 1992b), *TCRd*$^{-/-}$ (Itohara et al., 1993), *TCRbd*$^{-/-}$ (Itohara et al., 1993; Mombaerts et al., 1992a), *Il23a*$^{-/-}$ (Becker et al., 2006), *Il17af*$^{-/-}$ (Haas et al., 2012), *Il22*$^{-/-}$ (Kreymborg et al., 2007), *Clec4e*$^{-/-}$ ((Wells et al., 2008), kindly obtained from David Sancho), *Card9*$^{-/-}$ (Ferreira and Buch, unpublished data) and *Myd88*$^{-/-}$ (Adachi et al., 1998) mice were maintained and bred at the Institute of Laboratory Animals Science (LASC - University of Zurich, Zurich, Switzerland). *Clec4n*$^{-/-}$ (Saijo et al., 2010) *and Clec7a*$^{-/-}$ (Taylor et al., 2007) were kindly obtained from Benjamin Marsland (University of Lausanne, Switzerland). All mice were on the C57BL/6 background. The animals were kept in specific pathogen-free conditions and used at 6-12 weeks of age in sex- and age-matched groups. Female as well as male mice were used for experiments. Vehicle-treated and infected animals were kept separately to avoid cross-contamination. No *Malassezia* was detected by culture or PCR in our colony of mice under SPF conditions prior to infection.

Fungal Strains

The *M. pachydermatis* strain ATCC 14522 (= CBS 1879, (Guillot and Guého, 1995)) was purchased from ATCC. *M. sympodialis* strain ATCC 42132 (Gueho et al., 1987) and *M. furfur* strain JPLK23 (=CBS 14141, (Guillot and Guého, 1995)) were obtained from Joseph Heitman (Duke University, Durham). *M. sympodialis* and *M. slooffiae* clinical isolates for re-stimulation of human T cells were collected from AD patients at the Department of Dermatology, University Hospital Zurich, Switzerland and identified by ITS sequencing (Ciardo et al., 2006).

Experimental Model

For infection experiments with mice, *Malassezia* spp. were grown for 3-4 days at 30°C, 180 rpm in liquid modified Dixon medium (for 500 ml liquid medium: 18 g Malt Extract (Sigma Aldrich), 10 g desiccated Ox-bile (Sigma Aldrich), 5 ml Tween-40 (Sigma Aldrich), 3 g Peptone (Oxoid), 1 ml Glycerol (Honeywell), 1 ml Oleic Acid (Sigma Aldrich)). Cells were washed in PBS and suspended in olive oil (native olive oil extra, SPAR) at a density of 20 OD_{A600}/ml. 100 µl suspension (corresponding to 2 OD_{A600}) of yeast cells was applied topically onto the dorsal ear skin while mice were anaesthetized. In some experiments, the dorsal ear skin was disrupted by mild tape stripping (Transpore™ Hypoallergenic, 3M; 5 rounds per ear). Ear thickness was monitored prior and after infection using the Oditest S0247 0-5 mm measurement device (KROEPLIN). For determination of fungal loads in the skin, tissue was transferred in aqua dest. supplemented with 0.05 % Nonidet P40 (AxonLab), homogenized and plated on modified Dixon agar and incubated at 30°C for 3-4 days.

Atopic Patients and Healthy Controls

Blood from adult healthy (non-atopic) donors (3F, 2M; age 27y - 54y) and adult atopic individuals (4F, 2M; age 23y - 50y) was obtained at the Department of Dermatology of the University Hospital of Zurich. The female-male distribution was random as gender does not play a role in AD. All samples were anonymized. Healthy (non-atopic) status of individuals was defined as personal and family history without atopic diseases, such as allergic rhinitis, asthma or AD; and a negative skin prick test with 20 seasonal and perennial inhalant allergens. Atopy in individuals was defined as a positive personal history of atopic diseases and a skin prick test positive for at least one of the tested inhalant allergens.

METHOD DETAILS

Isolation of Skin and Lymph Node Cells

For digestion of total ear skin, ears were removed, cut into small pieces and transferred into Hank's medium (Ca^{2+}- and Mg^{2+}-free, Life Technology), supplemented with Liberase TM (0.15 mg/ml, Roche) and DNase I (0.12 mg/ml, Sigmar-Aldrich) and incubated for 1 hour at 37 °C. The cell suspension was filtered through a 40 µm cell strainer (Falcon) and rinsed with PBS supplemented with 5 mM ETDA (Life Technologies) and 1% FCS. Auricular lymph nodes were manually shredded using fine scissors and digested with DNAse I (2.4mg/ml Sigma-Aldrich) and Collagenase I (2.4mg/ml, Roche) in PBS for 20 min at 37°C. The cell suspension was filtered through a 40 µm cell strainer (Falcon) and rinsed with PBS supplemented with 5 mM ETDA (Life Technologies) and 1 % FCS.

Ex Vivo Murine T Cell Stimulation, Surface and Intracellular Staining

For *in vitro* stimulation of T cells, 1x10^6 auricular lymph node cells were co-cultured for 6 hours with 1 x 10^5 MutuDC1940 cells (Fuertes Marraco et al., 2012), pulsed with 2.5x10^5/ml heat-killed *Malassezia* spp. Unpulsed MutuDC1940 cells served as negative

control. Brefeldin A (10 μg/ml, Sigma-Aldrich) was added for the last 5 hours. After stimulation cells were surface stained, fixed and permeabilized with Cytofix/Cytoperm (BD Biosciences) and then stained for cytokine expression using the antibodies listed in the Key Resources Table.

Flow Cytometry and Cell Sorting

Single cell suspensions of skin and lymph nodes were stained in PBS supplemented with 1% FSC, 5mM EDTA and 0.02% NaN_3. LIVE/DEAD Near IR stain (Life Technologies) was used for exclusion of dead cells. The antibodies for surface and intracellular cytokine staining are listed in the Key Resources Table. For intracellular cytokine staining, cells were fixed and permeabilized using BD Cytofix/Cytoperm reagent (BD Bioscience) and subsequently incubated in Perm/Wash buffer (BD Bioscience). All extracellular and intracellular staining steps were carried out on ice. Cells were acquired on a FACS Gallios (Beckman Coulter) and the data were analyzed with FlowJo software (FlowJo LLC). The gating of the flow cytometric data was performed according to the guidelines for the use of flow cytometry and cell sorting in immunological studies (Cossarizza et al., 2017), including pre-gating on viable and single cells for analysis. Absolute cell numbers of myeloid and lymphoid cell populations were calculated based on a defined number of counting beads (BD Bioscience, Calibrite Beads), which were added to the samples before flow cytometric acquisition.

For sorting, single cell suspensions of ear skin were stained in PBS supplemented with 1% FSC and 5mM EDTA with antibodies listed in the Key Resources Table. Using a FACS Aria III, 50 target cells per cell population were sorted in individual wells of a 96-well plate (Eppendorf) containing RLT Plus RNeasy® lysis buffer (Qiagen). Lysates were snap-frozen and stored at -80°C until further processing.

RNA Isolation and Quantitative RT-PCR

Isolation of total RNA from ear skin was carried out according to standard protocols using TRI Reagent® (Sigma Aldrich). cDNA was generated by RevertAid reverse transcriptase (Thermo Fisher). For RNA isolation from sorted cells, the Smart-Seq2 protocol was applied as described (Picelli et al., 2014). Briefly, Agencourt RNAClean XP paramagnetic beads (Beckman Coulter) in combination with a DynaMag-96 side skirted magnet (Thermo Fisher) were applied to purify whole-genome RNA. Subsequently cDNA was generated using the SuperScript II Reverse Transcriptase Kit (Thermo Fisher), and further amplified with HiFi HotStart PCR Mix (KAPA Biosystems). For DNA clean-up, Agencourt AMPure XP beads (Beckman Coulter) were used as above. Quantitative PCR was performed using SYBR Green (Roche) and a QuantStudio 7 Flex (Life Technologies) instrument. The primers used for qPCR are listed in Table S1. All qRT-PCR assays were performed in duplicate and the relative expression (rel. expr.) of each gene was determined after normalization to β-actin transcript levels.

Histochemistry and Immunofluorescence

For histology, tissue was fixed in 4% PBS-buffered paraformaldehyde overnight and embedded in paraffin. Sagittal sections (9μm) were stained with Periodic-acidic Schiff (PAS) reagent and counterstained with Haematoxilin or with Haematoxylin-Eosin (H&E) and mounted with Pertex (Biosystem, Switzerland) according to standard protocols. For immunofluorescence staining, tissues were embedded in Tissue-TEK O.C.T compound (VWR International GmbH, Switzerland), snap frozen in liquid nitrogen and stored at -20°C. Sagittal cryo-sections (9 μm) were cut and mounted to super frost glass slides (Thermo Scientific). The specimen was allowed to dry at room temperature and were fixed either with methanol at -20°C for 20 minutes or with acetone a room temperature for 10 minutes. The following antibodies were used: anti-CD11b (M1/70, Biolegend) and anti-Ki67 (16A8, Biolegend). Alternatively, the specimen was stained with Calcofluor white (CFW, Sigmar Aldrich) diluted in Tris-HCl (0.1 M pH 9, 10 μg/ml final concentration) for 20 min on RT. The stained specimens were washed with aqua dest. and mounted with Mowiol and stored at 4°C. All images were acquired with a digital slide scanner (NanoZoomer 2.0-HT, Hamamatsu) and analyzed with NDP.view2.

Human Cell Sorting

Blood from healthy donors and atopic individuals was obtained from the Allergy Unit of the Department of Dermatology of the University Hospital of Zurich. Peripheral blood mononuclear cells (PBMCs) were isolated by Ficoll-Paque Plus (GE Healthcare) density gradient. Total $CD4^+$ T cells and monocytes were isolated by positive selection using CD4 and CD14 magnetic microbeads (Miltenyi Biotech), respectively. Memory $CD4^+CCR6^+$ and $CD4^+CCR6^-$ T cell subsets were sorted after exclusion of naïve T cells ($CD45RA^+CCR7^+$) and of $CD8^+CD14^+CD16^+CD19^+CD25^+CD56^+$ cells. The monoclonal antibodies used for FACS are listed in the Key Resources Table. Cells were sorted with FACSAria III (BD Biosciences).

Ex Vivo Human T Cell Stimulation, Surface and Intracellular Staining

For human T cell re-stimulation experiments, *Malassezia* spp. were grown in liquid modified Dixon medium as described above. *C. albicans* strain SC5314 (Odds et al., 2004) was grown in YNB-S medium for 18 hours at 30°C, 180 rpm starting at a density of OD_{600} = 0.1. The yeast cells were washed in PBS and heat-inactivated at 65°C for 30 minutes. The medium used for co-culture was RPMI 1640 supplemented with 2 mM glutamine, 1% non-essential amino acids, 1% sodium pyruvate, 1% penicillin/streptomycin (all from Life Technologies) and 5% of human serum (Swiss Red Cross). Sorted T cells were labeled with carboxyfluorescein succinimidyl ester (CFSE) and cultured at a ratio of 2:1 with irradiated autologous monocytes pre-pulsed for 3-5 hours with heat killed *M. furfur*, *M. sympodialis* or *M. slooffiae* that are frequently isolated from our cohort of AD patients. As control, some cultures were stimulated with heat-killed *C. albicans*. The ratio used for the human T cell *ex vivo* stimulation assay was 3 yeast particles per

monocyte. At day 5 culture supernatants were collected and cytokines (IFN-γ, IL-4, IL-5, IL-10, IL-17A and IL-22) were measured by cytometric bead arrays on FlexMAP 3D (Luminex). To measure proliferation and cytokine production and the single cell level, cultured cells were directly analyzed by FACS or stimulated with Phorbol 12-myristate 13-acetate (PMA) and Ionomycin (both from Sigma-Aldrich) for 5 hours with addition of Brefeldin A (Sigma-Aldrich) for the last 2.5 hours of stimulation. After stimulation, cells were surface stained, fixed and permeabilized with Cytofix/Cytoperm (BD Biosciences) and then stained for cytokine expression using the antibodies listed in the Key Resources Table.

QUANTIFICATION AND STATISTICAL ANALYSIS

For quantification of skin cell populations by flow cytometry, cell numbers were transformed using the formula Y = y(log10) or Y = y(log10 + 1) in case of lymphocyte enumeration. Bars of each data set indicate the arithmetic mean. For cfu data plotted on a logarithmic scale, the geomean and 95% confidence intervals are shown. RT-qPCR data were log-transformed and the mean of each group is indicated. In summary plots showing cfu data, quantification of flow cytometry data analysis and RT-qPCR data, each symbol represents an individual mouse. Ear thickness is shown as mean +/- SEM. Data are pooled from at least 2 independent experiments or are representative of at least 2 independent experiments with 3 to 5 animals per group. For human data, graphs show pooled data from all samples included in this study and analyzed on separate days. The mean + SEM of each group is indicated. The study design did not include randomization or blinding. Statistical significance was determined by unpaired Student's-test with Welch correction for multiple comparison, one-way or two-way ANOVA with Tukey's multiple comparison test as appropriate using GraphPad Prism software. Outlier calculation for mouse data was performed with the Grubbs' method. Significance is indicated as follows: $^{*/\#}$ $p< 0.05$; $^{**/\#\#}$ $p<0.01$; $^{***/\#\#\#}$ $p<0.001$; $^{****/\#\#\#\#}$ $p<0.0001$.

DATA AND SOFTWARE AVAILABILITY

All raw and analyzed data have been deposited in Zenodo under https://doi.org/10.5281/zenodo.2577503.

Cell Host & Microbe, Volume *25*

Supplemental Information

The Skin Commensal Yeast *Malassezia* Triggers a Type 17 Response that Coordinates Anti-fungal Immunity and Exacerbates Skin Inflammation

Florian Sparber, Corinne De Gregorio, Simone Steckholzer, Filipa M. Ferreira, Tamas Dolowschiak, Fiorella Ruchti, Florian R. Kirchner, Sarah Mertens, Immo Prinz, Nicole Joller, Thorsten Buch, Martin Glatz, Federica Sallusto, and Salomé LeibundGut-Landmann

SUPPLEMENTAL FIGURES AND TABLES

Figure S1 (related to Figure 1): Kinetics of *Malassezia* colonization after experimental skin infection. Fungal burden in the ear skin of *Malassezia* spp.-infected and vehicle-treated WT mice on day 2, 4, 7 and 12 post infection. The skin was tape-stripped prior to the infection. Each dot represents one animal. Graphs show pooled data from two independent experiments. The same vehicle-treated animals were used as control for *M. sympodialis*- and *M. furfur*-infected mice for each time point. The geomean and 95% confidence interval of each group is indicated. D.L., detection limit. Statistics were calculated using unpaired Student's T-Test.*p<0.05, **p<0.01, *** p<0.001, **** p<0.0001.

Figure S2 (related to Figure 2): Early recruitment of inflammatory leukocytes upon *Malassezia* infection is independent of skin barrier disruption. Myeloid cell populations in the ear skin were quantified by flow cytometry on day 2 post infection. Total leukocytes, neutrophils, monocytes, eosinophils and dendritic cells/macrophages were defined as shown in Figure 2. Summary graphs show the percentage of cell subsets on overall leukocytes and absolute numbers of cells per ½ ear for all myeloid cell populations. (**A**) WT mice were infected with *M. pachydermatis* or vehicle-treated without tape-stripping prior to infection. (**B**) WT mice were infected with *M. sympodialis* or *M. furfur,* or vehicle-treated as indicated. The ear skin was or was not tape-stripped before infection, as indicated**.** Each symbol represents one animal. Graphs show pooled data from two independent experiments. The mean of each group is indicated. Statistics were calculated using one-way ANOVA or unpaired Student's t-Test, as appropriate. *p<0.05, **p<0.01, ***p<0.001, ****p<0.0001.

Figure S3 (related to Figure 3): *Malassezia* spp. exposure of the skin results in a selective activation of the IL-17 pathway. A. WT mice were infected with *M. pachydermatis* (*M.p.*) or vehicle-treated (V) after mild tape stripping of the dorsal ear skin. Expression of *Ifng*, *Il5*, *Il13* and *Tslp* transcripts were analyzed in

the ear skin by RT-qPCR on day 2 post infection. **B.** WT mice were infected with *M. pachydermatis, M. sympodialis or M. furfur as indicated* without tape stripping prior to infection. Expression of *Il17a*, *Ifng* and *Tslp* transcripts was assessed by RT-qPCR analysis of the ear skin on day 2 post infection. **C-D.** WT mice were infected with *M. pachydermatis* or vehicle-treated after mild tape stripping of the dorsal ear skin. $CD45^+$ $CD90^+$ $CD11b^-$ lymphoid cell populations in the ear skin of infected and vehicle-treated WT mice were quantified by flow cytometry on day 2 post infection. $TCR\beta^+$ αβ T cells, $TCR\gamma\delta^{int}$ dermal γδ T cells, $TCR\gamma\delta^{hi}$ epidermal γδ T cells (DETCs) and TCR^- innate lymphoid cells (ILCs) were defined as indicated. Representative FACS plot with gating strategy (**C**) and summary graph with absolute numbers for each cell subset (**D**) are shown. (**E-F**) *Il17a*^{Cre}*R26R*^{eyfp} reporter mice were infected with *M. pachydermatis* or vehicle-treated after mild tape stripping of the dorsal ear skin. Expression of eYFP in lymphocyte subsets in the ear skin was analyzed by flow cytometry. Of note, the analysis was carried out on day 5 post infection due to delayed Cre-mediated eYFP expression. Representative FACS plots with gating strategy (**E**) and summary graphs with absolute numbers of $CD90^+$ and $CD90^+eYFP^+$ cells for each cell subset (**F**) are shown. Numbers in **C** and **E** indicate the % of cells in each gate. In **A**, **B**, **D** and **F**, each symbol represents one animal. Graphs show pooled data from two to three independent experiments. The mean of each group is indicated. The same vehicle-treated controls were used in **B** for the experiments with *M. sympodialis* and *M. furfur*. Statistics were calculated using unpaired Student's t-Test or one-way ANOVA as appropriate. *p<0.05, *p<0.01, ***p<0.001, ****p<0.0001.

Figure S4 (related to Figure 3): **Gating strategy of myeloid and lymphoid cell subsets in the *Malassezia*-exposed skin.** WT mice were infected with *M. pachydermatis* or vehicle-treated after mild tape stripping of the dorsal ear skin. (**A**) Myeloid and lymphoid cell populations were isolated by FACS-sorting as indicated on day 2 post infection. (**B**) Langerin expression was assessed in the indicated myeloid cell

subsets on day 2 post infection. Numbers in the contour plots indicate the % of cells in each gate, numbers in the histogram plots indicated median fluorescence intensity (MFI) for Langerin.

Figure S5 (related to Figure 3 and Figure 6): Induction of adaptive type-17 immunity in the draining LN upon *Malassezia* spp. infection is independent of skin barrier disruption. Auricular lymph node cells were analyzed on day 12 post infection for the production of Th17 (IL-17A), Th1 (INF-γ) and Th2 (IL-13) signature cytokines by intracellular staining and flow cytometry, after re-stimulated with dendritic cells that were pulsed with the corresponding heat-killed *Malassezia* spp. (**A**) WT mice were infected with *M. pachydermatis* (*M.p.*) or vehicle-treated (V) with tape stripping prior to infection. (**B-C**) WT mice were infected with *M. pachydermatis* or vehicle treated without tape stripping prior to infection. (**D-E**) WT mice were infected with *M. sympodialis* (*M.s.*) or *M. furfur* (*M.f.*), or vehicle-treated (V) as indicated. The ear skin was or was not tape-stripped before infection, as indicated**.** (**F**) WT mice were primed with *M. pachydermatis* (2°) or left uninfected (1°) 6 weeks prior to (re-)infection with the same strain of *Malassezia* or vehicle treatment as control. The ear skin was pretreated by tape stripping in all conditions. 4 and 6 days later, the percentage of INF-γ and IL-13-producing $CD90^+CD4^+$ T cells in the auricular lymph nodes was assessed by *ex vivo* re-stimulation with dendritic cells that were pulsed with heat-killed *M pachydermatis* followed by intracellular staining and flow cytometry. Representative FACS plots (**B, D**) and summary graphs (**A**, **C**, **E**, **F**) indicating the percentage of cytokine-positive $CD90^+CD4^+$ T cells are shown. In **A**, **C, E** and **F**, each symbol represents one animal. Graphs show pooled data from two independent experiments. The mean +/- SEM of each group is indicated. Statistics were calculated using one-way ANOVA or unpaired Student's t-Test, as appropriate. *p<0.05, **p<0.01, ***p<0.001, ****p<0.0001.

Figure S6 (related to Figure 7): Human memory T cells respond to *C. albicans* with type 17 cytokine secretion. (A-B) $CCR6^+$ and $CCR6^-$ human memory $CD4^+$ T cells were sorted from the peripheral blood of

non-atopic individuals and cytokine production was analyzed by Luminex after 5 days of co-culture with unpulsed autologous monocytes (**A**) or monocytes that were pulsed with heat-killed *C. albicans* (**B**) prior to co-culture. Graphs show the production of the type-17 cytokines IL-17A and IL-22, the type-1 cytokine IFN-γ and the type-2 cytokines IL-4, IL-5 by $CD4^+CCR6^-$ (white bars) and $CD4^+CCR6^+$ T cells (grey bars). Data are pooled from three independent experiments with 5 donors in total. The mean + SEM of each group is indicated.

Figure S7 (related to Figure 7): Human *Malassezia*-specific memory T cells display a strong Th17 signature. (**A-B**) $CCR6^+$ and $CCR6^-$ human memory $CD4^+$ T cells were sorted from the blood of atopic patients and non-atopic individuals and analyzed for type-17 (IL-17A, IL-22), type-1 (IFN-γ) and type-2 (IL-4) cytokine production by intracellular staining and flow cytometry after 5 days of co-culture with autologous monocytes that were pulsed with heat-killed *M. furfur*, *M. sympodialis*, *M. slooffiae* or *C. albicans*. Representative FACS plots (**A**) and summary graphs (**B**) with the percentages of cytokine-positive $CD4^+CCR6^+$ and $CD4^+CCR6^-$ T cells in non-atopic individuals (upper rows in **A**, grey bars in **B**) and atopic patients (lower rows in **A**, black bars in **B**). In **B**, each symbol represents one donor. Graphs show pooled data from three independent experiments. The mean + SEM of each group is indicated. Statistics were calculated using unpaired Student´s t-Test. *p<0.05, **p<0.01, ***p<0.001.

Table S1 (related to the Key Resource Table): Oligonucleotides used in this study

Figure S1:

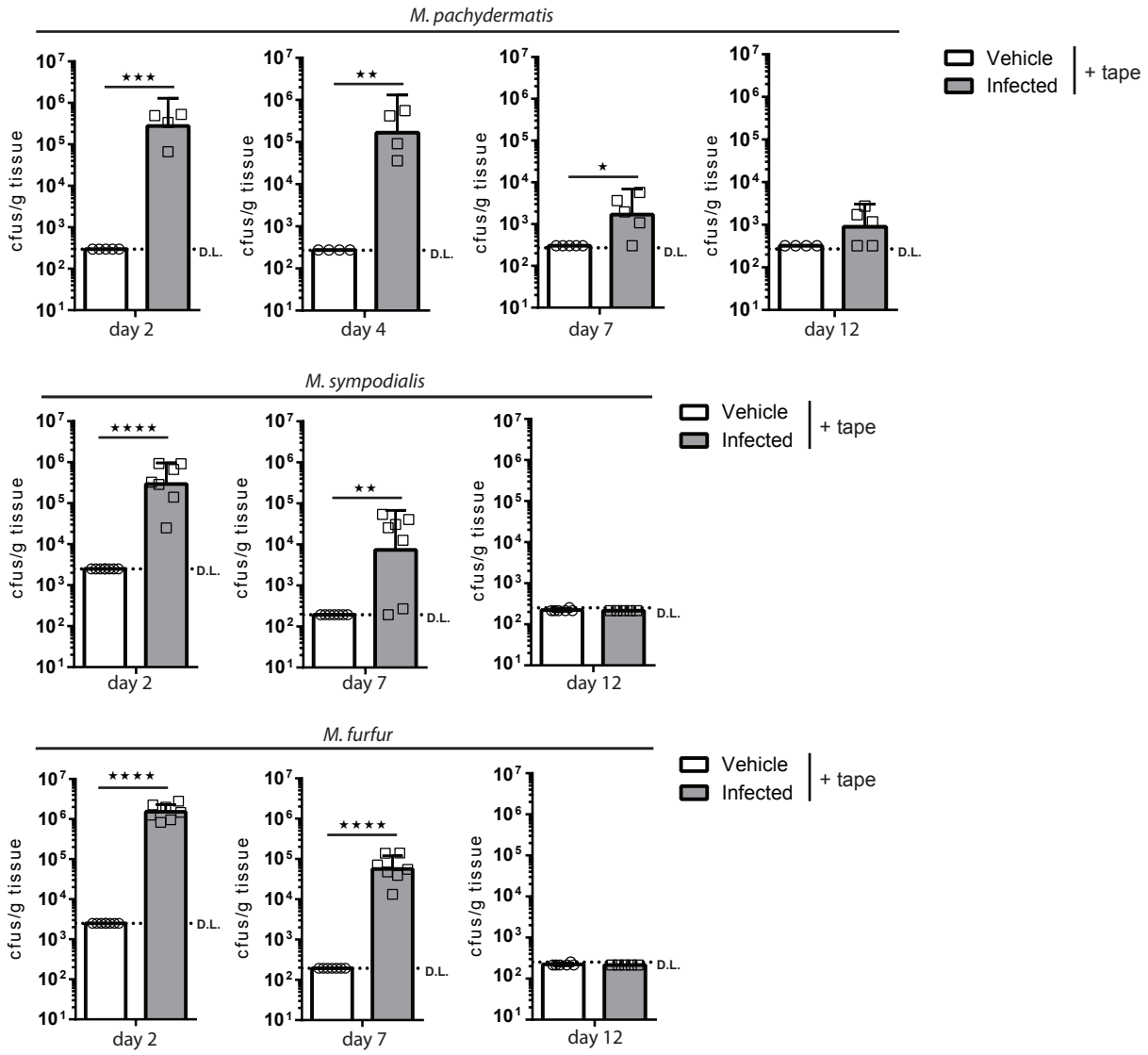

M. pachydermatis
M. sympodialis
M. furfur
Vehicle
Infected
+ tape
cfus/g tissue
D.L.
day 2
day 4
day 7
day 12

Figure S2:

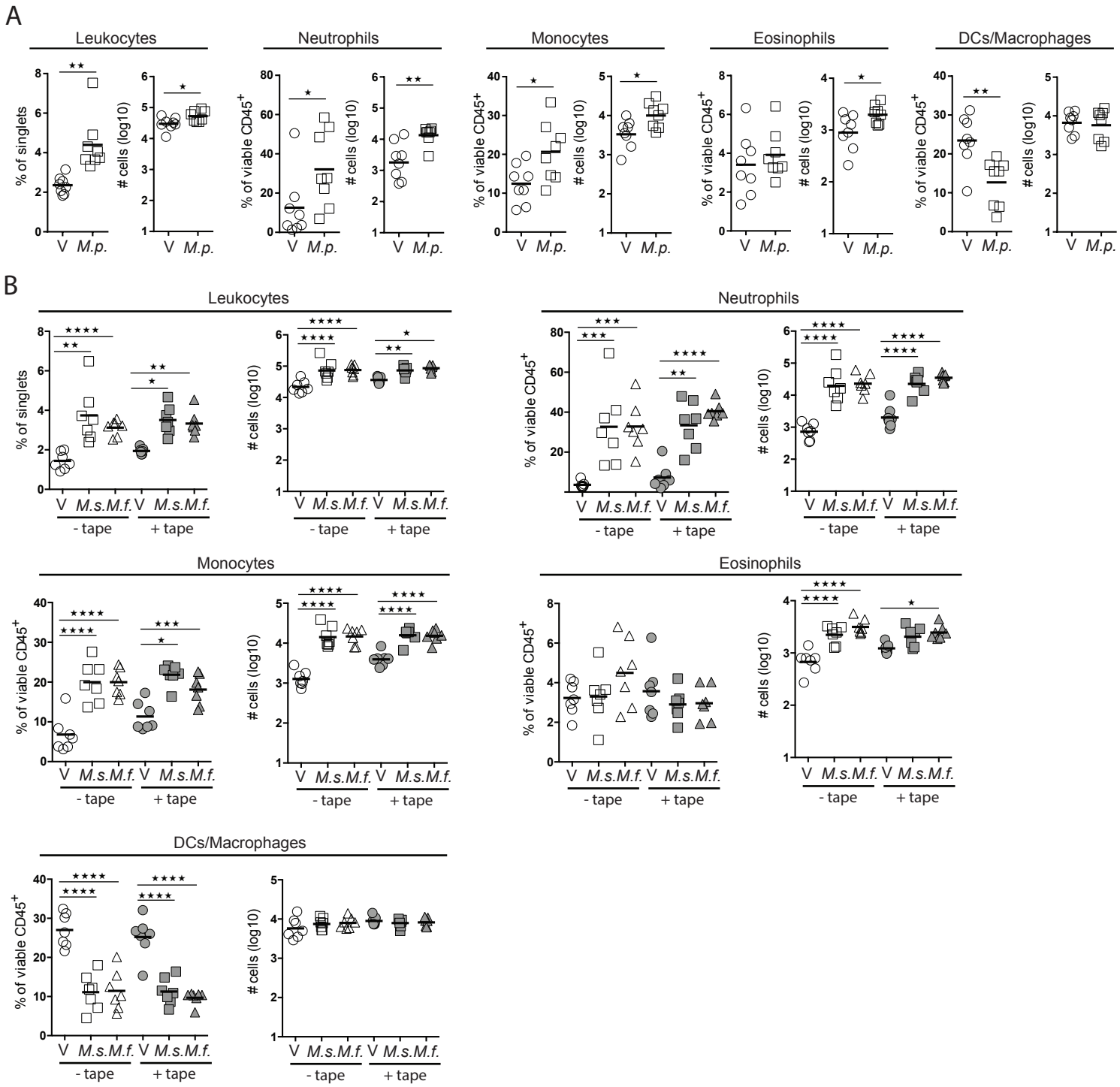

A
Leukocytes
Neutrophils
Monocytes
Eosinophils
DCs/Macrophages
% of singlets
% of viable CD45+
cells (log10)
V
M.p.
B
Leukocytes
Neutrophils
Monocytes
Eosinophils
DCs/Macrophages
% of singlets
% of viable CD45+
cells (log10)
V
M.s.M.f.
- tape
+ tape

Figure S3:

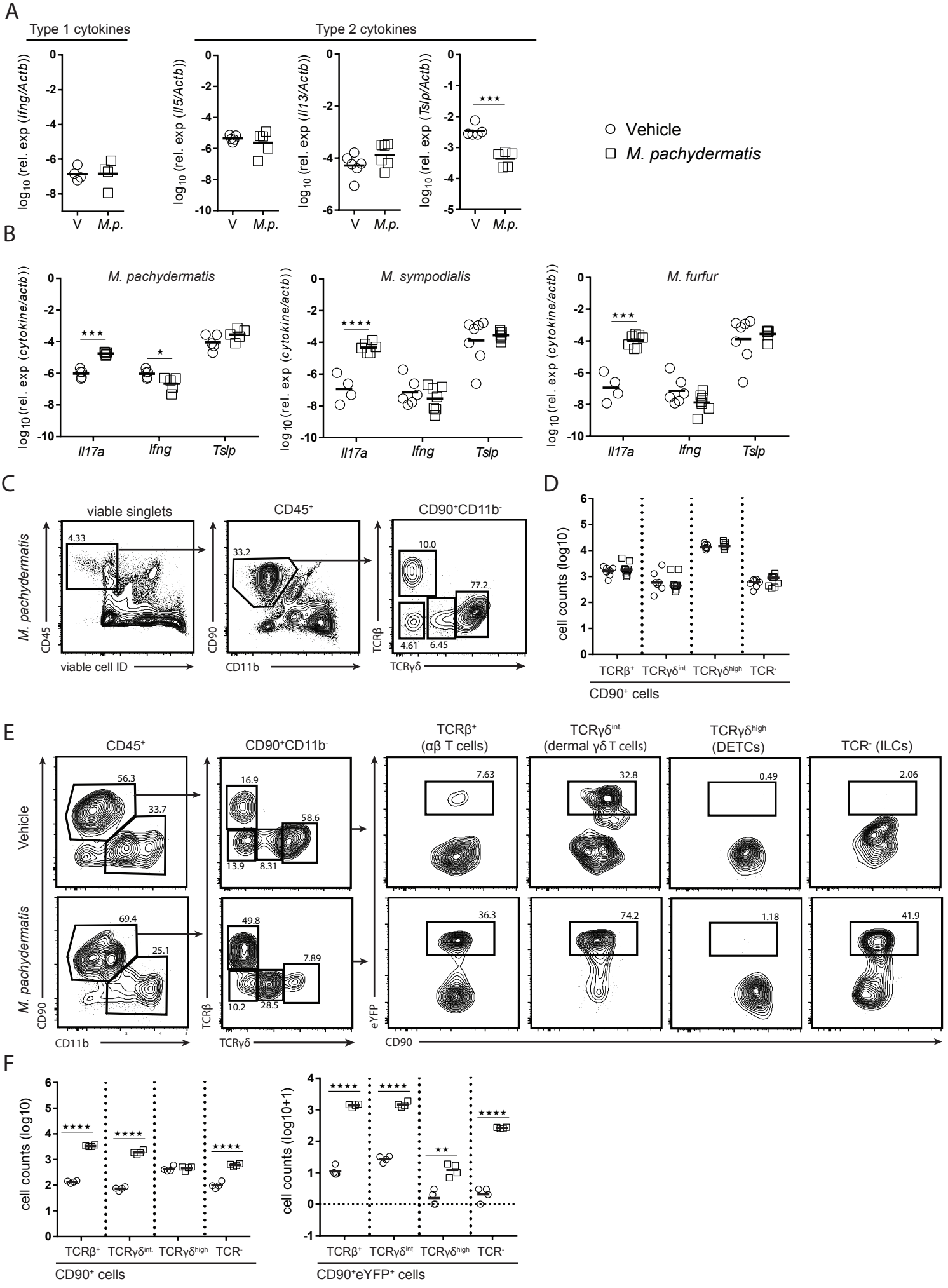
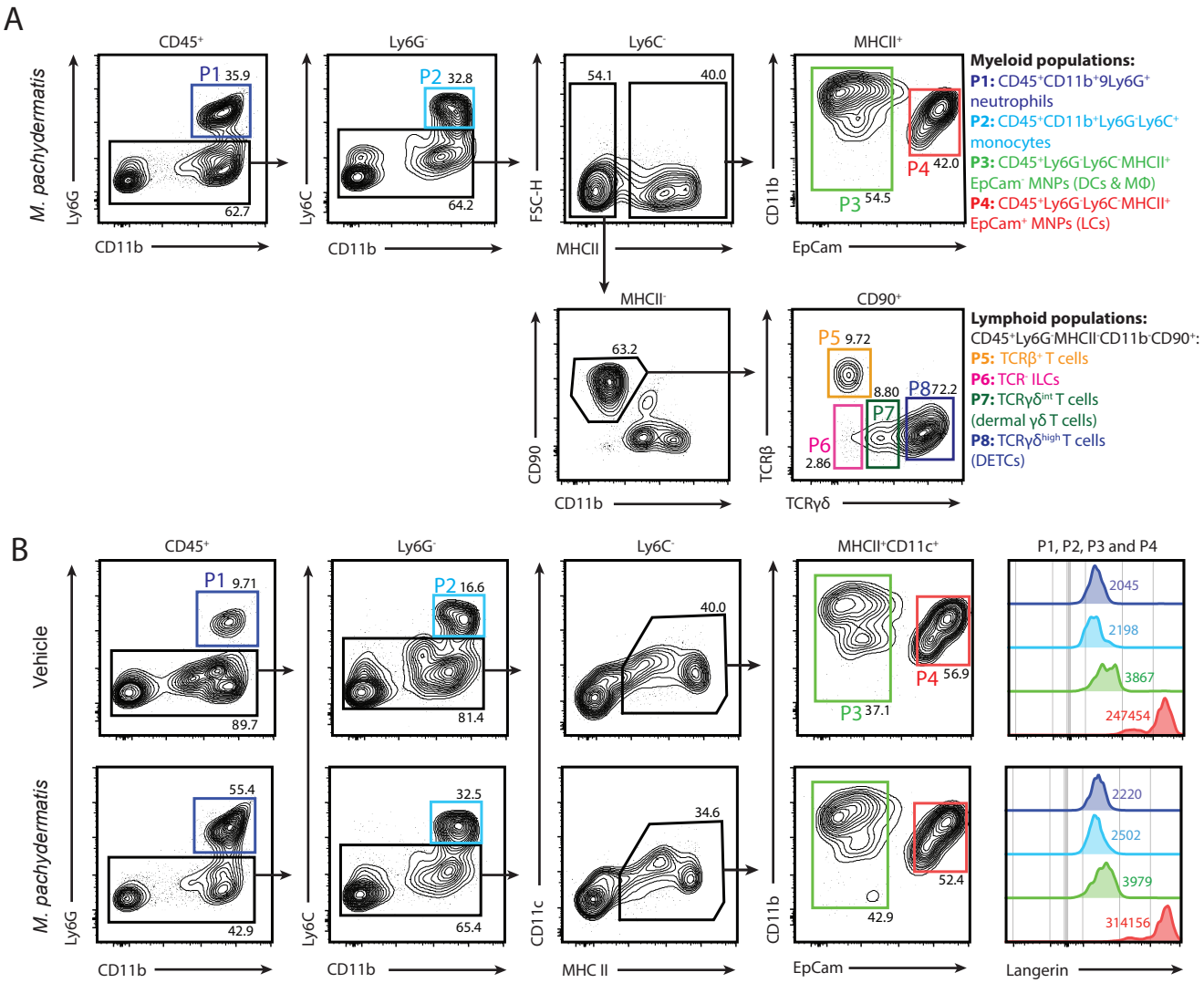

A
Type 1 cytokines
Type 2 cytokines
log10 (rel. exp (Ifng/Actb))
log10 (rel. exp (Il5/Actb))
log10 (rel. exp (Il13/Actb))
log10 (rel. exp (Tslp/Actb))
V
M.p.
Vehicle
M. pachydermatis
B
M. pachydermatis
M. sympodialis
M. furfur
log10 (rel. exp (cytokine/actb))
Il17a
Ifng
Tslp
C
viable singlets
CD45+
CD90+CD11b-
M. pachydermatis
CD45
viable cell ID
CD90
CD11b
TCRβ
TCRγδ
4.33
33.2
10.0
77.2
4.61
6.45
D
cell counts (log10)
TCRβ+
TCRγδint.
TCRγδhigh
TCR-
CD90+ cells
E
CD45+
CD90+CD11b-
TCRβ+ (αβ T cells)
TCRγδint. (dermal γδ T cells)
TCRγδhigh (DETCs)
TCR- (ILCs)
Vehicle
M. pachydermatis
56.3
33.7
16.9
58.6
13.9
8.31
7.63
32.8
0.49
2.06
69.4
25.1
49.8
7.89
10.2
28.5
36.3
74.2
1.18
41.9
CD90
CD11b
TCRβ
TCRγδ
eYFP
CD90
F
cell counts (log10)
cell counts (log10+1)
TCRβ+
TCRγδint.
TCRγδhigh
TCR-
CD90+ cells
CD90+eYFP+ cells

Figure S4:



P1: CD11b+Ly6G+ neutrophils, **P2**: Ly6G-Ly6C+CD11b+ monocytes, **P3**: MHCII+CD11c+EpCam- MNPs, **P4**: MHCII+CD11c+EpCam+ MNPs (LCs)

Figure S5:

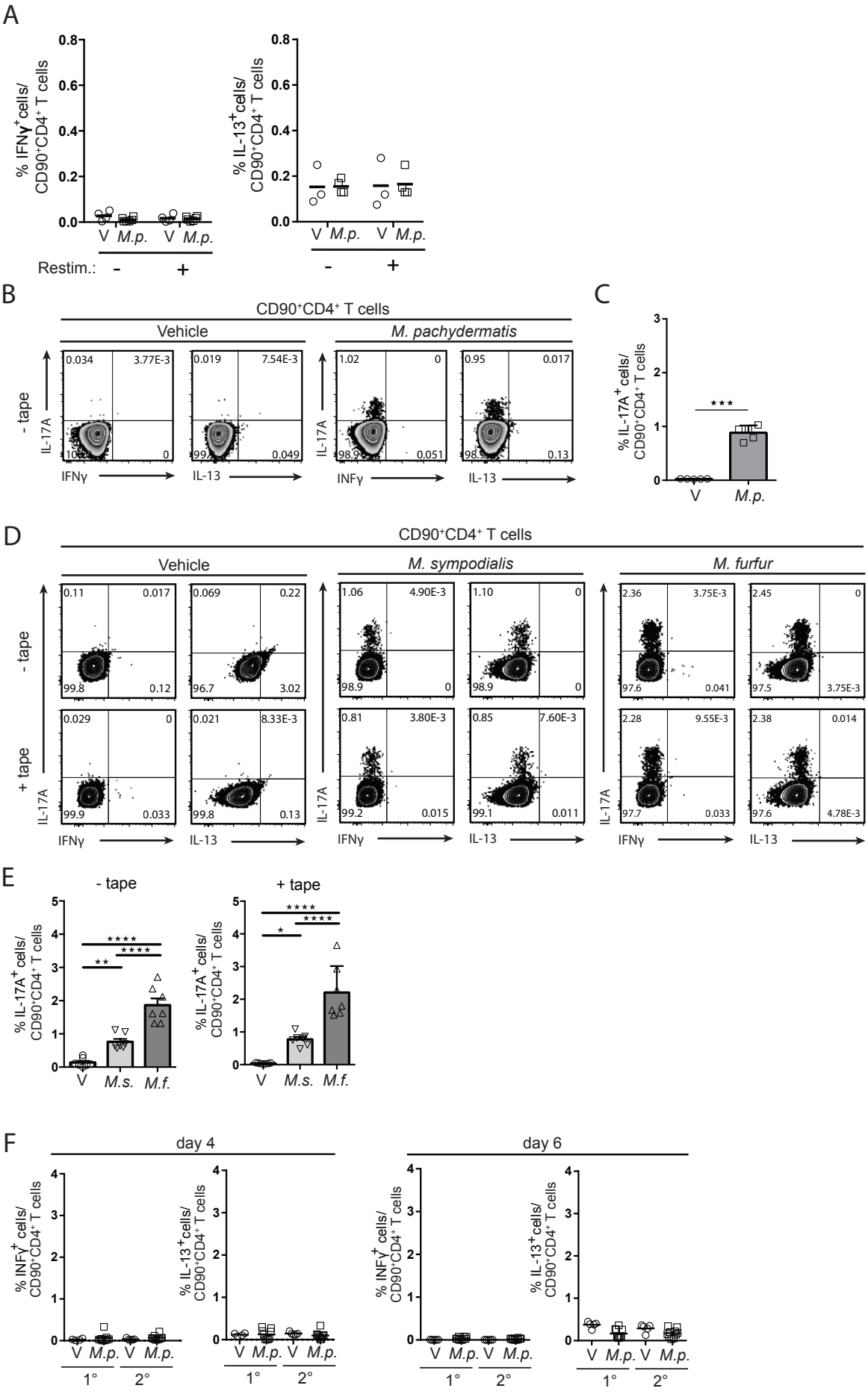

A
% IFNγ+cells/ CD90+CD4+ T cells
% IL-13+cells/ CD90+CD4+ T cells
V M.p. V M.p.
Restim.: - +
B
CD90+CD4+ T cells
Vehicle
M. pachydermatis
- tape
IL-17A
IFNγ
IL-13
0.034 3.77E-3 100 0
0.019 7.54E-3 99.9 0.049
1.02 0 98.9 0.051
0.95 0.017 98.8 0.13
C
% IL-17A+ cells/ CD90+CD4+ T cells
***
V M.p.
D
CD90+CD4+ T cells
Vehicle
M. sympodialis
M. furfur
- tape
+ tape
0.11 0.017 99.8 0.12
0.069 0.22 96.7 3.02
1.06 4.90E-3 98.9 0
1.10 0 98.9 0
2.36 3.75E-3 97.6 0.041
2.45 0 97.5 3.75E-3
0.029 0 99.9 0.033
0.021 8.33E-3 99.8 0.13
0.81 3.80E-3 99.2 0.015
0.85 7.60E-3 99.1 0.011
2.28 9.55E-3 97.7 0.033
2.38 0.014 97.6 4.78E-3
E
- tape
+ tape
% IL-17A+ cells/ CD90+CD4+ T cells
V M.s. M.f.
F
day 4
day 6
% INFγ+ cells/ CD90+CD4+ T cells
% IL-13+cells/ CD90+CD4+ T cells
V M.p. V M.p.
1° 2°

Figure S6:

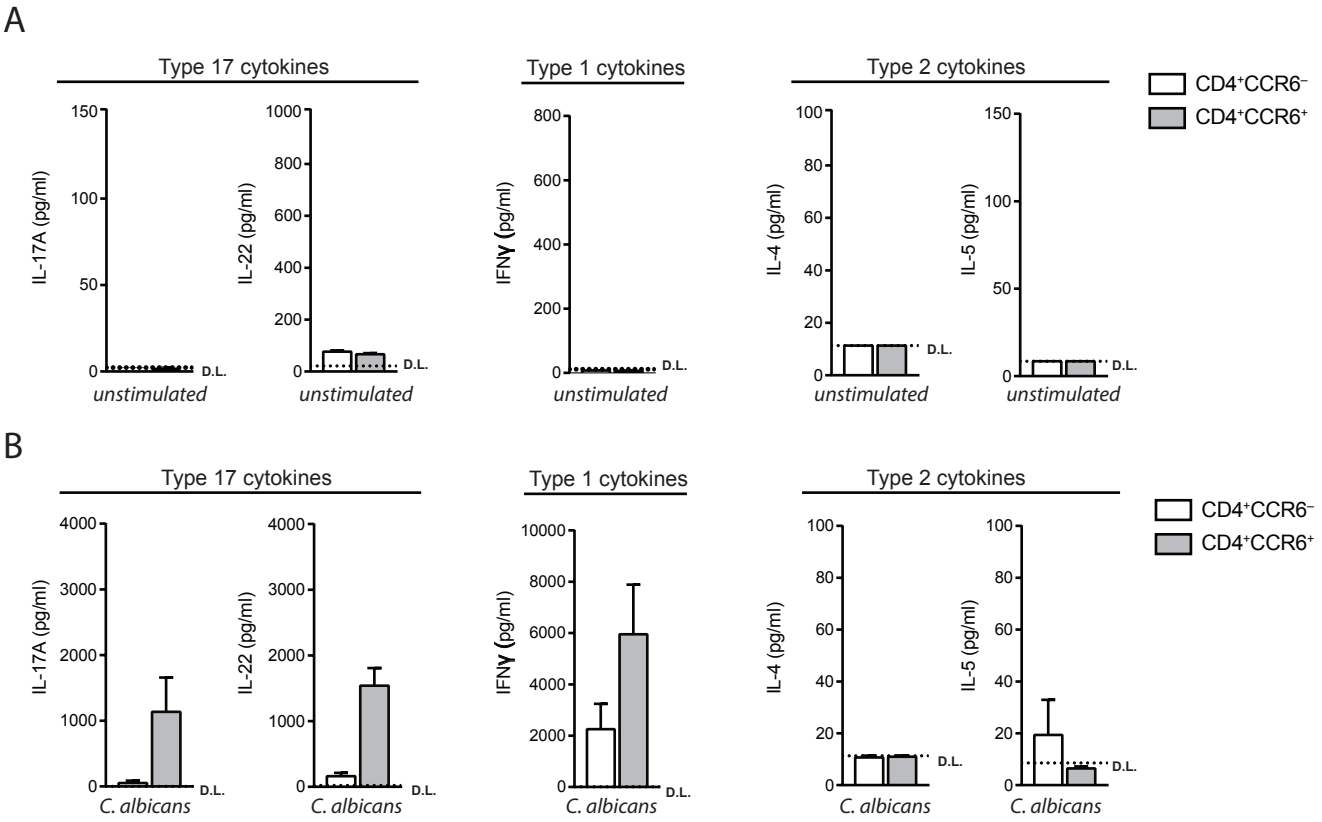
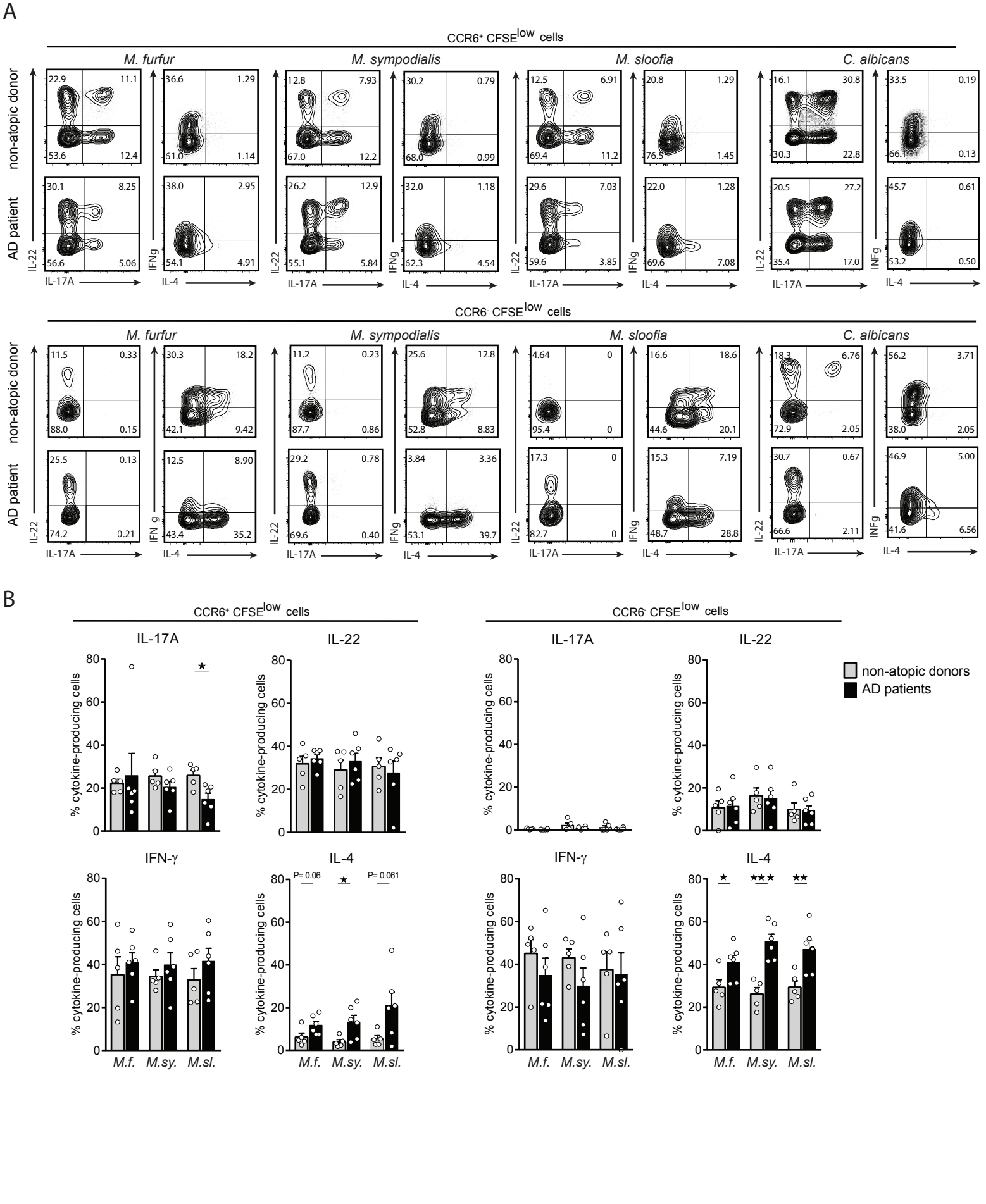

A
Type 17 cytokines
Type 1 cytokines
Type 2 cytokines
CD4+CCR6–
CD4+CCR6+
IL-17A (pg/ml)
IL-22 (pg/ml)
IFNγ (pg/ml)
IL-4 (pg/ml)
IL-5 (pg/ml)
D.L.
unstimulated
B
C. albicans

Figure S7:


A
CCR6+ CFSElow cells
M. furfur
M. sympodialis
M. sloofia
C. albicans
non-atopic donor
AD patient
IL-22
IL-17A
IFNg
IL-4
CCR6- CFSElow cells
B
CCR6+ CFSElow cells
CCR6- CFSElow cells
IL-17A
IL-22
IFN-γ
IL-4
% cytokine-producing cells
non-atopic donors
AD patients
P= 0.06
P= 0.061
M.f.
M.sy.
M.sl.

SUPPLEMENTAL TABLE S1: Oligonucleotides used in this study

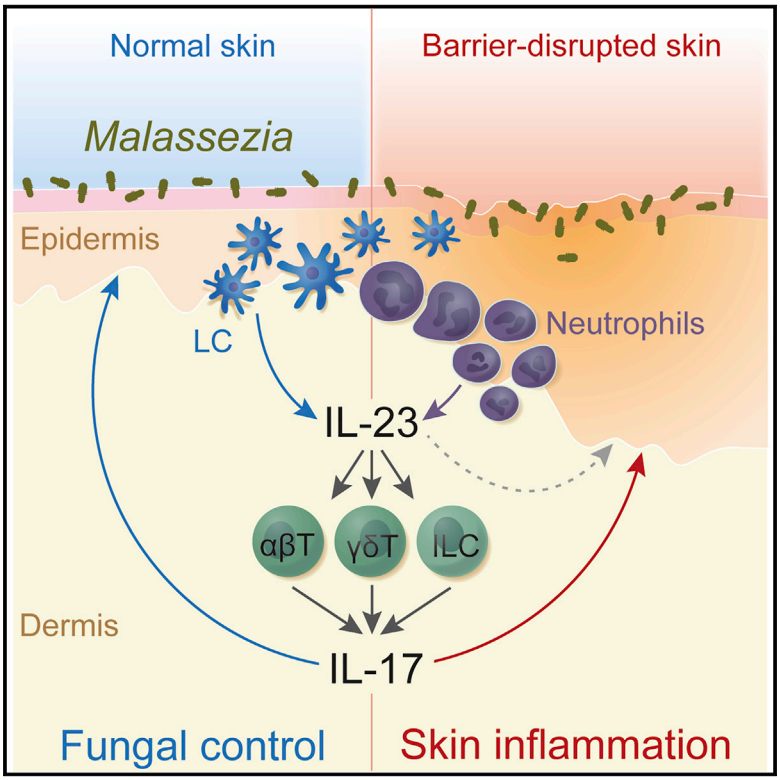
Oligonucleotides	SOURCE	IDENTIFIER
Actb: fwd 5´-CCCTGAAGTACCCCATTGAAC-3´, rev 5´-CTTTTCACGGTTGGCCTTAG-3´	Microsynth	N/A
Il17a: fwd 5´- GCTCCAGAAGGCCCTCAGA-3´, rev 5´-AGCTTTCCCTCCGCATTGA-3´	Microsynth	(Overbergh et al., 2003)
Il6: fwd 5´-GAGGAT ACCACTCCCAACAGACC-3´, rev 5´-AAGTGCATCATCGTTGTTCATACA-3´	Microsynth	(Liao et al., 2009)
Il23p19: fwd 5´- CCAGCAGCTCTCTCGGAATC-3´, *Il23p19* rev 5´-TCATATGTCCCGCTGGTGC-3´	Microsynth	(Zelante et al., 2007)
Tslp: fwd 5´-TCTGGAGATTGCATGAAGGA-3´, rev 5´-AGAGAAGCCCTCAATGACCA-3´	Microsynth	N/A
Il22: fwd 5´-CATGCAGGAGGTGGTGCCTT-3´*, Il22* rev 5´-CAGACGCAAGCATTTCTCAG-3´	Microsynth	(Chung et al., 2006)
Infg: fwd 5´-GAACTGGCAAAAGGATGGTGA-3´, rev 5´-TGTGGGTTGTTGACCTCAAAC-3´	Microsynth	N/A
Il5: fwd 5´-TCACCGAGCTCTGTTGACAA-3´, rev 5´-CCACACTTCTCTTTTTGGCG-3´	Microsynth	N/A
Il13: fwd 5´-CCAGGTCCACACTCCATACC-3´, rev 5´-TGCCAAGATCTGTGTCTCTCC-3´	Microsynth	N/A
Gcsf: fwd 5´-CTTAAGTCCCTGGAGCAAGTG-3´, *r*ev 5´-GTGGCCCAGCAACACCAG-3´	Microsynth	N/A
Cxcl1: fwd 5´-CCGCTCGCTTCTCTGTG-3´, rev 5´-GCAGCTCATTGGCGATAG-3´	Microsynth	N/A
Cxcl2: fwd 5´-AGTGAACTGCGCTGTCAATGC-3´, rev 5´-GCAAACTTTTTGACCGCCCT-3´	Microsynth	N/A
Ccl2: fwd 5´-GGGATCATCTTGCTGGTGAA-3´, *Ccl2* rev 5´-AGGTCCCTGTCATGCTTCTG-3´	Microsynth	N/A
Ccl5: fwd 5´-CCCACTTCTTCTCTGGGTTG-3´, rev 5´-GTGCCCACGTCAAGGAGTAT-3´	Microsynth	N/A
Ccl11: fwd 5´-CTATGGCTTTCAGGGTGCAT-3´, *Ccl11* rev 5´-TCACTTCCTTCACCTCCCAG-3´	Microsynth	N/A
Defb3: fwd 5´-GTCTCCACC TGCAGCTTTTAG, *Defb3* rev 5´-ACTGCCAATCTGACGAGTGTT	Microsynth	N/A
Il1b: *Il1b* rev 5´-AGGCCACAGGTATTTTGTCG-3´; *Il17a* fwd 5´- GCTCCAGAAGGCCCTCAGA-3´	Microsynth	N/A
Ccl24: fwd 5´-TCTTATGGCCCTTCTTGGTG-3´, rev 5´-AATTCCAGAAAACCGAGTGG-3´	Microsynth	N/A

Article

Cell Host & Microbe

The Skin Commensal Yeast *Malassezia* Triggers a Type 17 Response that Coordinates Anti-fungal Immunity and Exacerbates Skin Inflammation

Graphical Abstract



Authors

Florian Sparber, Corinne De Gregorio, Simone Steckholzer, ..., Martin Glatz, Federica Sallusto, Salomé LeibundGut-Landmann

Correspondence

salome.leibundgut-landmann@uzh.ch

In Brief

The skin commensal yeast *Malassezia* is associated with common skin disorders like atopic dermatitis, but how the mammalian host responds to *Malassezia* remains unclear. Using an epicutaneous infection model in mice, Sparber et al. demonstrate that the IL-23-IL-17 pathway controls fungal colonization and also drives *Malassezia*-induced inflammation in atopy-like skin.

Highlights

- The skin commensal yeast *Malassezia* drives type 17 immunity in the skin
- *Malassezia*-specific human memory T cells display a Th17 phenotype
- Mice deficient in IL-17AF or IL-23 show uncontrolled *Malassezia* growth on the skin
- In the disrupted skin, IL-23 and IL-17AF promote *Malassezia*-induced inflammation

Sparber et al., 2019, Cell Host & Microbe *25*, 389–403
March 13, 2019 © 2019 Elsevier Inc.
https://doi.org/10.1016/j.chom.2019.02.002

CellPress

Cell Host & Microbe
Article

The Skin Commensal Yeast *Malassezia* Triggers a Type 17 Response that Coordinates Anti-fungal Immunity and Exacerbates Skin Inflammation

Florian Sparber,[1] Corinne De Gregorio,[2] Simone Steckholzer,[1] Filipa M. Ferreira,[3] Tamas Dolowschiak,[4] Fiorella Ruchti,[1] Florian R. Kirchner,[1] Sarah Mertens,[1] Immo Prinz,[5] Nicole Joller,[4] Thorsten Buch,[3] Martin Glatz,[6] Federica Sallusto,[2,7] and Salomé LeibundGut-Landmann[1,8,*]

[1]Section of Immunology, Vetsuisse Faculty, University of Zürich, Zürich 8057, Switzerland
[2]Institute for Research in Biomedicine, Università della Svizzera Italiana, Bellinzona 6500, Switzerland
[3]Institute of Laboratory Animal Science, University of Zürich, Schlieren 8952, Switzerland
[4]Institute of Experimental Immunology, University of Zürich, Zürich 8057, Switzerland
[5]Institute of Immunology, Hannover Medical School, Hannover 30625, Germany
[6]Department of Dermatology, University and University Hospital of Zürich, Zürich 8091, Switzerland
[7]Institute of Microbiology, ETH Zürich, Zürich 8093, Switzerland
[8]Lead Contact
*Correspondence: salome.leibundgut-landmann@uzh.ch
https://doi.org/10.1016/j.chom.2019.02.002

SUMMARY

Commensal fungi of the mammalian skin, such as those of the genus *Malassezia*, are associated with atopic dermatitis and other common inflammatory skin disorders. Understanding of the causative relationship between fungal commensalism and disease manifestation remains incomplete. By developing a murine epicutaneous infection model, we found *Malassezia* spp. selectively induce IL-17 and related cytokines. This response is key in preventing fungal overgrowth on the skin, as disruption of the IL-23-IL-17 axis compromises *Malassezia*-specific cutaneous immunity. Under conditions of impaired skin integrity, mimicking a hallmark of atopic dermatitis, the presence of *Malassezia* dramatically aggravates cutaneous inflammation, which again was IL-23 and IL-17 dependent. Consistently, we found a CCR6$^+$ Th17 subset of memory T cells to be *Malassezia* specific in both healthy individuals and atopic dermatitis patients, whereby the latter showed enhanced frequency of these cells. Thus, the *Malassezia*-induced type 17 response is pivotal in orchestrating antifungal immunity and in actively promoting skin inflammation.

INTRODUCTION

Microbes coexist with mammalian organisms and create complex ecosystems on body surfaces, which contribute to health and disease. The constant exposure of the host to microbes shapes the immune reactivity of the host locally and at distant sites and even influences seemingly unrelated processes ranging from digestion to behavior (Belkaid and Tamoutounour, 2016). Perturbations that disrupt the equilibrium of the microbial ecosystem may lead to the overgrowth of species with pathogenic potential and in turn to the development of disease (Williams and Gallo, 2015). Fungi are increasingly being recognized as common members of the microbiota on nearly all surfaces, including the skin (Findley et al., 2013), and recent examples revealed that—similar to their bacterial counterparts—commensal fungi might have an important role in host physiology and immunity (Iliev and Leonardi, 2017).

Among the fungal communities on the mammalian skin, *Malassezia* species are by far the most abundant members, with >90% of all commensal fungi belonging to this genus (Findley et al., 2013; Gemmer et al., 2002). 17 species of *Malassezia* are currently known, 10 of which have been identified on human skin sites (Cabañes, 2014). *M. sympodialis* is among the most frequently identified and in turn best studied species, while *M. furfur* on the other hand is found enriched on diseased skin in humans (Prohic et al., 2016). *M. pachydermatis* is the most frequent species found in dogs and other homoeothermic animals (Cabañes, 2014). *Malassezia* spp. are well adapted to thrive in the temperate and sebaceous microenvironment of the skin. They are lipophilic, explaining their predilection for seborrheic skin sites such as the scalp and the trunk. They lack a fatty acid synthase and thus rely on exogenous fatty acid sources for their nutritive requirements (Wu et al., 2015).

Because of the constant presence of *Malassezia* on the host, the immune system is continuously exposed to the fungus, which is reflected by *Malassezia*-responsive T cells and antibodies in the blood of healthy individuals (Ashbee and Bond, 2010). Despite its high abundance on the mammalian skin, the mechanisms of immune surveillance of *Malassezia* remain unknown.

Besides their commensal lifestyle, *Malassezia* spp. have also been associated with several common skin disorders including pityriasis versicolor, seborrheic dermatitis, and more severe inflammatory skin pathologies such as atopic dermatitis (AD) in humans (Sugita et al., 2010) and dermatitis and otitis externa in dogs (Bond et al., 2010). The role of *Malassezia* in skin disease pathogenesis is not well understood. A causative link between *Malassezia* and disease development has been made only for

dandruff and pityriasis versicolor, while its role in AD remains correlative and not well defined (Casagrande et al., 2006; Johansson et al., 2002, 2004). It is generally believed that *Malassezia* actively promotes disease symptoms in predisposed atopic individuals, albeit firm evidence for this causal link is missing and the mechanistic basis has not been established. Alternatively, *Malassezia* may also exert a protective role in AD (Li et al., 2018).

AD is one of the most common allergies, affecting up to 30% of children and 10% of adults in developed countries (Weidinger and Novak, 2016). The incidence of AD has dramatically increased over the last three decades presumably in consequence of stringent hygiene and reduced exposure to microbes in early life (Flohr and Yeo, 2011). AD is characterized clinically by periodic flares of dry, red, itchy skin lesions that can severely affect the quality of life of those affected. A hallmark of AD is skin barrier defects (Cabanillas and Novak, 2016) that increase the likelihood of environmental factors and irritants to penetrate the skin and promote inflammation. *Malassezia* itself may contribute to barrier disruption through the production of free fatty acids that can damage the integrity of the skin and thereby contribute to irritation and inflammation (Saunders et al., 2012). The immune response to *Malassezia* may also enhance inflammation in the atopic skin (Glatz et al., 2015).

The interaction of *Malassezia* with the mammalian immune system, both during homeostasis and disease, is not well understood. The mechanisms of fungal recognition and the immune pathways that maintain commensalism and/or promote pathology remain to be defined. Most of what we know today about the host-fungal interplay is based on experiments with isolated host cells *in vitro* (Sparber and LeibundGut-Landmann, 2017). A suitable experimental model to study the interaction between *Malassezia* spp. and the host *in vivo* in the complex environment of the mammalian skin has not been available so far. To fill this gap, we developed an experimental model of *Malassezia* skin colonization in mice. This allowed us to identify cellular and molecular players of the host response to *Malassezia* that maintain homeostasis during commensalism and at the same time promote pathology under inflamed conditions.

RESULTS

Malassezia spp. Colonization of the Mouse Skin

To study the interaction of *Malassezia* spp. with the mammalian skin *in vivo*, we established an infection model in C57BL/6 mice. The yeast was not detectable in our colony of specific pathogen-free (SPF) mice under steady-state conditions. Epicutaneous application of *Malassezia* ssp. onto the dorsal ear skin resulted in robust colonization of the skin on day 2 post infection (p.i.), while no fungal counts were detected in mock-infected control mice. The colonization efficiency was comparable between *M. sympodialis*, *M. furfur*, and *M. pachydermatis* (Figure 1A), with yeast cells localizing exclusively to the keratinized layer of the epidermis (Figure 1B). Disrupting the barrier integrity of the skin by mild tape stripping prior to infection (Holzmann et al., 2004) did not alter the capacity of *Malassezia* spp. to colonize the *stratum corneum* (Figures 1C–1E). The fungal load remained high for up to a week and declined thereafter with some variations between the different species (Figure S1). The skin of *Malassezia*-free mice can thus readily be colonized by various species of *Malassezia*.

Malassezia spp. Trigger Infiltration of Myeloid Cells into the Colonized Skin

Given the robust colonization of the mouse skin with *Malassezia* spp., we were interested in understanding the immune response to the yeast. *M. pachydermatis* colonization of the epidermis in the mouse skin was accompanied by infiltration of leukocytes, in particular $CD11b^+$ myeloid cells, to the site of infection (Figure 2A). Detailed characterization of these infiltrates by flow cytometry revealed low numbers of cells in the *Malassezia*-negative skin but a sharp increase in $CD11b^+Ly6G^+$ neutrophils, $CD11b^+Ly6G^-Ly6C^{hi}$ monocytes, and $CD11b^+Ly6G^-Ly6C^{low}$Siglec-F^+ eosinophils upon encounter of *M. pachydermatis*, both in percentages and absolute numbers (Figures 2B and 2C). Consistent with the massive infiltration of neutrophils and monocytes, we detected a strong rise in the local expression of neutrophil- and monocyte-recruiting chemokines and growth factors in the *Malassezia*-exposed skin (Figure 2D). The remaining population of $Ly6G^-Ly6C^{low}$Siglec-F^- myeloid cells consisted mostly of $CD11c^+$MHC-II^+ mononuclear phagocytes (MNPs) including dendritic cells and macrophages. In contrast to the infiltrating neutrophils and monocytes, this population did not change or even declined upon *Malassezia* exposure (Figure 2C).

The recruitment of myeloid cell infiltrates to the epithelium in response to *Malassezia* was independent of the barrier integrity of the ear skin and occurred similarly under conditions with or without tape stripping (Figures 2C and S2A). Moreover, the response was not restricted to *M. pachydermatis*; it was also observed in response to *M. sympodialis* and *M. furfur* (Figure S2B). Of note, barrier disruption on its own stimulated only a very limited myeloid response in the skin compared to completely untreated conditions (Figures 2C and S2). Together, these results indicate that *Malassezia* triggers a robust response in the host upon contact with the mammalian skin.

Exposure of the Skin to *Malassezia* spp. Results in a Selective Activation of the IL-17 Pathway

Next, we explored the cytokine response to the fungus in the *Malassezia*-exposed skin. In particular, we were interested in interleukin (IL)-17 and related cytokines given their important function in barrier tissue immunity in response to other fungi. IL-17A and IL-17F, two closely related members of the IL-17 cytokine family, are essential for immunosurveillance of *Candida albicans* at mucosal surfaces as evidenced by studies of primary immunodeficiency patients suffering from chronic mucocutaneous candidiasis (Li et al., 2017) and by experimental infections in mice (Conti et al., 2009; Gladiator et al., 2013).

When analyzing cytokine expression in the *Malassezia*-exposed skin, we observed a pronounced and rapid induction of IL-17A and IL-22 transcripts in response to *M. pachydermatis* (Figure 3A), while transcripts encoding interferon (IFN)-γ and the type-2-associated cytokines IL-5, IL-13, and thymic stromal lymphopoietin (TSLP) remained unchanged or were even downregulated in the *M. pachydermatis*-colonized skin (Figure S3A). Consistent with our previous results, the local and selective induction of type 17 cytokines was independent of skin barrier integrity, and it was conserved across all three *Malassezia*

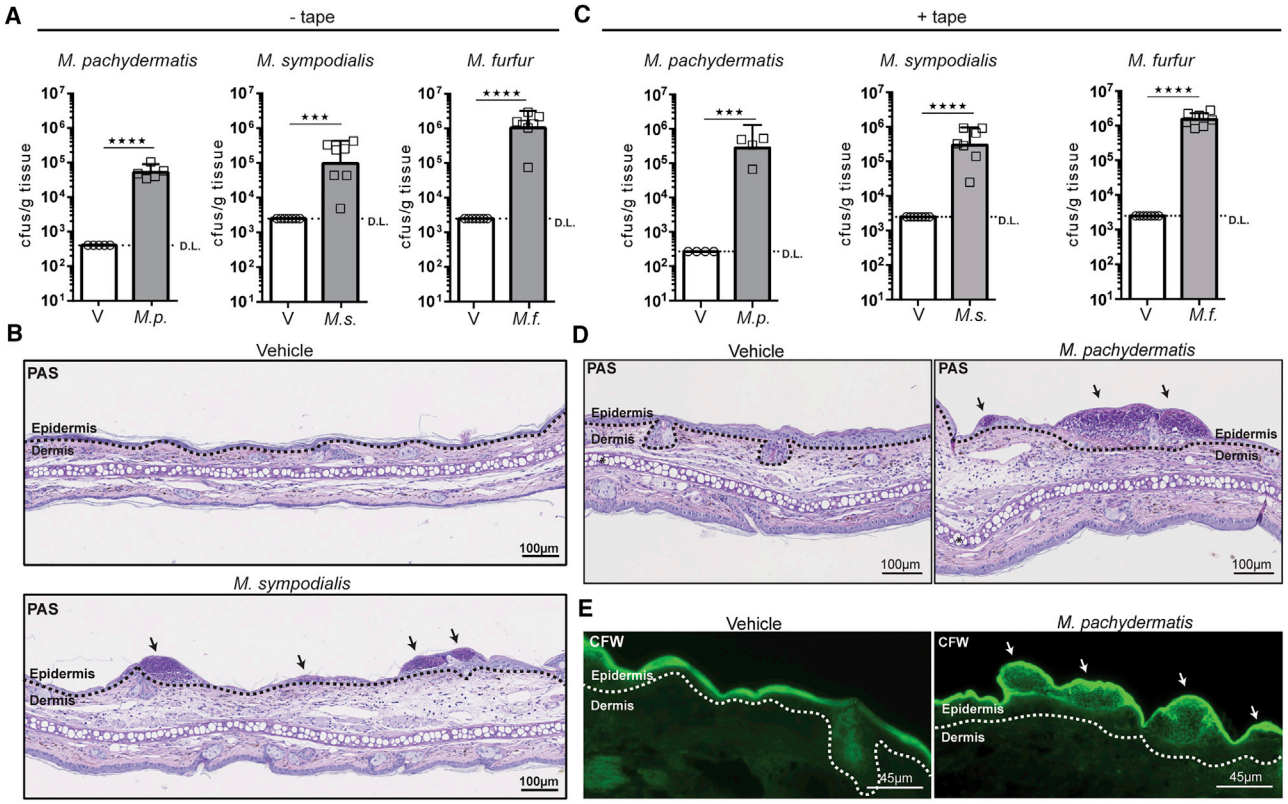


Figure 1. Experimental Colonization of Mice with *Malassezia* spp. *M. pachydermatis*, *M. sympodialis* or *M. furfur* in Olive Oil or Olive Oil Alone (Vehicle) Applied to the Dorsal Ear Skin of WT Mice

The skin was left untreated (A and B) or mildly tape-stripped (C–E) prior to infection. Fungal burden on day 2 p.i. (A and C). Histology of ear sections on day 2 p.i. stained with periodic acid-Schiff (PAS) (B and D) or calcofluor white (CFW) (E). D.L., detection limit; dotted line, basal membrane; arrows, accumulations of yeast cells; V, vehicle).

In (A) and (C), each symbol represents one animal. Graphs show pooled data from two independent experiments. The geomean and 95% confidence intervals are shown. Statistics were calculated using unpaired Student's t test. ***p<0.001, ****p<0.0001.

See also Figure S1.

species tested (Figure S3B). In line with the polarization of the *Malassezia*-induced cytokine response toward a type 17 profile, the expression of the key IL-17A- and IL-22-instructing factors IL-23, IL-1β, and IL-6 and the IL-17 target molecule β-defensin-3 were up-regulated in the *Malassezia*-exposed compared to the uninfected skin (Figures 3B and 3C).

To identify the cells involved in the local type-17 immune response, we applied a flow cytometry approach. Intracellular staining of IL-17A in lymphocytes that were freshly isolated from the skin of day-2-infected wild-type (WT) mice revealed dermal γδ T cells and αβ T cells as rapid producers of this cytokine (Figures 3D, 3E, S3C, and S3D). T cell receptor (TCR)-negative innate lymphocytes (ILCs) also expressed the cytokine, especially at a slightly later time point after infection, as revealed when analyzing *Il17a*^{Cre}*R26R*^{eYFP} reporter mice (Figures S3E and S3F). These data were further confirmed by *Il17a* expression analysis of sorted skin cell populations (Figures 3F and S4A). The response of γδ T cells, αβ T cells, and ILCs to *M. pachydermatis* skin exposure manifested also by expansion of the populations within the first 5 days p.i. (Figure S3F). In contrast, dendritic epidermal T cells (DETCs) neither expanded nor contributed considerably to IL-17A production in response to *M. pachydermatis* (Figures 3D–3F, S3E, and S3F). The tripartite cellular source of IL-17A in the *Malassezia*-exposed skin was reminiscent of the situation in the oral mucosa during experimental oropharyngeal candidiasis (Sparber et al., 2018).

Next, we set out to identify the cell type(s) producing the IL-17-instructing cytokine IL-23 in the infected skin. For this, we fluorescence-activated cell sorting (FACS)-sorted various myeloid skin cell subsets on day 2 p.i., including Ly6G^{+} neutrophils, Ly6C^{hi} monocytes, EpCam^{-} MNPs, and EpCam^{+} MNPs, the latter representing epidermal Langerhans cells (Figure S4). Of those, neutrophils and Langerhans cells were found to express the highest levels of *Il23a* transcripts (Figure 3G).

Finally, we asked the question of whether complementary to the local cytokine response, which we observed as early as 2 days after infection, *Malassezia* spp. would also activate the adaptive immune system in our experimental setting. Indeed, we found a strong induction of *Malassezia*-specific CD4^{+} T cells in the skin-draining lymph nodes that were polarized toward IL-17A-secreting Th17 effector cells (Figures 3H and 3I), while no concurrent induction of Th1 or Th2 cells was detected (Figure S5A). The selective Th17 response to the fungus was observed irrespectively of whether the skin was barrier disrupted or not prior to

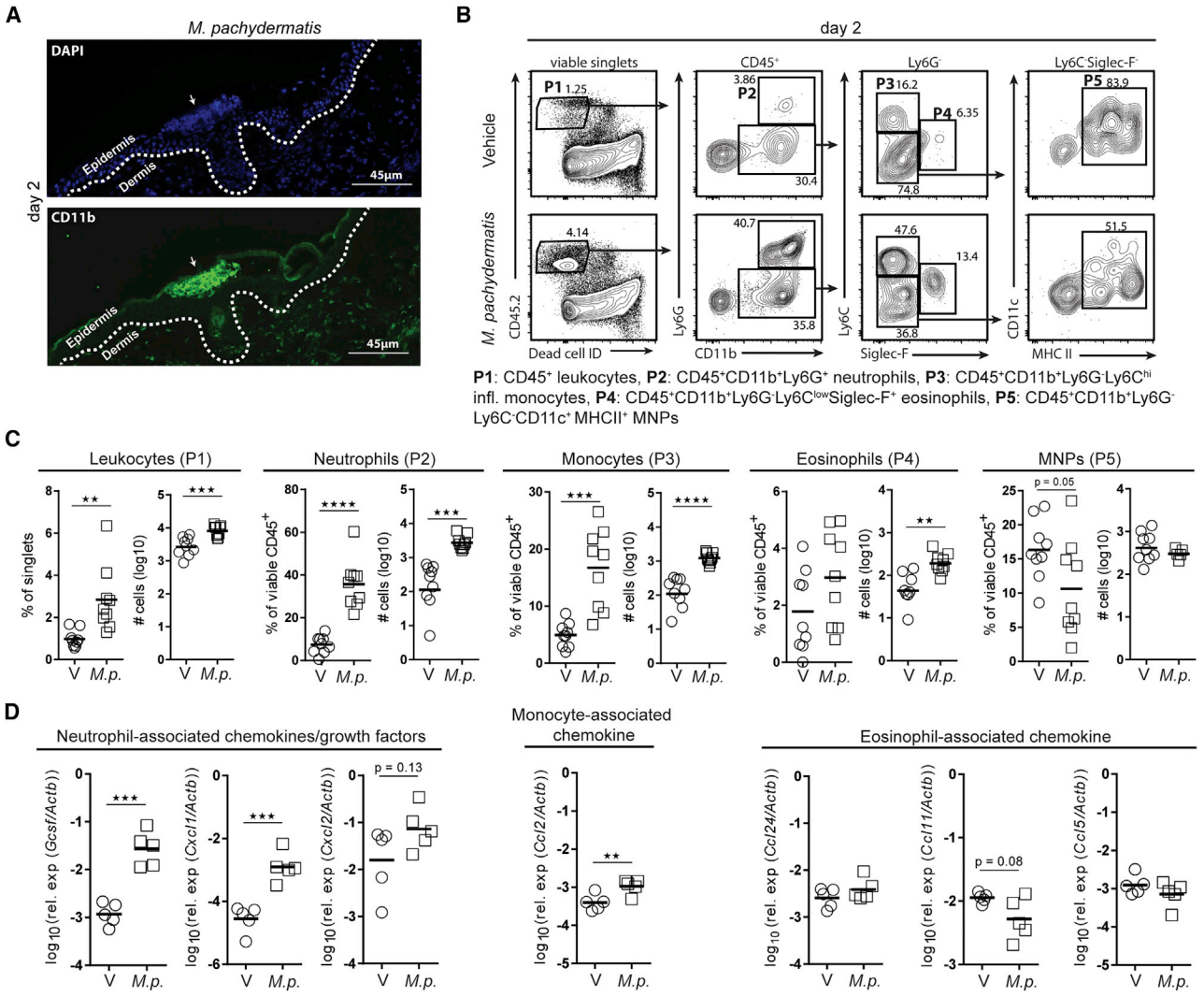


Figure 2. *Malassezia* Triggers a Rapid Infiltration of Myeloid Cells into the Infected Tissue

WT mice infected with *M. pachydermatis* (*M.p.*) or vehicle treated (V) after mild tape stripping of the dorsal ear skin and analyzed on day 2 p.i.

(A) Ear sections stained with DAPI and anti-CD11b. Dotted line, basal membrane; arrow, micro abscesses.

(B and C) FACS gating strategy for neutrophils (P2), inflammatory monocytes (P3), eosinophils (P4), and mononuclear phagocytes (MNPs, comprising DC and macrophages) (P5) in the ear skin (B) and summary graphs with the percentage and absolute number of cells per ½ ear (C). Numbers in (B) indicate the % of cells in each gate.

(D) Chemokine expression in the ear skin.

In (C) and (D), each symbol represents one animal. Graphs show pooled data from three (C) or two (D) independent experiments. The mean of each group is indicated. Statistics were calculated using unpaired Student's t test. **p<0.01, ***p<0.001, ****p<0.0001.

See also Figure S2.

infection (Figures 3H, 3I, S5B, and S5C). *M. sympodialis* displayed a similar capacity as *M. pachydermatis* to instruct IL-17A production by CD4+ T cells, while *M. furfur* was an even stronger inducer of Th17 immunity, both in the barrier-disrupted as well as in the unperturbed skin (Figures S5D and S5E). In summary, we revealed a very robust and selective activation of the IL-17 pathway by *Malassezia* spp., both via innate and adaptive immunity.

The IL-17 Pathway Is Critical for Preventing Uncontrolled Fungal Growth

Given the strong and selective induction of type 17 immunity in response to *Malassezia* skin exposure, we aimed at determining the role of this pathway in fungal control. For this, we assessed Rag1-deficient animals and animals with a selective defect in the T cell compartment, and we used *M. pachydermatis* as a representative fungal species. Rag1- and TCRβδ-deficient mice displayed very high skin colonization levels on day 12 p.i., a time point when WT mice had almost completely cleared the fungus from the skin (Figures 4A and S1). Compared with WT control animals, TCRδ-deficient mice lacking γδ but not αβ T cells also had a significantly higher fungal burden, indicating a crucial contribution of γδ T cells to fungal control (Figure 4B). Consistently, mice lacking a functional IL-17 pathway owing to a genetic defect in the IL-17A- and IL-17F- or in

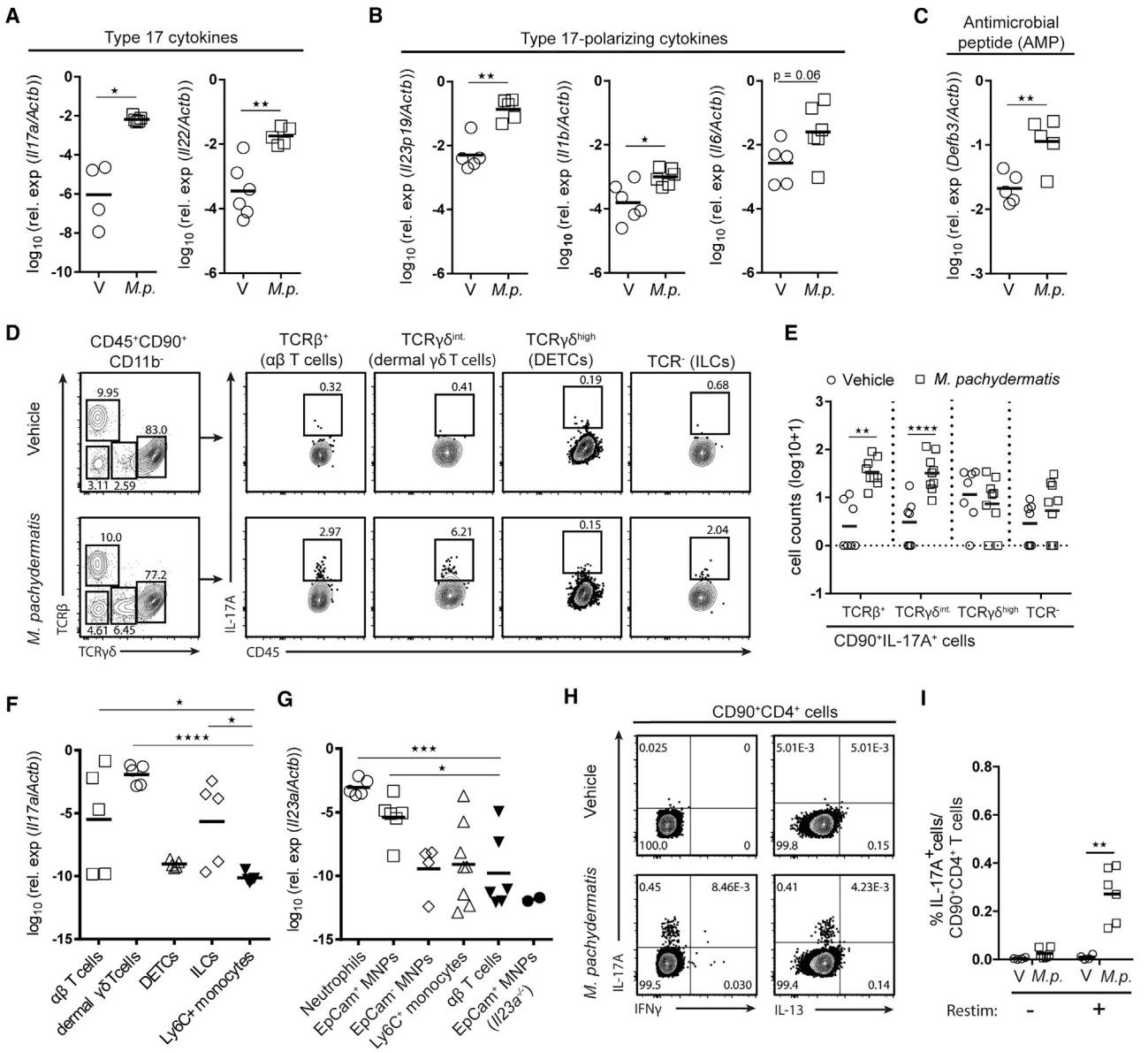


Figure 3. *Malassezia* Exposure of the Skin Results in a Selective Activation of the IL-17 Pathway

WT mice infected with *M. pachydermatis* (*M.p.*) or vehicle treated (V) after mild tape stripping of the dorsal ear skin.

(A–C) Expression of type 17 cytokine transcripts (A), type-17-polarizing cytokine transcripts (B), and antimicrobial peptide transcripts (C) in the ear skin on day 2 p.i.

(D and E) FACS gating strategy for αβ T cells, innate lymphoid cells (ILCs), dermal γδ T cells, and epidermal γδ T cells (DETCs) in the ear skin (D) and summary graph with absolute numbers of IL-17A$^+$ subsets per ear on day 2 p.i. (E). Plots in (D) represent concatenated samples from two ears each; numbers indicate the % of cells in each gate.

(F and G) *Il17a* (F) and *Il23a* transcripts (G) in the indicated cell populations sorted from the ear skin on day 2 p.i.

(H and I) IL-17A production by CD90$^+$CD4$^+$ T cells in the auricular lymph nodes on day 12 p.i.

Numbers in (H) indicate the % of cells in each quadrant.

In (A–C), (E–G), and (I), each symbol represents one animal. Graphs show pooled data from two to three independent experiments. The mean of each group is shown. Statistics were calculated using Student's t test or one-way ANOVA as appropriate. *p<0.05, **p<0.01, ***p<0.001, ****p<0.0001.

See also Figures S3, S4, and S5A–S5E.

IL-23-encoding genes, respectively, were unable to clear the fungus (Figure 4C). In contrast, IL-22, which is functionally related to IL-17A and IL-17F and which was also strongly induced in the *M. pachydermatis*-exposed skin (Figure 3A), was not required for the control of fungal colonization (Figure 4D). The defect in fungal control in the absence of a functional IL-17 pathway was underlined by the reduced expression of antimicrobial peptides, many of which were bearing antifungal activity

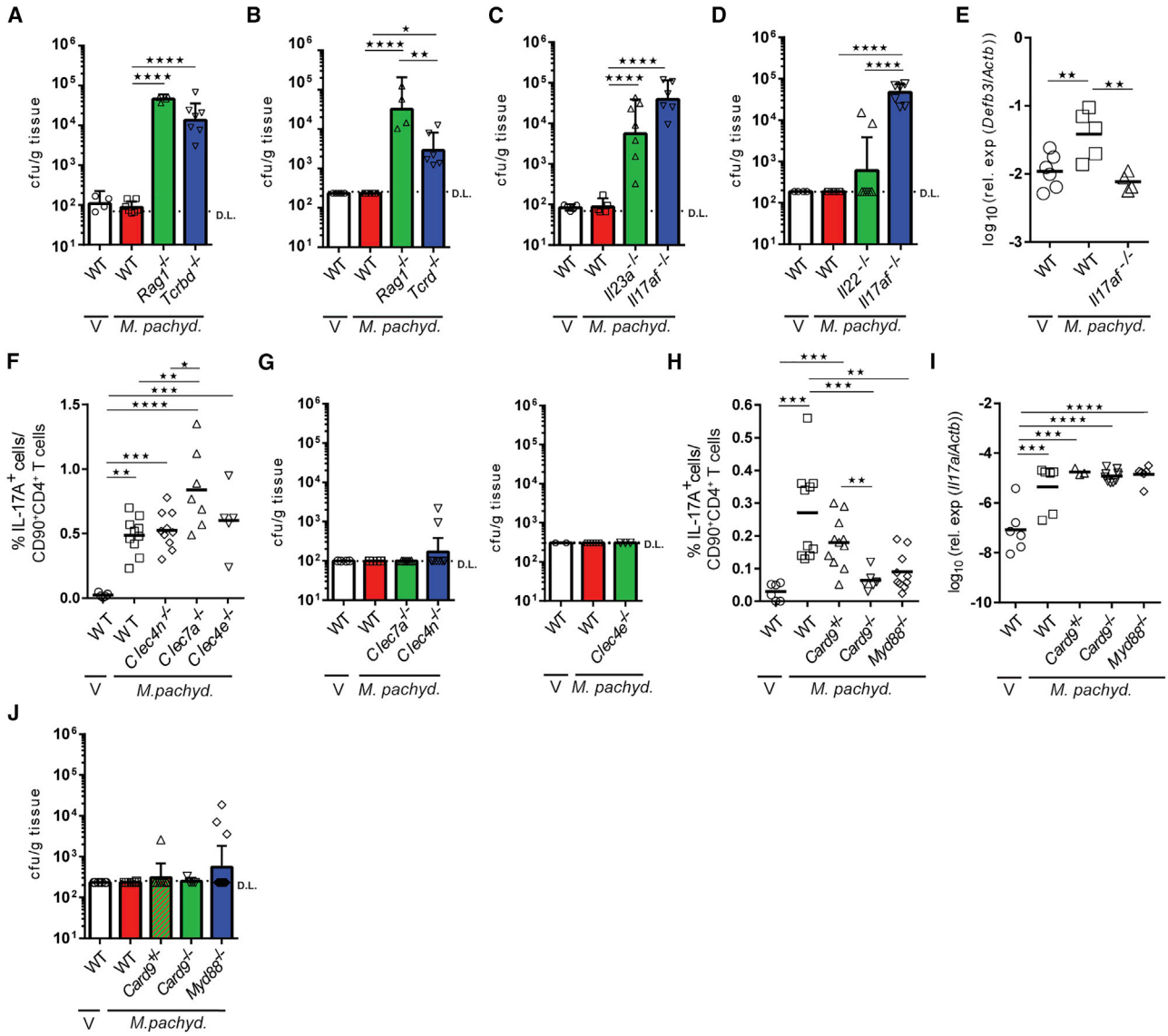


Figure 4. The IL-17 Pathway Is Critical for Preventing Uncontrolled Fungal Growth

(A–E) WT, *Rag1*$^{-/-}$ and *Tcrbd*$^{-/-}$ mice (A), WT, *Rag1*$^{-/-}$ and *Tcrd*$^{-/-}$ mice (B), WT, *Il23a*$^{-/-}$ and *Il17af*$^{-/-}$ mice (C), WT, *Il22*$^{-/-}$ and *Il17af*$^{-/-}$ mice (D) or WT and *Il17af*$^{-/-}$ mice (E) mildly tape stripped on the dorsal ear skin and infected with *M. pachydermatis* or vehicle treated (V). Fungal burden in the ear skin on day 12 p.i. (A–D). *Defb3* mRNA expression in the ear skin on day 2 p.i. (E).

(F–J) WT, *Clec7a*$^{-/-}$, *Clec4n*$^{-/-}$ and *Clec4e*$^{-/-}$, mice (F, G) or *Card9*$^{-/-}$, *Myd88*$^{-/-}$, and *Card9*$^{+/-}$ littermate control mice (H–J) mildly tape stripped on the dorsal ear skin and infected with *M. pachydermatis* or vehicle treated. IL-17A-production by CD90^{+}CD4^{+} T cells in the auricular lymph nodes on day 12 p.i. (F and H). Skin fungal burden on day 12 p.i. (G and J). *Il17a* mRNA expression in the ear skin on day 2 p.i. (I).

Each symbol represents one animal. In (E), (F), (H), and (I), the mean of each group is indicated. Graphs in (A–D), (G), and (J) show the geomean and 95% confidence interval. D.L., detection limit. All graphs show pooled data from two to three independent experiments. Statistics were calculated using one-way ANOVA. *p<0.05, **p<0.01, ***p<0.001, ****p<0.0001.

(Swidergall and Ernst, 2014), in the *Malassezia*-exposed skin of IL-17AF-deficient animals (Figure 4E). Together, these results demonstrate a critical role of the IL-23-IL-17 axis in cutaneous immunity against *Malassezia*.

The Role of C-type Lectin Receptor Signaling in the Host Response to *Malassezia* in the Mammalian Skin

C-type lectin receptor (CLR) family members are specialized in sensing fungal microbes and linking fungal recognition to the initiation of T cell responses, in particular those of the Th17 type (LeibundGut-Landmann et al., 2007). Mincle and Dectin-2 as well as the downstream signaling kinase Syk have previously been implicated in *Malassezia*-induced immune activation (Ishikawa et al., 2013; Kistowska et al., 2014; Yamasaki et al., 2009). However, mice lacking Mincle (*Clec4e*$^{-/-}$), Dectin-2 (*Clec4n*$^{-/-}$), or the prototypic CLR Dectin-1 (*Clec7a*$^{-/-}$) mice mounted a normal or even enhanced Th17 response to *M. pachydermatis* skin colonization if compared to their WT counterparts (Figure 4F). Likewise, fungal

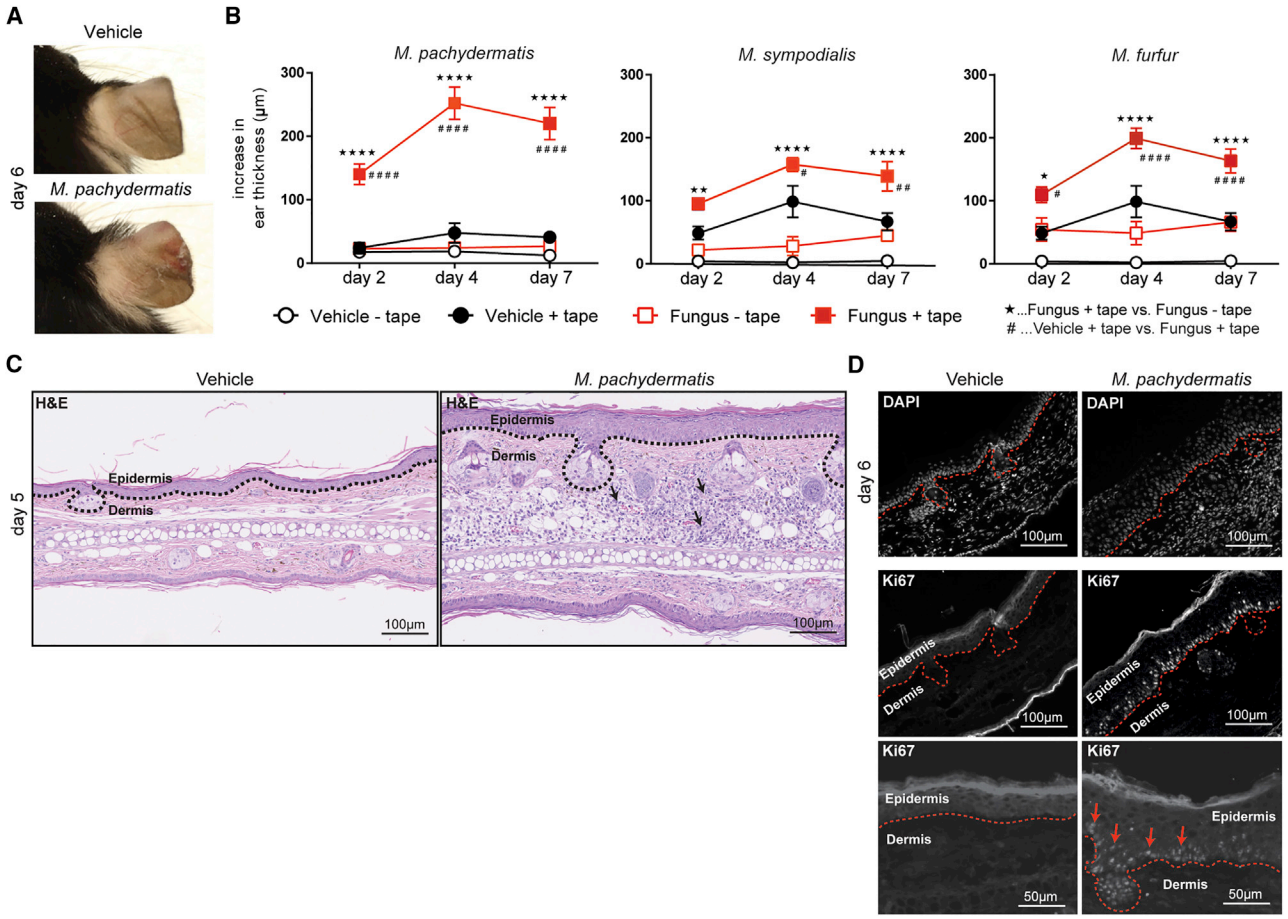


Figure 5. Epicutaneous Application of *Malassezia* spp. Promotes Inflammation in the Barrier-Disrupted Skin

WT mice mildly tape stripped on the dorsal ear skin and/or infected with *M. pachydermatis*, *M. sympodialis*, or *M. furfur* or vehicle treated (V).

(A) Macroscopic images of the dorsal ear on day 6 p.i.

(B) Increase in ear thickness over time. Graphs shows mean +/– SEM of two independent experiments with at least 3 mice per group each.

(C) Histology of ear sections stained with H&E on day 5 p.i. Arrows, leukocyte infiltrates; dotted line: basal membrane.

(D) Ear sections stained with DAPI or anti-Ki67 antibody as indicated on day 6 p.i. Bottom panels: increased magnification of anti-Ki67-stained sections. Arrows: $Ki67^{+}$ keratinocytes; dotted line: basal membrane.

Statistics were calculated using one-way ANOVA. Stars indicate the comparison of tape-stripped versus non-tape stripped groups; hashes indicate the comparison between vehicle-treated and *Malassezia* spp.-infected groups. $^{*/\#}p<0.05$, $^{**/\#\#}p<0.01$, $^{****/\#\#\#\#}p<0.0001$.

control was not impaired in any of the three receptor-deficient mouse lines (Figure 4G), indicating that none of the three CLRs on its own was essential for driving type 17 immunity and fungal control of *Malassezia* in the skin. Redundancy may however mask a partial contribution of individual receptors. Indeed, a broader abrogation of CLR signaling by genetic deletion of the common adaptor Card9 resulted in a severely impaired Th17 response to *Malassezia* (Figure 4H). In addition, the TLR-IL-1R signaling pathway also contributed critically to the induction of the antifungal Th17 response (Figure 4H). Interestingly and in contrast to the adaptive response, early IL-17 expression on day 2 p.i. was independent of Card9 and MyD88 in the *Malassezia*-exposed skin (Figure 4I) and consequently, fungal control was not compromised in the absence of Card9 or MyD88 (Figure 4J). Together, these results indicate a critical role of both the CLR and MyD88 pathway in the regulation of adaptive immunity to *Malassezia*.

Epicutaneous Application of *Malassezia* spp. Promotes Inflammation in the Barrier-Disrupted Skin

After having established the host protective principles that regulate *Malassezia* colonization in the skin, we aspired to explore the potential of the fungus to promote inflammation in our experimental system under AD-like conditions, which we mimicked by tape stripping of the skin prior to epicutaneous application of the fungus. While barrier disruption on its own induced only a mild inflammatory response, the addition of *Malassezia* strongly enhanced inflammation both macroscopically and microscopically (Figures 5A–5C). The ear skin of the barrier-disrupted mice was massively thickened upon exposure of any of the three tested *Malassezia* species if compared to the uninfected tape-stripped skin (Figures 5B and 5C) and was characterized by edema, inflammatory infiltrates throughout the ear tissue, and strong epithelial hyperplasia (Figures 5C and 5D). The increase in epithelial cell proliferation was confirmed by

Ki67 staining of keratinocytes in the *stratum basale* of the ear skin of *M. pachydermatis*-infected and tape-stripped animals (Figure 5D). The overall response peaked between day 4 and day 7 p.i. and thereby followed the kinetics of the fungal load in the skin, which had its maximum on days 2 to 4 p.i. and declined thereafter (Figure S1). This temporal discordance supported the idea that the inflammatory phenotype was secondary to the presence of the fungus and the antifungal response in the skin. Together, these results provide evidence that *Malassezia* spp. actively drive skin inflammation in the barrier-disrupted skin, promoting pathological features that resemble lesions in human AD.

Malassezia-Induced Skin Inflammation Is Driven by the Type 17 Pathway

Given the prominent induction of IL-17 and related cytokines by *Malassezia* spp., we hypothesized that the antifungal response might actively contribute to the inflammatory phenotype in the barrier-disrupted skin of colonized animals. Indeed, IL-17AF-deficiency curtailed the increase in skin thickening upon the application of *M. pachydermatis* to the barrier-disrupted skin (Figure 6A). The phenotype was even more strongly impaired in *Il23a*$^{-/-}$ compared to *Il17af*$^{-/-}$ mice (Figure 6A), suggesting that other IL-23-dependent factors may partially compensate for the lack of IL-17 in *Il17af*$^{-/-}$ mice. IL-22 was linked to AD before (Cavani et al., 2012; Gittler et al., 2012), and in our system, IL-22 was strongly induced in the *Malassezia*-exposed skin, irrespective of the presence or absence of IL-17A and IL-17F (Figure 6B). However, IL-22-deficient mice did not display a phenotype in our experimental system (Figure 6C). We therefore concluded that, in contrast to IL-17AF, IL-22 was not responsible for driving inflammation in the *Malassezia*-exposed, barrier-disrupted skin, although redundancy between IL-17AF and IL-22 cannot be excluded. In line with a lymphocytic source of IL-17 cytokines in the *Malassezia*-exposed skin, the lack of T cells, and in particular γδ T cells, also abolished *Malassezia*-induced skin inflammation (Figures 6D and 6E). In summary, our results indicate that the IL-23-IL-17 axis and γδ T cells play a central role in stimulating an aggravated inflammatory response and enhanced skin thickening in response to *Malassezia*.

Finally, we aimed at evaluating the impact of pre-existing T cell memory to *Malassezia*, as it exists in humans and dogs that are naturally colonized with the yeast, on promoting skin inflammation in our model. To generate a population of *Malassezia*-specific memory T cells, we applied *M. pachydermatis* onto the dorsal ear skin as described before. 5 weeks later, a time point at which the fungus was no longer detectable, we re-challenged the animals with the fungus via the same route. The presence of *Malassezia*-specific memory Th17 cells in the primed mice was evidenced by the rapid production of IL-17A by CD90^{+}CD4^{+} T cells following challenge infection, while during a primary infection, the response was not apparent earlier than 6 days p.i. (Figure 6F). Again, no IL-13 or IFN-γ production could be evidenced under these experimental conditions (Figure S5F). Importantly, the presence of *Malassezia*-specific memory T cells accelerated the kinetics of the inflammatory reaction to the fungus in the barrier-disrupted mouse skin (Figure 6G). Together, these data indicate that *Malassezia*-specific Th17 cells can promote the pathological skin inflammation under AD-like conditions.

Human *Malassezia*-Specific Memory T Cells from Healthy and Atopic Individuals Display a Th17 Phenotype

To corroborate the findings obtained in mice on the relevance of the IL-17 pathway in *Malassezia* immunity and *Malassezia*-driven skin inflammation, we turned to analyze the T cell response to the commensal yeast in humans. As a consequence of the continuous exposure of the barrier tissues to commensal microbes, the circulating pool of lymphocytes in humans comprises memory T helper cell populations with specificities toward these organisms (Acosta-Rodriguez et al., 2007). We initially analyzed the memory T cell compartment in healthy non-atopic individuals by sorting CD4^{+}CCR6^{+} and CD4^{+}CCR6^{-} memory T cells (containing Th17 and an untypical subset of Th1 cells termed Th1*, or Th1 and Th2 subsets, respectively [Sallusto, 2016]), CFSE-labeling and re-stimulating them with autologous monocytes that were pulsed with various species of *Malassezia*. Analysis of cell division by means of carboxyfluorescein succinimidyl ester (CFSE) dilution revealed proliferation of both CCR6^{+} and CCR6^{-} memory T cells in response to *Malassezia* spp., whereby the CCR6^{+} subset responded somewhat stronger under all conditions tested (Figures 7A and 7B). We then analyzed the cytokine production by *Malassezia*-responsive T cells by Luminex. The CCR6^{+} subset produced high amounts of IL-17A and IL-22 when stimulated with any of the three *Malassezia* species tested (Figure 7C). In addition, we detected IFN-γ and IL-5 secretion by the CCR6^{-} subset (Figure 7C). Re-stimulation of T cells with monocytes that were not pulsed with Ag or pulsed with heat-killed *C. albicans* served as negative and reference control, respectively (Figures S6A and S6B). A similar result was also obtained when analyzing cytokine production by intracellular cytokine staining and flow cytometry (Figure S7).

Next, we compared the T cell polarization profile of memory T cells from healthy individuals with that of AD patients. The frequency and cytokine response of *Malassezia*-responsive memory CD4^{+} T cells were increased in AD patients compared to non-atopic donors (Figure 7D). Consistent with the literature (Johansson et al., 2009; Valli et al., 2010), we found production of type 2 cytokines, which were derived predominantly from CCR6^{-} memory T cells (Figure 7E). Strikingly, the *Malassezia*-specific production of IL-17 and IL-22 was also increased in the memory T cell compartment from AD patients compared to healthy controls (Figure 7E). As expected, the IL-17 and IL-22 response was most pronounced in the CCR6^{+} subset. The increase in cytokine concentration appeared to be the result of an increase in the expansion of the overall *Malassezia*-specific T cell compartment (Figure 7D) as cytokine production on a per-cell basis was not altered in AD patients compared to healthy donors when cytokine-production was quantified by flow cytometry (Figure S7). Together, these data revealed a so far unrecognized contribution of IL-17 and related cytokines to the overall T cell response to *Malassezia* spp. in humans, both in healthy subjects and in AD patients, and thereby underpin the relevance of our findings from our experimental model of *Malassezia* colonization.

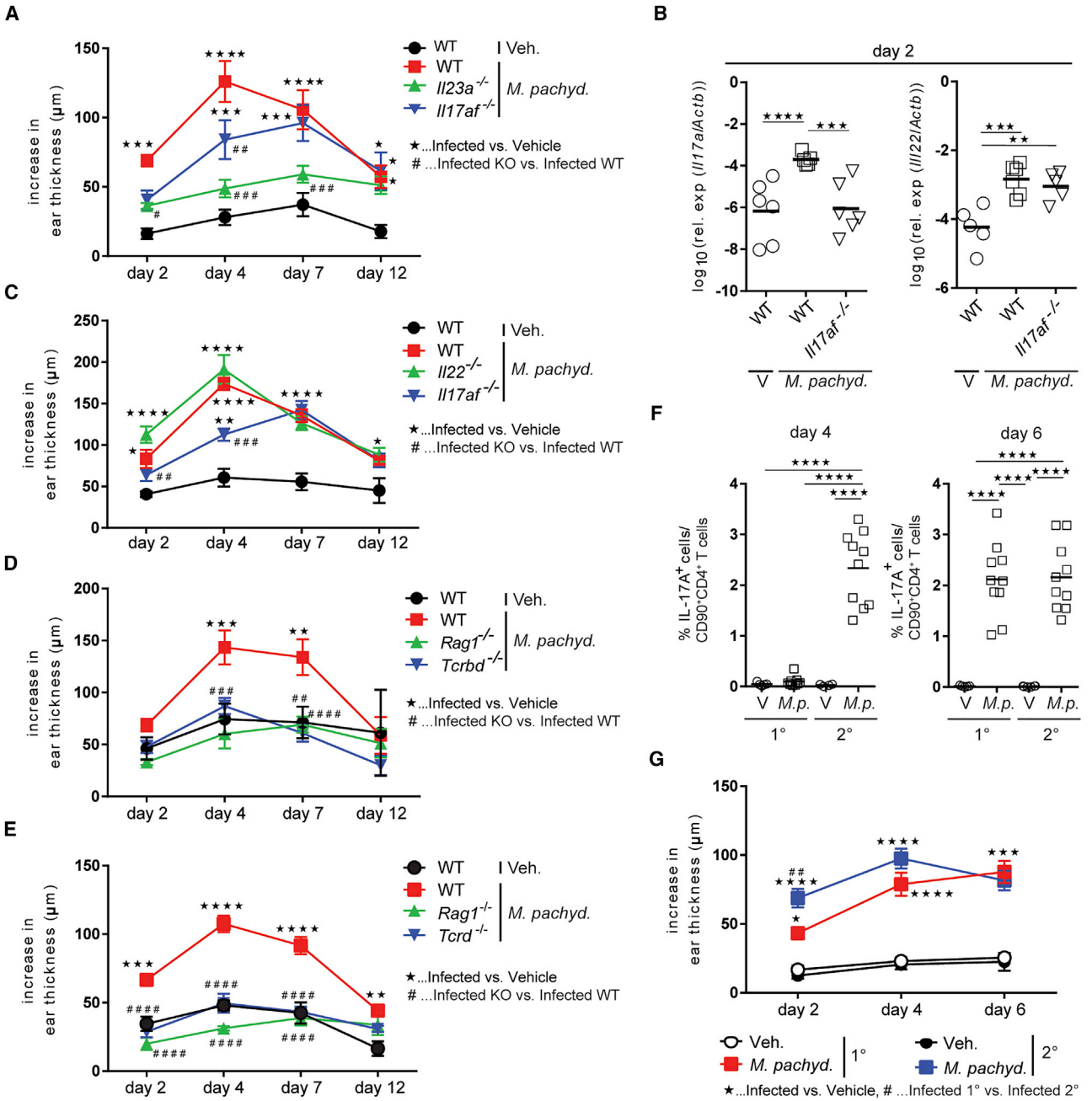


Figure 6. The IL-23-IL-17 Immune Axis Plays a Critical Role in Promoting Excessive Skin Inflammation

(A–E) WT, *Il23a*$^{-/-}$, and *Il17af*$^{-/-}$ mice (A, B), WT, *Il17af*$^{-/-}$, and *Il22*$^{-/-}$ mice (C), WT, *Rag1*$^{-/-}$, and *Tcrbd*$^{-/-}$ mice (D), or WT, *Rag1*$^{-/-}$, and *Tcrd*$^{-/-}$ mice (E) mildly tape stripped and infected with *M. pachydermatis* or vehicle treated (V). Increase in ear thickness over time (A, C, D, and E) and *Il17a* and *Il22* mRNA expression in the skin on day 2 p.i. (B).

(F and G) WT mice were primed with *M. pachydermatis* (2°) or left uninfected (1°) 6 weeks prior to (re-)infection. The ear skin was pretreated by tape stripping in all conditions. IL-17A production by CD90^{+}CD4^{+} T cells in the auricular lymph nodes 4 and 6 days after (re-)infection (F) and increase in ear thickness on days 2, 4, and 6 after (re-)infection (G).

In (B) and (F), each symbol represents one animal. Graphs show pooled data from two independent experiments; the mean of each group is indicated. Graphs in (A), (C–E), and (G) show the mean +/– SEM of each group with pooled data from 2 to 3 independent experiments with 4–5 mice per group. Statistics were calculated using one-way ANOVA. In (A) and (C–E), stars indicate the comparison of vehicle-treated and *M. pachydermatis*-infected groups; hashes indicate the comparison between infected knockout (KO) and infected WT groups. In (G), stars indicate the comparison of vehicle-treated and *M. pachydermatis*-infected groups; hashes indicate the comparison between 1° and 2° infected groups. $^{*/\#}p<0.05$, $^{**/\#\#}p<0.01$, $^{***/\#\#\#}p<0.001$, $^{****/\#\#\#\#}p<0.0001$.

See also Figure S5F.

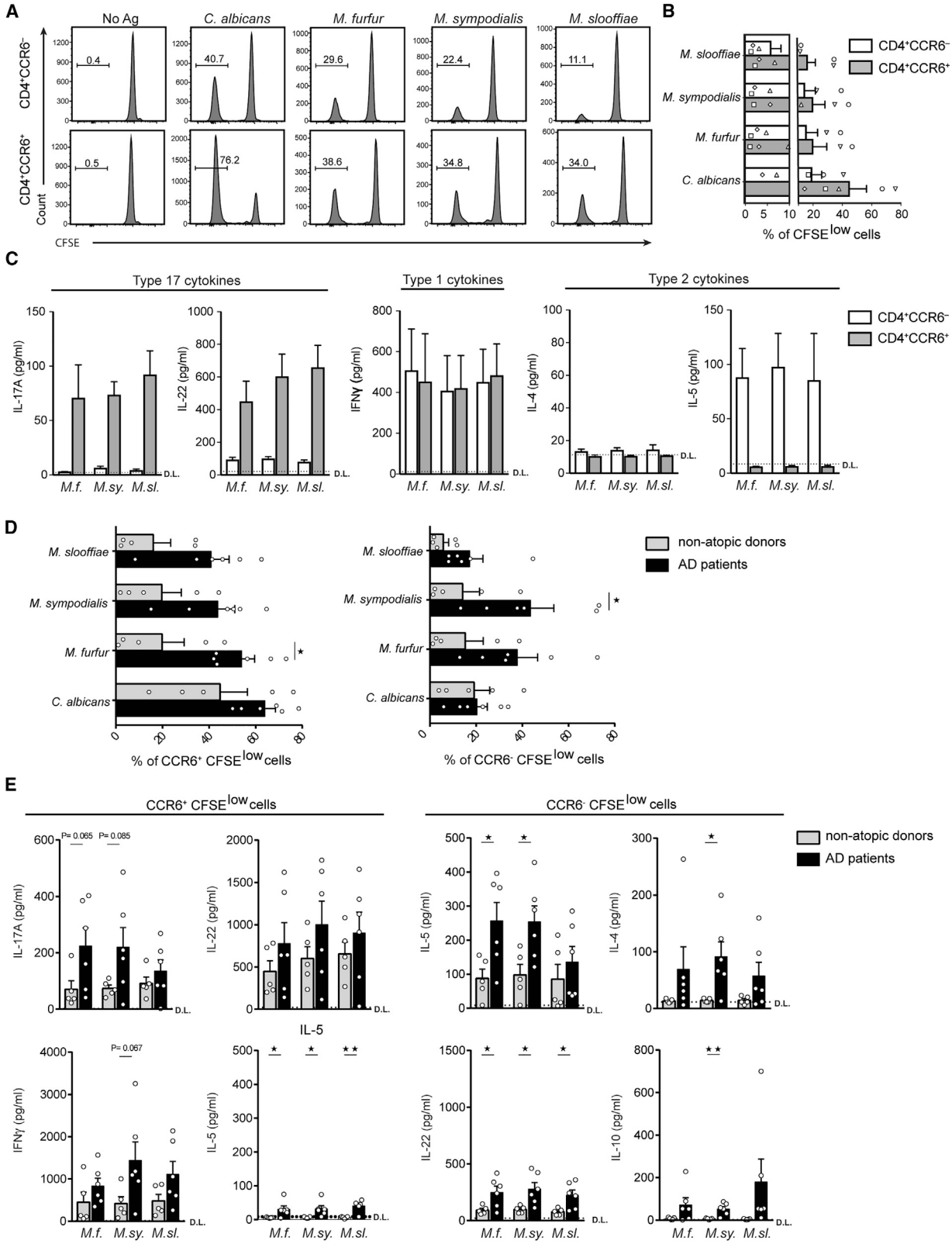


Figure 7. Human *Malassezia*-Specific Memory T Cells Display a Strong Th17 Signature

(A–C) CCR6$^+$ and CCR6$^-$ human memory CD4$^+$ T cells sorted from the peripheral blood of non-atopic individuals and co-cultured for 5 days with autologous monocytes that were pulsed with heat-killed *Malassezia* spp. Unpulsed monocytes and monocytes pulsed with heat-killed *C. albicans* served as controls.

(legend continued on next page)

DISCUSSION

Malassezia is by far the most abundant fungal commensal on the mammalian skin. Besides its commensal lifestyle, *Malassezia* can also mediate common skin diseases (Velegraki et al., 2015) and, beyond that, may be implicated in extracutaneous pathologies (Sokol et al., 2017). Despite its prevalence and clinical relevance, the yeast obtained little attention in the past, and it remains largely unknown how it contributes to immune homeostasis and disease. *Malassezia* continuously interacts with the host, but the complex interplay with the skin immune system is not well understood (Sparber and LeibundGut-Landmann, 2017). Our experimental model allowed us to study these aspects *in vivo* in the complex environment of the mammalian skin. We thereby revealed a distinct polarization of the *Malassezia*-specific immune response toward a type 17 profile, which was central for preventing uncontrolled fungal growth in the skin. Moreover, the IL-23-IL-17 axis promoted the inflammatory response in the barrier-disrupted skin, which mimics AD-like conditions. Consistent with the key role of the IL-17 pathway in the interaction of the skin immune system with *Malassezia*, we also identified a strong Th17 signature in human *Malassezia*-specific T cells.

Type 17 immunity is well known for its host-protective effects against fungal infections in barrier tissues, in particular those caused by *C. albicans*. This is evidenced most strikingly by inborn errors in genes involved in IL-17 signaling or IL-17 induction that lead to increased susceptibility to chronic mucocutaneous candidiasis. The IL-17 pathway is also associated with immunity against other fungal diseases, at least in preclinical settings including dermatophytosis (Burstein et al., 2018), pulmonary infections with dimorphic fungi (Wüthrich et al., 2011), and ocular mold infections (Taylor et al., 2014). Our findings highlight the relevance of type 17 immunity to the abundant mammalian skin commensal yeast *Malassezia*. Upon primary exposure of the murine skin to *Malassezia*, we observed a rapid induction of IL-17 expression. Reminiscent of what is known from other experimental models of fungal infection in mice (Conti et al., 2014; Gladiator et al., 2013; Hernández-Santos et al., 2018; Kagami et al., 2010; Kashem et al., 2015; Sparber et al., 2018), the initial peak of IL-17 expression by innate immune cells, in particular $\gamma\delta$ T cells, appears long before the adaptive immune system is fully activated. The swift activation of the innate immune system in our experimental model results in fungal elimination within $\sim$2 weeks p.i. Despite this important difference to the situation in naturally colonized hosts, the model allows delineating the key pathways that regulate the crosstalk between *Malassezia* spp. and the host.

Whether the IL-17 pathway also regulates fungal homeostasis in the human skin remains to be determined. The hypothesis is supported by a prominent population of Th17 cells within the *Malassezia*-specific memory T cell pool. So far, *Malassezia* overgrowth has not been reported in individuals bearing genetic defects in the IL-17 pathway. However, these individuals are very rare, and changes in *Malassezia* colonization density on the human skin may not become readily apparent if fungal loads are not determined in a quantitative manner. Moreover, increased fungal loads may not be directly associated with the emergence of disease symptoms. Changes in *Malassezia* colonization levels were correlated with the manifestation of AD in dogs (Cafarchia et al., 2005), but such a link remains uncertain in human AD (Chng et al., 2016; Darabi et al., 2009; Sandström Falk et al., 2005).

Our study revealed a dual role of IL-17 in the host response to *Malassezia*. Beyond its antifungal effect, IL-17 promotes inflammatory pathology in the *Malassezia*-colonized barrier-disrupted skin, and *Malassezia*-specific Th17 cells constitute a prominent subset among the overall *Malassezia*-specific T cell population in human AD patients. Previous studies analyzing the polarization of *Malassezia*-specific T cells in atopic individuals focused on type 2 immunity (Glatz et al., 2015), as allergic diseases have generally been regarded as Th2 driven. Consistent with Balaji et al. (2011), our results from humans and mice suggest the contribution of type 17 immunity to AD.

The potential of IL-17 in driving pathology in the skin is best understood in psoriasis, and targeting IL-17 in psoriatic patients has produced spectacular outcomes (Hawkes et al., 2017). The relevance of type 17 immunity in the pathogenesis of allergic diseases has been recognized more recently and appears to be of particular importance in some subtypes of AD (Cosmi et al., 2016; Esaki et al., 2016; Koga et al., 2008; Leonardi et al., 2015). The contribution of *Malassezia*-induced IL-17 to the manifestation of inflammatory skin pathology that we observed in our experimental model is reminiscent of the recently reported role of IL-17 in driving skin inflammation in response to *Staphylococcus aureus* (Liu et al., 2017; Nakagawa et al., 2017). *S. aureus* is the most well-known bacterial microbe associated with AD, and the prevalence rate of *S. aureus* colonization correlates with disease severity (Geoghegan et al., 2018). *S. aureus* toxins can trigger the production of IL-17 cytokines in experimentally infected mice, which in turn promotes cutaneous inflammation (Liu et al., 2017; Nakagawa et al., 2017). In contrast to the situation reported here with *Malassezia*, IL-17A and IL-17F were however not implicated in bacterial control (Nakagawa et al., 2017). Mechanistically, *S. aureus*-induced IL-17 production in the murine skin was shown to be initiated by keratinocyte-derived IL-1 and IL-36. Whether similar mechanisms regulate the IL-17 response to *Malassezia* remains to be determined. Factors beyond IL-17 cytokines also contribute to *Malassezia*-driven inflammation as indicated by our observation that the skin

Representative FACS plots (A) and summary graph (B) show the percentages of proliferating ($CFSE^{low}$) $CD4^+CCR6^-$ (upper row, gray bars) and $CD4^+CCR6^+$ T cells (lower row, white bars). (C) Type 17 (IL-17A and IL-22), type 1 (IFN-γ), and type 2 cytokines (IL-4 and IL-5) by $CD4^+CCR6^-$ (white bars) and $CD4^+CCR6^+$ T cells (gray bars). The mean + SEM of each group is indicated.

(D and E) Comparison of proliferation (D) and cytokine production (E) by *Malassezia* spp.-responsive $CCR6^+$ and $CCR6^-$ memory T cells from atopic patients (black bars) with those from non-atopic individuals (from A–C, gray bars). Each symbol represents one donor. Graphs show pooled data from 3 independent experiments with 5 donors per group. The mean + SEM of each group is indicated. Statistics were calculated using one-way ANOVA or unpaired Student's t test, as appropriate. *$p<0.05$, **$p<0.01$.

See also Figures S6 and S7.

phenotype was more severely curtailed in *Il23a*$^{-/-}$ animals than in *Il17af*$^{-/-}$ animals.

In humans, T cell dysregulation and a prevalent type 2 profile dominate the allergic response, and as such, *Malassezia*-specific Th2 cells are abundant in atopic individuals (Glatz et al., 2015). What initiates the transition from a Th17 response in healthy individuals to a mixed Th17-Th2 response in AD patients remains unknown. *Malassezia*-specific Th2 cells may emerge as a result of T cell plasticity, or they may be generated *de novo* in diseased individuals. Alternatively, the large pool of Th2 cells in AD patients may arise from selective expansion of *Malassezia*-specific Th2 cells that exist in small numbers in non-atopic individuals. The detailed analysis of the T cell repertoire in healthy individuals and in AD patients during flares and remission phases might provide valuable insights (Becattini et al., 2015).

Malassezia research was hampered in the past by the lack of adequate experimental systems. The establishment of an animal model represents a major advancement in the field. It opens the door for future explorations of fundamental principles of fungal-host interactions that contribute to homeostasis in the mammalian skin and of the mechanistic processes that control the balance between protective immunity and allergic inflammation, both in the intact skin and under conditions of barrier deficiency or Th2 polarization (Moosbrugger-Martinz et al., 2017), both of which represent key hallmarks of AD. Recent reports on the assembly and annotation of several *Malassezia* genomes (Gioti et al., 2013; Wu et al., 2015; Zhu et al., 2017) and the development of insertional and targeted mutagenesis in *Malassezia* (Ianiri et al., 2016, 2017) make the identification of fungal determinants that govern the interaction of the fungus with the host tangible. Our experimental model will facilitate the functional validation of such factors under diverse host conditions and thereby further promotes a comprehensive understanding of the *Malassezia*-host interplay.

STAR★METHODS

Detailed methods are provided in the online version of this paper and include the following:

- KEY RESOURCES TABLE
- CONTACT FOR REAGENT AND RESOURCE SHARING
- EXPERIMENTAL MODEL AND SUBJECT DETAILS
  - Ethic Statement
  - Animals
  - Fungal Strains
  - Experimental Model
  - Atopic Patients and Healthy Controls
- METHOD DETAILS
  - Isolation of Skin and Lymph Node Cells
  - *Ex Vivo* Murine T Cell Stimulation, Surface and Intracellular Staining
  - Flow Cytometry and Cell Sorting
  - RNA Isolation and Quantitative RT-PCR
  - Histochemistry and Immunofluorescence
  - Human Cell Sorting
  - *Ex Vivo* Human T Cell Stimulation, Surface and Intracellular Staining
- QUANTIFICATION AND STATISTICAL ANALYSIS
- DATA AND SOFTWARE AVAILABILITY

SUPPLEMENTAL INFORMATION

Supplemental Information can be found online at https://doi.org/10.1016/j.chom.2019.02.002.

ACKNOWLEDGMENTS

The authors would like to thank AD patients and healthy donors for blood donation; G.D. Brown, Y. Iwakura, J.-C. Reneault, C. Wells, B. Marsland, D. Sancho, and B. Becher for mice; J. Heitman and T. Boekhout for *Malassezia* strains; the staff of the Laboratory Animal Service Center of University of Zurich for animal husbandry; the Laboratory for Animal Model Pathology of University of Zurich and the Flow Cytometry Facility of University of Zurich for support; and members of the LeibundGut-lab for helpful advice and discussions. This work was supported by the University of Zürich and in part by the European Research Council (# 323183 PREDICT to F. Sallusto). F. Sallusto and the Institute for Research in Biomedicine are supported by the Helmut Horten Foundation. T.D. was funded by the Forschungskredit of the University of Zurich (# FK-17-044). The work in N.J.'s lab is supported by the Swiss National Science Foundation (# PP00P3_150663 to N.J.) and the European Research Council (# 677200 Immune Regulation to N.J.). The work in T.B.'s lab is supported by the Swiss Multiple Sclerosis Society and the Hertie Foundation (# P1150013).

AUTHOR CONTRIBUTIONS

Conceptualization, F. Sparber, F. Sallusto, and S.L.-L.; Methodology, F. Sparber, C.D.G., and T.D.; Investigation, F. Sparber, C.D.G., F.R.K., S.S., T.D., F.R., S.M., and S.L.-L.; Formal Analysis, F. Sparber and C.D.G.; Validation, F. Sparber and S.L.-L.; Resources, F.M.F., T.B., and I.P.; Visualization, F. Sparber; Project Administration, M.G. and S.L.-L.; Funding Acquisition, F. Sparber and S.L.-L.; Supervision, S.L.-L.; Writing – Original Draft, F. Sparber and S.L.-L.; Writing – Review & Editing, C.D.G., F. Sallusto, I.P., N.J., T.B., and M.G.

DECLARATION OF INTERESTS

The authors declare no competing interests.

Received: July 25, 2018
Revised: November 28, 2018
Accepted: February 5, 2019
Published: March 13, 2019

REFERENCES

Acosta-Rodriguez, E.V., Rivino, L., Geginat, J., Jarrossay, D., Gattorno, M., Lanzavecchia, A., Sallusto, F., and Napolitani, G. (2007). Surface phenotype and antigenic specificity of human interleukin 17-producing T helper memory cells. Nat. Immunol. *8*, 639–646.

Adachi, O., Kawai, T., Takeda, K., Matsumoto, M., Tsutsui, H., Sakagami, M., Nakanishi, K., and Akira, S. (1998). Targeted disruption of the MyD88 gene results in loss of IL-1- and IL-18-mediated function. Immunity *9*, 143–150.

Ashbee, H.R., and Bond, R. (2010). Malassezia species and immunity: host-pathogen interactions. In Malassezia and the Skin, Science., Clinical Practice, T. Boekhout, P. Mayser, E. Guého-Kellermann, and A. Velegraki, eds. (Springer), pp. 139–173.

Balaji, H., Heratizadeh, A., Wichmann, K., Niebuhr, M., Crameri, R., Scheynius, A., and Werfel, T. (2011). Malassezia sympodialis thioredoxin-specific T cells are highly cross-reactive to human thioredoxin in atopic dermatitis. J. Allergy Clin. Immunol. *128*, 92–99.e4.

Becattini, S., Latorre, D., Mele, F., Foglierini, M., De Gregorio, C., Cassotta, A., Fernandez, B., Kelderman, S., Schumacher, T.N., Corti, D., et al. (2015). T cell immunity. Functional heterogeneity of human memory CD4^{+} T cell clones primed by pathogens or vaccines. Science *347*, 400–406.

Becker, C., Dornhoff, H., Neufert, C., Fantini, M.C., Wirtz, S., Huebner, S., Nikolaev, A., Lehr, H.A., Murphy, A.J., Valenzuela, D.M., et al. (2006). Cutting edge: il-23 cross-regulates IL-12 production in T cell-dependent experimental colitis. J. Immunol. *177*, 2760–2764.

Belkaid, Y., and Tamoutounour, S. (2016). The influence of skin microorganisms on cutaneous immunity. Nat. Rev. Immunol. *16*, 353–366.

Bond, R., Guillot, J., and Cabañes, F.J. (2010). Malassezia yeasts in animal disease. In Malassezia and the Skin: Science and Clinical Practice, T. Boekhout, P. Mayser, E. Guého-Kellermann, and A. Velegraki, eds. (Springer), pp. 271–299.

Burstein, V.L., Guasconi, L., Beccacece, I., Theumer, M.G., Mena, C., Prinz, I., Cervi, L., Herrero, M., Masih, D.T., and Chiapello, L.S. (2018). IL-17-mediated immunity controls skin infection and T Helper 1 response during experimental Microsporum canis dermatophytosis. J. Invest. Dermatol. *138*, 1744–1753.

Cabañes, F.J. (2014). Malassezia yeasts: how many species infect humans and animals? PLoS Pathog. *10*, e1003892.

Cabanillas, B., and Novak, N. (2016). Atopic dermatitis and filaggrin. Curr. Opin. Immunol. *42*, 1–8.

Cafarchia, C., Gallo, S., Romito, D., Capelli, G., Chermette, R., Guillot, J., and Otranto, D. (2005). Frequency, body distribution, and population size of Malassezia species in healthy dogs and in dogs with localized cutaneous lesions. J. Vet. Diagn. Invest. *17*, 316–322.

Casagrande, B.F., Flückiger, S., Linder, M.T., Johansson, C., Scheynius, A., Crameri, R., and Schmid-Grendelmeier, P. (2006). Sensitization to the yeast Malassezia sympodialis is specific for extrinsic and intrinsic atopic eczema. J. Invest. Dermatol. *126*, 2414–2421.

Cavani, A., Pennino, D., and Eyerich, K. (2012). Th17 and Th22 in skin allergy. Chem. Immunol. Allergy *96*, 39–44.

Chng, K.R., Tay, A.S., Li, C., Ng, A.H., Wang, J., Suri, B.K., Matta, S.A., McGovern, N., Janela, B., Wong, X.F., et al. (2016). Whole metagenome profiling reveals skin microbiome-dependent susceptibility to atopic dermatitis flare. Nat. Microbiol. *1*, 16106.

Ciardo, D.E., Schär, G., Böttger, E.C., Altwegg, M., and Bosshard, P.P. (2006). Internal transcribed spacer sequencing versus biochemical profiling for identification of medically important yeasts. J. Clin. Microbiol. *44*, 77–84.

Conti, H.R., Peterson, A.C., Brane, L., Huppler, A.R., Hernández-Santos, N., Whibley, N., Garg, A.V., Simpson-Abelson, M.R., Gibson, G.A., Mamo, A.J., et al. (2014). Oral-resident natural Th17 cells and γδ T cells control opportunistic Candida albicans infections. J. Exp. Med. *211*, 2075–2084.

Conti, H.R., Shen, F., Nayyar, N., Stocum, E., Sun, J.N., Lindemann, M.J., Ho, A.W., Hai, J.H., Yu, J.J., Jung, J.W., et al. (2009). Th17 cells and IL-17 receptor signaling are essential for mucosal host defense against oral candidiasis. J. Exp. Med. *206*, 299–311.

Cosmi, L., Liotta, F., and Annunziato, F. (2016). Th17 regulating lower airway disease. Curr. Opin. Allergy Clin. Immunol. *16*, 1–6.

Cossarizza, A., Chang, H.D., Radbruch, A., Akdis, M., Andrä, I., Annunziato, F., Bacher, P., Barnaba, V., Battistini, L., Bauer, W.M., et al. (2017). Guidelines for the use of flow cytometry and cell sorting in immunological studies. Eur. J. Immunol. *47*, 1584–1797.

Darabi, K., Hostetler, S.G., Bechtel, M.A., and Zirwas, M. (2009). The role of Malassezia in atopic dermatitis affecting the head and neck of adults. J. Am. Acad. Dermatol. *60*, 125–136.

Esaki, H., Brunner, P.M., Renert-Yuval, Y., Czarnowicki, T., Huynh, T., Tran, G., Lyon, S., Rodriguez, G., Immaneni, S., Johnson, D.B., et al. (2016). Early-onset pediatric atopic dermatitis is TH2 but also TH17 polarized in skin. J. Allergy Clin. Immunol. *138*, 1639–1651.

Findley, K., Oh, J., Yang, J., Conlan, S., Deming, C., Meyer, J.A., Schoenfeld, D., Nomicos, E., Park, M., et al.; NIH Intramural Sequencing Center Comparative Sequencing Program (2013). Topographic diversity of fungal and bacterial communities in human skin. Nature *498*, 367–370.

Flohr, C., and Yeo, L. (2011). Atopic dermatitis and the hygiene hypothesis revisited. Curr. Probl. Dermatol. *41*, 1–34.

Fuertes Marraco, S.A., Grosjean, F., Duval, A., Rosa, M., Lavanchy, C., Ashok, D., Haller, S., Otten, L.A., Steiner, Q.G., Descombes, P., et al. (2012). Novel murine dendritic cell lines: a powerful auxiliary tool for dendritic cell research. Front. Immunol. *3*, 331.

Gemmer, C.M., DeAngelis, Y.M., Theelen, B., Boekhout, T., and Dawson, T.L., Jr. (2002). Fast, noninvasive method for molecular detection and differentiation of Malassezia yeast species on human skin and application of the method to dandruff microbiology. J. Clin. Microbiol. *40*, 3350–3357.

Geoghegan, J.A., Irvine, A.D., and Foster, T.J. (2018). Staphylococcus aureus and atopic dermatitis: a complex and evolving relationship. Trends Microbiol. *26*, 484–497.

Gioti, A., Nystedt, B., Li, W., Xu, J., Andersson, A., Averette, A.F., Münch, K., Wang, X., Kappauf, C., Kingsbury, J.M., et al. (2013). Genomic insights into the atopic eczema-associated skin commensal yeast Malassezia sympodialis. mBio *4*, e00572–12.

Gittler, J.K., Shemer, A., Suárez-Fariñas, M., Fuentes-Duculan, J., Gulewicz, K.J., Wang, C.Q., Mitsui, H., Cardinale, I., de Guzman Strong, C., Krueger, J.G., et al. (2012). Progressive activation of T(H)2/T(H)22 cytokines and selective epidermal proteins characterizes acute and chronic atopic dermatitis. J. Allergy Clin. Immunol. *130*, 1344–1354.

Gladiator, A., Wangler, N., Trautwein-Weidner, K., and LeibundGut-Landmann, S. (2013). Cutting edge: il-17-secreting innate lymphoid cells are essential for host defense against fungal infection. J. Immunol. *190*, 521–525.

Glatz, M., Bosshard, P.P., Hoetzenecker, W., and Schmid-Grendelmeier, P. (2015). The role of Malassezia spp. in atopic dermatitis. J. Clin. Med. *4*, 1217–1228.

Gueho, E., Simmons, R.B., Pruitt, W.R., Meyer, S.A., and Ahearn, D.G. (1987). Association of Malassezia pachydermatis with systemic infections of humans. J. Clin. Microbiol. *25*, 1789–1790.

Guillot, J., and Guého, E. (1995). The diversity of Malassezia yeasts confirmed by rRNA sequence and nuclear DNA comparisons. Antonie Leeuwenhoek *67*, 297–314.

Haas, J.D., Ravens, S., Düber, S., Sandrock, I., Oberdörfer, L., Kashani, E., Chennupati, V., Föhse, L., Naumann, R., Weiss, S., et al. (2012). Development of interleukin-17-producing γδ T cells is restricted to a functional embryonic wave. Immunity *37*, 48–59.

Hawkes, J.E., Chan, T.C., and Krueger, J.G. (2017). Psoriasis pathogenesis and the development of novel targeted immune therapies. J. Allergy Clin. Immunol. *140*, 645–653.

Hernández-Santos, N., Wiesner, D.L., Fites, J.S., McDermott, A.J., Warner, T., Wüthrich, M., and Klein, B.S. (2018). Lung epithelial cells coordinate innate lymphocytes and immunity against pulmonary fungal infection. Cell Host Microbe *23*, 511–522.e5.

Holzmann, S., Tripp, C.H., Schmuth, M., Janke, K., Koch, F., Saeland, S., Stoitzner, P., and Romani, N. (2004). A model system using tape stripping for characterization of Langerhans cell-precursors in vivo. J. Invest. Dermatol. *122*, 1165–1174.

Ianiri, G., Applen Clancey, S., Lee, S.C., and Heitman, J. (2017). FKBP12-dependent inhibition of calcineurin mediates immunosuppressive antifungal drug action in Malassezia. MBio *8*.

Ianiri, G., Averette, A.F., Kingsbury, J.M., Heitman, J., and Idnurm, A. (2016). Gene function analysis in the ubiquitous human commensal and pathogen Malassezia genus. MBio *7*.

Iliev, I.D., and Leonardi, I. (2017). Fungal dysbiosis: immunity and interactions at mucosal barriers. Nat. Rev. Immunol. *17*, 635–646.

Ishikawa, T., Itoh, F., Yoshida, S., Saijo, S., Matsuzawa, T., Gonoi, T., Saito, T., Okawa, Y., Shibata, N., Miyamoto, T., et al. (2013). Identification of distinct ligands for the C-type lectin receptors Mincle and Dectin-2 in the pathogenic fungus Malassezia. Cell Host Microbe *13*, 477–488.

Itohara, S., Mombaerts, P., Lafaille, J., Iacomini, J., Nelson, A., Clarke, A.R., Hooper, M.L., Farr, A., and Tonegawa, S. (1993). T cell receptor delta gene mutant mice: independent generation of alpha beta T cells and programmed rearrangements of gamma delta TCR genes. Cell *72*, 337–348.

Johansson, C., Ahlborg, N., Andersson, A., Lundeberg, L., Karlsson, M.A., Scheynius, A., and Tengvall Linder, M. (2009). Elevated peripheral allergen-

specific T cell response is crucial for a positive atopy patch test reaction. Int. Arch. Allergy Immunol. *150*, 51–58.

Johansson, C., Eshaghi, H., Linder, M.T., Jakobson, E., and Scheynius, A. (2002). Positive atopy patch test reaction to Malassezia furfur in atopic dermatitis correlates with a T helper 2-like peripheral blood mononuclear cells response. J. Invest. Dermatol. *118*, 1044–1051.

Johansson, C., Tengvall Linder, M., Aalberse, R.C., and Scheynius, A. (2004). Elevated levels of IgG and IgG4 to Malassezia allergens in atopic eczema patients with IgE reactivity to Malassezia. Int. Arch. Allergy Immunol. *135*, 93–100.

Kagami, S., Rizzo, H.L., Kurtz, S.E., Miller, L.S., and Blauvelt, A. (2010). IL-23 and IL-17A, but not IL-12 and IL-22, are required for optimal skin host defense against Candida albicans. J. Immunol. *185*, 5453–5462.

Kashem, S.W., Riedl, M.S., Yao, C., Honda, C.N., Vulchanova, L., and Kaplan, D.H. (2015). Nociceptive sensory fibers drive interleukin-23 production from CD301b+ dermal dendritic cells and drive protective cutaneous immunity. Immunity *43*, 515–526.

Kistowska, M., Fenini, G., Jankovic, D., Feldmeyer, L., Kerl, K., Bosshard, P., Contassot, E., and French, L.E. (2014). Malassezia yeasts activate the NLRP3 inflammasome in antigen-presenting cells via Syk-kinase signalling. Exp. Dermatol. *23*, 884–889.

Koga, C., Kabashima, K., Shiraishi, N., Kobayashi, M., and Tokura, Y. (2008). Possible pathogenic role of Th17 cells for atopic dermatitis. J. Invest. Dermatol. *128*, 2625–2630.

Kreymborg, K., Etzensperger, R., Dumoutier, L., Haak, S., Rebollo, A., Buch, T., Heppner, F.L., Renauld, J.C., and Becher, B. (2007). IL-22 is expressed by Th17 cells in an IL-23-dependent fashion, but not required for the development of autoimmune encephalomyelitis. J. Immunol. *179*, 8098–8104.

LeibundGut-Landmann, S., Gross, O., Robinson, M.J., Osorio, F., Slack, E.C., Tsoni, S.V., Schweighoffer, E., Tybulewicz, V., Brown, G.D., Ruland, J., et al. (2007). Syk- and CARD9-dependent coupling of innate immunity to the induction of T helper cells that produce interleukin 17. Nat. Immunol. *8*, 630–638.

Leonardi, S., Cuppari, C., Manti, S., Filippelli, M., Parisi, G.F., Borgia, F., Briuglia, S., Cannavò, P., Salpietro, A., Arrigo, T., et al. (2015). Serum interleukin 17, interleukin 23, and interleukin 10 values in children with atopic eczema/dermatitis syndrome (AEDS): association with clinical severity and phenotype. Allergy Asthma Proc. *36*, 74–81.

Li, H., Goh, B.N., Teh, W.K., Jiang, Z., Goh, J.P.Z., Goh, A., Wu, G., Hoon, S.S., Raida, M., Camattari, A., et al. (2018). Skin commensal Malassezia globosa secreted protease attenuates Staphylococcus aureus biofilm formation. J. Invest. Dermatol. *138*, 1137–1145.

Li, J., Vinh, D.C., Casanova, J.L., and Puel, A. (2017). Inborn errors of immunity underlying fungal diseases in otherwise healthy individuals. Curr. Opin. Microbiol. *40*, 46–57.

Liu, H., Archer, N.K., Dillen, C.A., Wang, Y., Ashbaugh, A.G., Ortines, R.V., Kao, T., Lee, S.K., Cai, S.S., Miller, R.J., et al. (2017). Staphylococcus aureus epicutaneous exposure drives skin inflammation via IL-36-Mediated T cell responses. Cell Host Microbe *22*, 653–666.e5.

Mombaerts, P., Clarke, A.R., Rudnicki, M.A., Iacomini, J., Itohara, S., Lafaille, J.J., Wang, L., Ichikawa, Y., Jaenisch, R., and Hooper, M.L. (1992a). Mutations in T-cell antigen receptor genes alpha and beta block thymocyte development at different stages. Nature *360*, 225–231.

Mombaerts, P., Iacomini, J., Johnson, R.S., Herrup, K., Tonegawa, S., and Papaioannou, V.E. (1992b). RAG-1-deficient mice have no mature B and T lymphocytes. Cell *68*, 869–877.

Moosbrugger-Martinz, V., Schmuth, M., and Dubrac, S. (2017). A mouse model for atopic dermatitis using topical application of vitamin D3 or of its analog MC903. Methods Mol. Biol. *1559*, 91–106.

Nakagawa, S., Matsumoto, M., Katayama, Y., Oguma, R., Wakabayashi, S., Nygaard, T., Saijo, S., Inohara, N., Otto, M., Matsue, H., et al. (2017). Staphylococcus aureus Virulent PSMalpha peptides induce keratinocyte Alarmin release to orchestrate IL-17-dependent skin inflammation. Cell Host Microbe *22*, 667–677.e5.

Odds, F.C., Brown, A.J., and Gow, N.A. (2004). Candida albicans genome sequence: a platform for genomics in the absence of genetics. Genome Biol. *5*, 230.

Picelli, S., Faridani, O.R., Björklund, A.K., Winberg, G., Sagasser, S., and Sandberg, R. (2014). Full-length RNA-seq from single cells using Smart-seq2. Nat. Protoc. *9*, 171–181.

Prohic, A., Jovovic Sadikovic, T., Krupalija-Fazlic, M., and Kuskunovic-Vlahovljak, S. (2016). Malassezia species in healthy skin and in dermatological conditions. Int. J. Dermatol. *55*, 494–504.

Russel, W.M.S., and Burch, R.L. (1959). The Principles of Humane Experimental Technique (Methuen & Co.).

Saijo, S., Ikeda, S., Yamabe, K., Kakuta, S., Ishigame, H., Akitsu, A., Fujikado, N., Kusaka, T., Kubo, S., Chung, S.H., et al. (2010). Dectin-2 recognition of alpha-mannans and induction of Th17 cell differentiation is essential for host defense against Candida albicans. Immunity *32*, 681–691.

Sallusto, F. (2016). Heterogeneity of human CD4(+) T cells against microbes. Annu. Rev. Immunol. *34*, 317–334.

Sandström Falk, M.H., Tengvall Linder, M., Johansson, C., Bartosik, J., Bäck, O., Särnhult, T., Wahlgren, C.F., Scheynius, A., and Faergemann, J. (2005). The prevalence of Malassezia yeasts in patients with atopic dermatitis, seborrhoeic dermatitis and healthy controls. Acta Derm. Venereol. *85*, 17–23.

Saunders, C.W., Scheynius, A., and Heitman, J. (2012). Malassezia fungi are specialized to live on skin and associated with dandruff, eczema, and other skin diseases. PLoS Pathog. *8*, e1002701.

Sokol, H., Leducq, V., Aschard, H., Pham, H.P., Jegou, S., Landman, C., Cohen, D., Liguori, G., Bourrier, A., Nion-Larmurier, I., et al. (2017). Fungal microbiota dysbiosis in IBD. Gut *66*, 1039–1048.

Sparber, F., Dolowschiak, T., Mertens, S., Lauener, L., Clausen, B.E., Joller, N., Stoitzner, P., Tussiwand, R., and LeibundGut-Landmann, S. (2018). Langerin+ DCs regulate innate IL-17 production in the oral mucosa during Candida albicans-mediated infection. PLoS Pathog. *14*, e1007069.

Sparber, F., and LeibundGut-Landmann, S. (2017). Host responses to Malassezia spp. in the mammalian skin. Front. Immunol. *8*, 1614.

Sugita, T., Boekhout, T., Velegraki, A., Guillot, J., Hadina, S., and Cabanes, F.J. (2010). Epidemiology of Malassezia-related skin diseases. In Malassezia and the Skin, T. Boekhout, E. Guého, P. Mayser, and A. Velegraki, eds. (Springer-Verlag), pp. 65–119.

Swidergall, M., and Ernst, J.F. (2014). Interplay between Candida albicans and the antimicrobial peptide armory. Eukaryot. Cell *13*, 950–957.

Taylor, P.R., Leal, S.M., Jr., Sun, Y., and Pearlman, E. (2014). Aspergillus and Fusarium corneal infections are regulated by Th17 cells and IL-17-producing neutrophils. J. Immunol. *192*, 3319–3327.

Taylor, P.R., Tsoni, S.V., Willment, J.A., Dennehy, K.M., Rosas, M., Findon, H., Haynes, K., Steele, C., Botto, M., Gordon, S., et al. (2007). Dectin-1 is required for beta-glucan recognition and control of fungal infection. Nat. Immunol. *8*, 31–38.

Valli, J.L., Williamson, A., Sharif, S., Rice, J., and Shewen, P.E. (2010). In vitro cytokine responses of peripheral blood mononuclear cells from healthy dogs to distemper virus, Malassezia and Toxocara. Vet. Immunol. Immunopathol. *134*, 218–229.

Velegraki, A., Cafarchia, C., Gaitanis, G., Iatta, R., and Boekhout, T. (2015). Malassezia infections in humans and animals: pathophysiology, detection, and treatment. PLoS Pathog. *11*, e1004523.

Weidinger, S., and Novak, N. (2016). Atopic dermatitis. Lancet *387*, 1109–1122.

Wells, C.A., Salvage-Jones, J.A., Li, X., Hitchens, K., Butcher, S., Murray, R.Z., Beckhouse, A.G., Lo, Y.L., Manzanero, S., Cobbold, C., et al. (2008). The macrophage-inducible C-type lectin, mincle, is an essential component of the innate immune response to Candida albicans. J. Immunol. *180*, 7404–7413.

Williams, M.R., and Gallo, R.L. (2015). The role of the skin microbiome in atopic dermatitis. Curr. Allergy Asthma Rep. *15*, 65.

Wu, G., Zhao, H., Li, C., Rajapakse, M.P., Wong, W.C., Xu, J., Saunders, C.W., Reeder, N.L., Reilman, R.A., Scheynius, A., et al. (2015). Genus-wide

comparative genomics of Malassezia delineates its phylogeny, physiology, and niche adaptation on human skin. PLoS Genet. *11*, e1005614.

Wüthrich, M., Gern, B., Hung, C.Y., Ersland, K., Rocco, N., Pick-Jacobs, J., Galles, K., Filutowicz, H., Warner, T., Evans, M., et al. (2011). Vaccine-induced protection against 3 systemic mycoses endemic to North America requires Th17 cells in mice. J. Clin. Invest. *121*, 554–568.

Yamasaki, S., Matsumoto, M., Takeuchi, O., Matsuzawa, T., Ishikawa, E., Sakuma, M., Tateno, H., Uno, J., Hirabayashi, J., Mikami, Y., et al. (2009). C-type lectin Mincle is an activating receptor for pathogenic fungus, Malassezia. Proc. Natl. Acad. Sci. U S A *106*, 1897–1902.

Zhu, Y., Engström, P.G., Tellgren-Roth, C., Baudo, C.D., Kennell, J.C., Sun, S., Billmyre, R.B., Schröder, M.S., Andersson, A., Holm, T., et al. (2017). Proteogenomics produces comprehensive and highly accurate protein-coding gene annotation in a complete genome assembly of Malassezia sympodialis. Nucleic Acids Res. *45*, 2629–2643.

STAR★METHODS

KEY RESOURCES TABLE

REAGENT or RESOURCE	SOURCE	IDENTIFIER
Antibodies		
Alexa Fluor 700 Anti-mCD45.2 (104)	Biolegend	Cat# 109821, RRID: AB_493730
PeCy7 Anti-mCD11b (M1/70)	Thermo Fisher	Cat# 25-0112-81, RRID: AB_469587
APC Anti-mCD11c (N418)	Biolegend	Cat# 117309, RRID: AB_313778
Pacific Blue Anti-mMHCII (M5/114.15.2)	Biolegend	Cat# 107619, RRID: AB_493528
BV510 Anti-mLy6C (HK1.4)	Biolegend	Cat# 128033, RRID: AB_2562351
FITC Anti-mLy6G (1A8)	Biolegend	Cat# 127605, RRID: AB_1236488
PE Anti-mSiglecF (E50-2440)	BD Bioscience	Cat# 552126, RRID: AB_394341
FITC Anti-mCD3 (145-2C11)	Biolegend	Cat# 100305, RRID: AB_312670
Pacific Blue Anti-mCD4 (RM4-5)	Biolegend	Cat# 100534, RRID: AB_493375
PeCy7 Anti-mIL-17A (TC11-18H10.1)	Biolegend	Cat# 506921, RRID: AB_2125011
APC Anti-mIFNγ (XMG1.2)	Biolegend	Cat# 505809, RRID: AB_315403
eFluor 610 Anti-mIL-13 (eBio13A)	Thermo Fisher	Cat# 61-7133-82, RRID: AB_2574654
Alexa Fluor 488 Anti-mKi67 (16A8)	Biolegend	Cat# 652417, RRID: AB_256423
Alexa Fluor 488 Anti-mCD11b (M1/70)	Biolegend	Cat# 101219, RRID: AB_493545
BV570 Anti-mCD90 (30-H12)	Biolegend	Cat# 105329, RRID: AB_10917055
PeCy7 Anti-mTCRγδ (GL3)	Biolegend	Cat# 118123, RRID: AB_11203530
APC Anti-mTCRβ (H57-597)	Biolegend	Cat# 109211, RRID: AB_313434
Alexa fluor 647 Anti-mLangerin (929F3.01)	Dendritics	Cat# DDX0362A647-100, RRID: AB_1148741
Qdot 655 Anti-hCD45RA (MEM-56)	Thermo Fisher	Cat# Q10069, RRID: AB_2556451
PE Texas Red Anti-hCD4 (S3.5)	Thermo Fisher	Cat# MHCD0417, RRID: AB_10371766
PECy5 Anti-hCD8 (B9.11)	Beckman Coulter	Cat# A07758, RRID: AB_2713928
PECy5 Anti-hCD14 (RMO52)	Beckman Coulter	Cat# A07765, RRID: AB_2621824
PECy5 Anti-hCD16 (3G8)	Beckman Coulter	Cat# A07767
PECy5 Anti-hCD19 (J3-119)	Beckman Coulter	Cat# A07771
PECy5 Anti-hCD25 (B1.49.9)	Beckman Coulter	Cat# IM2646, RRID: AB_131142
PECy5 Anti-hCD56 (N901)	Beckman Coulter	Cat# A07789, RRID: AB_1575976
PE Anti-hCCR6 (11A9)	BD Bioscience	Cat# 561019, RRID: AB_10565962
BV421 Anti-hCCR7 (G043H7)	Biolegend	Cat# 353207, RRID: AB_10915137
Pacific Blue Anti-hICOS (C398.4A)	Biolegend	Cat# 313521, RRID: AB_10895762
BV785 Anti-hCD25 (BC96)	Biolegend	Cat# 302637, RRID: AB_11219197
PECy7 Anti-hIL-10 (JES3-9D7)	Biolegend	Cat# 501419, RRID: AB_2280292
PE Anti-hIL-9 (MH9A4)	Biolegend	Cat# 507604, RRID: AB_315486
BV650 Anti-hIFN-γ (4S.B3)	Biolegend	Cat# 502537, RRID: AB_11126140
BV605 Anti-hIL-17A (BL168)	Biolegend	Cat# 512325, RRID: AB_11218595
APC Anti-hIL-4 (MP4-25D2)	BD Bioscience	Cat# 554486, RRID: AB_398562
Percp-eFluor 710 Anti-hIL-22 (22URTI)	Thermo Fisher	Cat# 46-7229-42, RRID: AB_10596639
hCD4 magnetic microbeads	Milteny	Cat# 130-045-101
hCD14 magnetic microbeads	Milteny	Cat# 130-050-201
Biological Samples		
Human peripheral blood samples from healthy donors	Department of Dermatology, University Hospital Zurich	N/A
Human peripheral blood samples from atopic patients	Department of Dermatology, University Hospital Zurich	N/A
Human Serum (5%)	Swiss Red Cross	N/A

(*Continued on next page*)

Continued

REAGENT or RESOURCE	SOURCE	IDENTIFIER
Fetal Calve Serum	Bioconcept	Cat# 2-01F10-I
Chemicals, Peptides, and Recombinant Proteins		
Phosphate Buffered Salt Solutions (PBS, 1x)	Amimed/Bioconcept	Cat# 3-05F39
RPMI 1640	Life Technologies	Cat# 21875034
2-Mercaptoethanol	Life Technologies	Cat# 31350-010
EDTA (0.5M, pH 8)	Life Technologies	Cat# AM9260G
Hanks Buffered Salt Solution (HBSS, 1x)	Life Technologies	Cat# 14175-053
Brefeldin A	Sigma-Aldrich	Cat# B6542-25MG
DNAse I	Sigma-Aldrich	Cat# DN25-100MG
Collagenase I	Life Technologies	Cat# 17100017
Liberase TM	Roche	Cat# 05401119001
TRI Reagent	Sigma-Aldrich	Cat# T9424-100ML
SYBR Green	Roche	Cat# 04913914001
Revert Aid Transcriptase	Thermo Fisher	Cat# EP0451
SuperScript II Reverse Transcriptase Kit	Thermo Fisher	Cat# 18064014
LIVE/DEAD Near IR Dead cell Stain Kit	Thermo Fisher	Cat# L10119
LIVE/DEAD Aqua Dead Cell Stain Kit	Thermo Fisher	Cat# L34957
BD Cytofix/Cytoperm reagent	BD Bioscience	Cat# 554714
Paraformaldehyde	Sigma-Aldrich	Cat# P6148-500G
Ficoll-Plaque PLUS	GE Healthcare	Cat# 17144002
L-Glutamine	Thermo Fisher	Cat# X0550-100
Penicillin/Streptomycin	Amimed/Bioconcept	Cat# 4-01F00-H
Phorbol 12-myristate 13-acetate (PMA)	Sigma-Aldrich	Cat# P8139
Ionomycin	Sigma-Aldrich	Cat# I0634-1MG
O.C.T. compound	Tissue-TEK	Cat# 4583
Methanol	Merck	Cat# 1.06009.2500
Nonidet P40	Axonlab	Cat# A1694,0250
Malt extract	Sigma-Aldrich	Cat# 70167-500G
Glycerol (99%)	Honeywell	Cat# 10314830
Ox-bile	Sigma-Aldrich	Cat# 70168-100G
Tween-40	Sigma-Aldrich	Cat# P1504-100ML
Peptone	Oxoid	Cat# LP0037
Oleic Acid	Sigma-Aldrich	Cat#75090-5ML
Native Olive Oil	Commerc. available	N/A
Agar	Sigma-Aldrich	Cat# A1296-1KG
Ketasol	Graeub AG	Lot# 6680416
Rompun (2%)	Bayer	Lot# KP0BFHR
Calcofluor White	Sigma-Aldrich	Cat# 18909-100ML-F
Deposited Data		
Raw and analyzed data	This paper	Zenodo: https://doi.org/10.5281/zenodo.2577503
Experimental Models: Cell Lines		
MutuDC1940 cells	Hans Acha-Orbea, University of Lausanne (Fuertes Marraco et al., 2012)	N/A
Experimental Models: Organisms/Strains		
Mouse: WT: C57BL/6JRj	Janvier Elevage	C57BL/6JRj
Mouse: *Rag1*$^{-/-}$: B6.129S7-Rag1^{tm1Mom}/J	Swiss Immunological Mouse Repository (SwImMR) hosted by the University of Zurich, (Mombaerts et al., 1992b)	MGI: 1857241

(*Continued on next page*)

Continued

REAGENT or RESOURCE	SOURCE	IDENTIFIER
Mouse: *TCRd*$^{-/-}$: B6;129P2- TCRd^{tm1Mom}	Burkhard Becher, University of Zurich, (Itohara et al., 1993)	MGI: 1857257
Mouse: *TCRbd*$^{-/-}$: B6;129P2-TCRb^{tm1Mom} x TCRd^{tm1Mom}	Swiss Immunological Mouse Repository (SwImMR) hosted by the University of Zurich, (Itohara et al., 1993; Mombaerts et al., 1992a)	MGI: 1857256, MGI: 1857257
Mouse: *Il23a*$^{-/-}$: B6.129-IL23^{tm1Gdy}	Burkhard Becher, University of Zurich, (Becker et al., 2006)	MGI: 3625894
Mouse: *Il17af*$^{-/-}$: C57BL/6.Il17a/Il17f$^{tm1.1Impr}$	Hannover Medical School (Haas et al., 2012)	MGI: 5438791, MGI: 5438793
Mouse: *Il22*$^{-/-}$: C57BL/6.Il22^{tm1Jcrd}	Burkard Becher, University of Zurich, (Kreymborg et al., 2007)	MGI: 4453827
Mouse: *Clec4e*$^{-/-}$: C57BL/6.Clec4e$^{tm1.1Cfg}$	David Sancho (CNIC), (Wells et al., 2008)	MGI: 5052164
Mouse: *Clec4n*$^{-/-}$: C57BL/6.Clec4n^{tm1Yiw}	Benjamin Marsland, University of Lausanne, (Saijo et al., 2010)	MGI: 4459637
Mouse: *Clec7a*$^{-/-}$: C57BL/6.Clec7a^{tmGdb}	Benjamin Marsland, University of Lausanne, (Taylor et al., 2007)	MGI: 3695710
Mouse: *Myd88*$^{-/-}$: C57BL/6.Myd88^{tm1Ak}	Swiss Immunological Mouse Repository (SwImMR) hosted by the University of Zurich, (Adachi et al., 1998)	MGI: 2385681
Mouse: *Card9*$^{-/-}$: C57BL/6-Card9^{em1ThBu}	Thorsten Buch University of Zurich (unpublished data)	N/A
M. pachydermatis: strain ATCC 14522	ATCC (Guillot and Guého, 1995)	ATCC 14522, CBS 1879
M. sympodialis: strain ATCC 42132	Joseph Heitman, Duke University (Gueho et al., 1987)	ATCC 42132, M1154/77
M. furfur: strain JPLK23	Joseph Heitman, Duke University (Guillot and Guého, 1995)	JPLK23
M. sympodialis: clinical isolate	this report	N/A
M. slooffiae: clinical isolate	this report	N/A
C. albicans: strain SC5314	(Odds et al., 2004)	SC5314
Oligonucleotides		
See Table S1		N/A
Software and Algorithms		
GraphPad Prism V6	GraphPad	www.graphpad.com
NDP.view2.	Hamamatsu	U12388-01, www.hamamatsu.com
FlowJo V10	FlowJo LLC	www.flowjo.com
Other		
Gallios Flow Cytometer	Beckman Coulter	www.beckmancoulter.com
FACS Aria III	BD Bioscience	www.bdbiosciences.com
FlexMAP 3D	Luminex	www.luminexcorp.com
NanoZoomer 2.0-HT	Hamamatsu	www.hamamatsu.com
Transpore Hypoallergic Tape	3M	Cat# 1527-1
Oditest 0-5mm measurement device	KROEPLIN	Cat# S0247
BD Calibrite Beads	BD Bioscience	Cat# 349502

CONTACT FOR REAGENT AND RESOURCE SHARING

Further information and requests for resources and reagents should be directed to and will be fulfilled by the Lead Contact, Salomé LeibundGut-Landmann (salome.leibundgut-landmann@uzh.ch). *Il17af*$^{-/-}$ (Hannover Medical School), *Il22*$^{-/}$ (Ludwig Cancer Research Brussels), *Clec4n*$^{-/-}$ (The Tokyo University of Science) and *Clec4e*$^{-/-}$ (The University of Melbourne) mice as well as the DC^{1940} cell line (University of Lausanne) were obtained via an MTA between the University of Zurich and the respective entities.

EXPERIMENTAL MODEL AND SUBJECT DETAILS

Ethic Statement

All mouse experiments in this study were conducted in strict accordance with the guidelines of the Swiss Animals Protection Law and were performed under the protocols approved by the Veterinary office of the Canton Zurich, Switzerland (license number 183/2015). All efforts were made to minimize suffering and ensure the highest ethical and humane standards according to the 3R principles (Russel and Burch, 1959). Samples from humans comprised blood samples and skin swabs. Those samples were collected from volunteers after informed consent. Sampling of humans was approved by the ethics committee of the Canton Zurich (ID 2016-00301).

Animals

WT C57BL/6j mice were purchased by Janvier Elevage. *Rag1*$^{-/-}$ (Mombaerts et al., 1992b), *TCRd*$^{-/-}$ (Itohara et al., 1993), *TCRbd*$^{-/-}$ (Itohara et al., 1993; Mombaerts et al., 1992a), *Il23a*$^{-/-}$ (Becker et al., 2006), *Il17af*$^{-/-}$ (Haas et al., 2012), *Il22*$^{-/-}$ (Kreymborg et al., 2007), *Clec4e*$^{-/-}$ ((Wells et al., 2008), kindly obtained from David Sancho), *Card9*$^{-/-}$ (Ferreira and Buch, unpublished data) and *Myd88*$^{-/-}$ (Adachi et al., 1998) mice were maintained and bred at the Institute of Laboratory Animals Science (LASC - University of Zurich, Zurich, Switzerland). *Clec4n*$^{-/-}$ (Saijo et al., 2010) *and Clec7a*$^{-/-}$ (Taylor et al., 2007) were kindly obtained from Benjamin Marsland (University of Lausanne, Switzerland). All mice were on the C57BL/6 background. The animals were kept in specific pathogen-free conditions and used at 6-12 weeks of age in sex- and age-matched groups. Female as well as male mice were used for experiments. Vehicle-treated and infected animals were kept separately to avoid cross-contamination. No *Malassezia* was detected by culture or PCR in our colony of mice under SPF conditions prior to infection.

Fungal Strains

The *M. pachydermatis* strain ATCC 14522 (= CBS 1879, (Guillot and Guého, 1995)) was purchased from ATCC. *M. sympodialis* strain ATCC 42132 (Gueho et al., 1987) and *M. furfur* strain JPLK23 (=CBS 14141, (Guillot and Guého, 1995)) were obtained from Joseph Heitman (Duke University, Durham). *M. sympodialis* and *M. slooffiae* clinical isolates for re-stimulation of human T cells were collected from AD patients at the Department of Dermatology, University Hospital Zurich, Switzerland and identified by ITS sequencing (Ciardo et al., 2006).

Experimental Model

For infection experiments with mice, *Malassezia* spp. were grown for 3-4 days at 30°C, 180 rpm in liquid modified Dixon medium (for 500 ml liquid medium: 18 g Malt Extract (Sigma Aldrich), 10 g desiccated Ox-bile (Sigma Aldrich), 5 ml Tween-40 (Sigma Aldrich), 3 g Peptone (Oxoid), 1 ml Glycerol (Honeywell), 1 ml Oleic Acid (Sigma Aldrich)). Cells were washed in PBS and suspended in olive oil (native olive oil extra, SPAR) at a density of 20 OD_{A600}/ml. 100 µl suspension (corresponding to 2 OD_{A600}) of yeast cells was applied topically onto the dorsal ear skin while mice were anaesthetized. In some experiments, the dorsal ear skin was disrupted by mild tape stripping (Transpore™ Hypoallergenic, 3M; 5 rounds per ear). Ear thickness was monitored prior and after infection using the Oditest S0247 0-5 mm measurement device (KROEPLIN). For determination of fungal loads in the skin, tissue was transferred in aqua dest. supplemented with 0.05 % Nonidet P40 (AxonLab), homogenized and plated on modified Dixon agar and incubated at 30°C for 3-4 days.

Atopic Patients and Healthy Controls

Blood from adult healthy (non-atopic) donors (3F, 2M; age 27y - 54y) and adult atopic individuals (4F, 2M; age 23y - 50y) was obtained at the Department of Dermatology of the University Hospital of Zurich. The female-male distribution was random as gender does not play a role in AD. All samples were anonymized. Healthy (non-atopic) status of individuals was defined as personal and family history without atopic diseases, such as allergic rhinitis, asthma or AD; and a negative skin prick test with 20 seasonal and perennial inhalant allergens. Atopy in individuals was defined as a positive personal history of atopic diseases and a skin prick test positive for at least one of the tested inhalant allergens.

METHOD DETAILS

Isolation of Skin and Lymph Node Cells

For digestion of total ear skin, ears were removed, cut into small pieces and transferred into Hank's medium (Ca^{2+}- and Mg^{2+}-free, Life Technology), supplemented with Liberase TM (0.15 mg/ml, Roche) and DNase I (0.12 mg/ml, Sigmar-Aldrich) and incubated for 1 hour at 37 °C. The cell suspension was filtered through a 40 µm cell strainer (Falcon) and rinsed with PBS supplemented with 5 mM ETDA (Life Technologies) and 1% FCS. Auricular lymph nodes were manually shredded using fine scissors and digested with DNAse I (2.4mg/ml Sigma-Aldrich) and Collagenase I (2.4mg/ml, Roche) in PBS for 20 min at 37°C. The cell suspension was filtered through a 40 µm cell strainer (Falcon) and rinsed with PBS supplemented with 5 mM ETDA (Life Technologies) and 1 % FCS.

Ex Vivo Murine T Cell Stimulation, Surface and Intracellular Staining

For *in vitro* stimulation of T cells, 1x10^6 auricular lymph node cells were co-cultured for 6 hours with 1 x 10^5 MutuDC1940 cells (Fuertes Marraco et al., 2012), pulsed with 2.5x10^5/ml heat-killed *Malassezia* spp. Unpulsed MutuDC1940 cells served as negative

control. Brefeldin A (10 μg/ml, Sigma-Aldrich) was added for the last 5 hours. After stimulation cells were surface stained, fixed and permeabilized with Cytofix/Cytoperm (BD Biosciences) and then stained for cytokine expression using the antibodies listed in the Key Resources Table.

Flow Cytometry and Cell Sorting

Single cell suspensions of skin and lymph nodes were stained in PBS supplemented with 1% FSC, 5mM EDTA and 0.02% NaN_3. LIVE/DEAD Near IR stain (Life Technologies) was used for exclusion of dead cells. The antibodies for surface and intracellular cytokine staining are listed in the Key Resources Table. For intracellular cytokine staining, cells were fixed and permeabilized using BD Cytofix/Cytoperm reagent (BD Bioscience) and subsequently incubated in Perm/Wash buffer (BD Bioscience). All extracellular and intracellular staining steps were carried out on ice. Cells were acquired on a FACS Gallios (Beckman Coulter) and the data were analyzed with FlowJo software (FlowJo LLC). The gating of the flow cytometric data was performed according to the guidelines for the use of flow cytometry and cell sorting in immunological studies (Cossarizza et al., 2017), including pre-gating on viable and single cells for analysis. Absolute cell numbers of myeloid and lymphoid cell populations were calculated based on a defined number of counting beads (BD Bioscience, Calibrite Beads), which were added to the samples before flow cytometric acquisition.

For sorting, single cell suspensions of ear skin were stained in PBS supplemented with 1% FSC and 5mM EDTA with antibodies listed in the Key Resources Table. Using a FACS Aria III, 50 target cells per cell population were sorted in individual wells of a 96-well plate (Eppendorf) containing RLT Plus RNeasy® lysis buffer (Qiagen). Lysates were snap-frozen and stored at -80°C until further processing.

RNA Isolation and Quantitative RT-PCR

Isolation of total RNA from ear skin was carried out according to standard protocols using TRI Reagent® (Sigma Aldrich). cDNA was generated by RevertAid reverse transcriptase (Thermo Fisher). For RNA isolation from sorted cells, the Smart-Seq2 protocol was applied as described (Picelli et al., 2014). Briefly, Agencourt RNAClean XP paramagnetic beads (Beckman Coulter) in combination with a DynaMag-96 side skirted magnet (Thermo Fisher) were applied to purify whole-genome RNA. Subsequently cDNA was generated using the SuperScript II Reverse Transcriptase Kit (Thermo Fisher), and further amplified with HiFi HotStart PCR Mix (KAPA Biosystems). For DNA clean-up, Agencourt AMPure XP beads (Beckman Coulter) were used as above. Quantitative PCR was performed using SYBR Green (Roche) and a QuantStudio 7 Flex (Life Technologies) instrument. The primers used for qPCR are listed in Table S1. All qRT-PCR assays were performed in duplicate and the relative expression (rel. expr.) of each gene was determined after normalization to β-actin transcript levels.

Histochemistry and Immunofluorescence

For histology, tissue was fixed in 4% PBS-buffered paraformaldehyde overnight and embedded in paraffin. Sagittal sections (9μm) were stained with Periodic-acidic Schiff (PAS) reagent and counterstained with Haematoxilin or with Haematoxylin-Eosin (H&E) and mounted with Pertex (Biosystem, Switzerland) according to standard protocols. For immunofluorescence staining, tissues were embedded in Tissue-TEK O.C.T compound (VWR International GmbH, Switzerland), snap frozen in liquid nitrogen and stored at -20°C. Sagittal cryo-sections (9 μm) were cut and mounted to super frost glass slides (Thermo Scientific). The specimen was allowed to dry at room temperature and were fixed either with methanol at -20°C for 20 minutes or with acetone a room temperature for 10 minutes. The following antibodies were used: anti-CD11b (M1/70, Biolegend) and anti-Ki67 (16A8, Biolegend). Alternatively, the specimen was stained with Calcofluor white (CFW, Sigmar Aldrich) diluted in Tris-HCl (0.1 M pH 9, 10 μg/ml final concentration) for 20 min on RT. The stained specimens were washed with aqua dest. and mounted with Mowiol and stored at 4°C. All images were acquired with a digital slide scanner (NanoZoomer 2.0-HT, Hamamatsu) and analyzed with NDP.view2.

Human Cell Sorting

Blood from healthy donors and atopic individuals was obtained from the Allergy Unit of the Department of Dermatology of the University Hospital of Zurich. Peripheral blood mononuclear cells (PBMCs) were isolated by Ficoll-Paque Plus (GE Healthcare) density gradient. Total $CD4^+$ T cells and monocytes were isolated by positive selection using CD4 and CD14 magnetic microbeads (Miltenyi Biotech), respectively. Memory $CD4^+CCR6^+$ and $CD4^+CCR6^-$ T cell subsets were sorted after exclusion of naïve T cells ($CD45RA^+CCR7^+$) and of $CD8^+CD14^+CD16^+CD19^+CD25^+CD56^+$ cells. The monoclonal antibodies used for FACS are listed in the Key Resources Table. Cells were sorted with FACSAria III (BD Biosciences).

Ex Vivo Human T Cell Stimulation, Surface and Intracellular Staining

For human T cell re-stimulation experiments, *Malassezia* spp. were grown in liquid modified Dixon medium as described above. *C. albicans* strain SC5314 (Odds et al., 2004) was grown in YNB-S medium for 18 hours at 30°C, 180 rpm starting at a density of OD_{600} = 0.1. The yeast cells were washed in PBS and heat-inactivated at 65°C for 30 minutes. The medium used for co-culture was RPMI 1640 supplemented with 2 mM glutamine, 1% non-essential amino acids, 1% sodium pyruvate, 1% penicillin/streptomycin (all from Life Technologies) and 5% of human serum (Swiss Red Cross). Sorted T cells were labeled with carboxyfluorescein succinimidyl ester (CFSE) and cultured at a ratio of 2:1 with irradiated autologous monocytes pre-pulsed for 3-5 hours with heat killed *M. furfur*, *M. sympodialis* or *M. slooffiae* that are frequently isolated from our cohort of AD patients. As control, some cultures were stimulated with heat-killed *C. albicans*. The ratio used for the human T cell *ex vivo* stimulation assay was 3 yeast particles per

monocyte. At day 5 culture supernatants were collected and cytokines (IFN-γ, IL-4, IL-5, IL-10, IL-17A and IL-22) were measured by cytometric bead arrays on FlexMAP 3D (Luminex). To measure proliferation and cytokine production and the single cell level, cultured cells were directly analyzed by FACS or stimulated with Phorbol 12-myristate 13-acetate (PMA) and Ionomycin (both from Sigma-Aldrich) for 5 hours with addition of Brefeldin A (Sigma-Aldrich) for the last 2.5 hours of stimulation. After stimulation, cells were surface stained, fixed and permeabilized with Cytofix/Cytoperm (BD Biosciences) and then stained for cytokine expression using the antibodies listed in the Key Resources Table.

QUANTIFICATION AND STATISTICAL ANALYSIS

For quantification of skin cell populations by flow cytometry, cell numbers were transformed using the formula Y = y(log10) or Y = y(log10 + 1) in case of lymphocyte enumeration. Bars of each data set indicate the arithmetic mean. For cfu data plotted on a logarithmic scale, the geomean and 95% confidence intervals are shown. RT-qPCR data were log-transformed and the mean of each group is indicated. In summary plots showing cfu data, quantification of flow cytometry data analysis and RT-qPCR data, each symbol represents an individual mouse. Ear thickness is shown as mean +/- SEM. Data are pooled from at least 2 independent experiments or are representative of at least 2 independent experiments with 3 to 5 animals per group. For human data, graphs show pooled data from all samples included in this study and analyzed on separate days. The mean + SEM of each group is indicated. The study design did not include randomization or blinding. Statistical significance was determined by unpaired Student's-test with Welch correction for multiple comparison, one-way or two-way ANOVA with Tukey's multiple comparison test as appropriate using GraphPad Prism software. Outlier calculation for mouse data was performed with the Grubbs' method. Significance is indicated as follows: $^{*/\#}$ $p< 0.05$; $^{**/\#\#}$ $p<0.01$; $^{***/\#\#\#}$ $p<0.001$; $^{****/\#\#\#\#}$ $p<0.0001$.

DATA AND SOFTWARE AVAILABILITY

All raw and analyzed data have been deposited in Zenodo under https://doi.org/10.5281/zenodo.2577503.

Cell Host & Microbe, Volume *25*

Supplemental Information

The Skin Commensal Yeast *Malassezia* Triggers a Type 17 Response that Coordinates Anti-fungal Immunity and Exacerbates Skin Inflammation

Florian Sparber, Corinne De Gregorio, Simone Steckholzer, Filipa M. Ferreira, Tamas Dolowschiak, Fiorella Ruchti, Florian R. Kirchner, Sarah Mertens, Immo Prinz, Nicole Joller, Thorsten Buch, Martin Glatz, Federica Sallusto, and Salomé LeibundGut-Landmann

SUPPLEMENTAL FIGURES AND TABLES

Figure S1 (related to Figure 1): Kinetics of *Malassezia* colonization after experimental skin infection. Fungal burden in the ear skin of *Malassezia* spp.-infected and vehicle-treated WT mice on day 2, 4, 7 and 12 post infection. The skin was tape-stripped prior to the infection. Each dot represents one animal. Graphs show pooled data from two independent experiments. The same vehicle-treated animals were used as control for *M. sympodialis*- and *M. furfur*-infected mice for each time point. The geomean and 95% confidence interval of each group is indicated. D.L., detection limit. Statistics were calculated using unpaired Student's T-Test.*p<0.05, **p<0.01, *** p<0.001, **** p<0.0001.

Figure S2 (related to Figure 2): Early recruitment of inflammatory leukocytes upon *Malassezia* infection is independent of skin barrier disruption. Myeloid cell populations in the ear skin were quantified by flow cytometry on day 2 post infection. Total leukocytes, neutrophils, monocytes, eosinophils and dendritic cells/macrophages were defined as shown in Figure 2. Summary graphs show the percentage of cell subsets on overall leukocytes and absolute numbers of cells per ½ ear for all myeloid cell populations. (**A**) WT mice were infected with *M. pachydermatis* or vehicle-treated without tape-stripping prior to infection. (**B**) WT mice were infected with *M. sympodialis* or *M. furfur,* or vehicle-treated as indicated. The ear skin was or was not tape-stripped before infection, as indicated**.** Each symbol represents one animal. Graphs show pooled data from two independent experiments. The mean of each group is indicated. Statistics were calculated using one-way ANOVA or unpaired Student's t-Test, as appropriate. *p<0.05, **p<0.01, ***p<0.001, ****p<0.0001.

Figure S3 (related to Figure 3): *Malassezia* spp. exposure of the skin results in a selective activation of the IL-17 pathway. A. WT mice were infected with *M. pachydermatis* (*M.p.*) or vehicle-treated (V) after mild tape stripping of the dorsal ear skin. Expression of *Ifng*, *Il5*, *Il13* and *Tslp* transcripts were analyzed in

the ear skin by RT-qPCR on day 2 post infection. **B.** WT mice were infected with *M. pachydermatis, M. sympodialis or M. furfur as indicated* without tape stripping prior to infection. Expression of *Il17a*, *Ifng* and *Tslp* transcripts was assessed by RT-qPCR analysis of the ear skin on day 2 post infection. **C-D.** WT mice were infected with *M. pachydermatis* or vehicle-treated after mild tape stripping of the dorsal ear skin. $CD45^+$ $CD90^+$ $CD11b^-$ lymphoid cell populations in the ear skin of infected and vehicle-treated WT mice were quantified by flow cytometry on day 2 post infection. $TCR\beta^+$ αβ T cells, $TCR\gamma\delta^{int}$ dermal γδ T cells, $TCR\gamma\delta^{hi}$ epidermal γδ T cells (DETCs) and TCR^- innate lymphoid cells (ILCs) were defined as indicated. Representative FACS plot with gating strategy (**C**) and summary graph with absolute numbers for each cell subset (**D**) are shown. (**E-F**) *Il17a*^{Cre}*R26R*^{eyfp} reporter mice were infected with *M. pachydermatis* or vehicle-treated after mild tape stripping of the dorsal ear skin. Expression of eYFP in lymphocyte subsets in the ear skin was analyzed by flow cytometry. Of note, the analysis was carried out on day 5 post infection due to delayed Cre-mediated eYFP expression. Representative FACS plots with gating strategy (**E**) and summary graphs with absolute numbers of $CD90^+$ and $CD90^+eYFP^+$ cells for each cell subset (**F**) are shown. Numbers in **C** and **E** indicate the % of cells in each gate. In **A**, **B**, **D** and **F**, each symbol represents one animal. Graphs show pooled data from two to three independent experiments. The mean of each group is indicated. The same vehicle-treated controls were used in **B** for the experiments with *M. sympodialis* and *M. furfur*. Statistics were calculated using unpaired Student's t-Test or one-way ANOVA as appropriate. *p<0.05, *p<0.01, ***p<0.001, ****p<0.0001.

Figure S4 (related to Figure 3): **Gating strategy of myeloid and lymphoid cell subsets in the *Malassezia*-exposed skin.** WT mice were infected with *M. pachydermatis* or vehicle-treated after mild tape stripping of the dorsal ear skin. (**A**) Myeloid and lymphoid cell populations were isolated by FACS-sorting as indicated on day 2 post infection. (**B**) Langerin expression was assessed in the indicated myeloid cell

subsets on day 2 post infection. Numbers in the contour plots indicate the % of cells in each gate, numbers in the histogram plots indicated median fluorescence intensity (MFI) for Langerin.

Figure S5 (related to Figure 3 and Figure 6): Induction of adaptive type-17 immunity in the draining LN upon *Malassezia* spp. infection is independent of skin barrier disruption. Auricular lymph node cells were analyzed on day 12 post infection for the production of Th17 (IL-17A), Th1 (INF-γ) and Th2 (IL-13) signature cytokines by intracellular staining and flow cytometry, after re-stimulated with dendritic cells that were pulsed with the corresponding heat-killed *Malassezia* spp. (**A**) WT mice were infected with *M. pachydermatis* (*M.p.*) or vehicle-treated (V) with tape stripping prior to infection. (**B-C**) WT mice were infected with *M. pachydermatis* or vehicle treated without tape stripping prior to infection. (**D-E**) WT mice were infected with *M. sympodialis* (*M.s.*) or *M. furfur* (*M.f.*), or vehicle-treated (V) as indicated. The ear skin was or was not tape-stripped before infection, as indicated**.** (**F**) WT mice were primed with *M. pachydermatis* (2°) or left uninfected (1°) 6 weeks prior to (re-)infection with the same strain of *Malassezia* or vehicle treatment as control. The ear skin was pretreated by tape stripping in all conditions. 4 and 6 days later, the percentage of INF-γ and IL-13-producing $CD90^+CD4^+$ T cells in the auricular lymph nodes was assessed by *ex vivo* re-stimulation with dendritic cells that were pulsed with heat-killed *M pachydermatis* followed by intracellular staining and flow cytometry. Representative FACS plots (**B, D**) and summary graphs (**A**, **C**, **E**, **F**) indicating the percentage of cytokine-positive $CD90^+CD4^+$ T cells are shown. In **A**, **C, E** and **F**, each symbol represents one animal. Graphs show pooled data from two independent experiments. The mean +/- SEM of each group is indicated. Statistics were calculated using one-way ANOVA or unpaired Student's t-Test, as appropriate. *p<0.05, **p<0.01, ***p<0.001, ****p<0.0001.

Figure S6 (related to Figure 7): Human memory T cells respond to *C. albicans* with type 17 cytokine secretion. (A-B) $CCR6^+$ and $CCR6^-$ human memory $CD4^+$ T cells were sorted from the peripheral blood of

non-atopic individuals and cytokine production was analyzed by Luminex after 5 days of co-culture with unpulsed autologous monocytes (**A**) or monocytes that were pulsed with heat-killed *C. albicans* (**B**) prior to co-culture. Graphs show the production of the type-17 cytokines IL-17A and IL-22, the type-1 cytokine IFN-γ and the type-2 cytokines IL-4, IL-5 by $CD4^+CCR6^-$ (white bars) and $CD4^+CCR6^+$ T cells (grey bars). Data are pooled from three independent experiments with 5 donors in total. The mean + SEM of each group is indicated.

Figure S7 (related to Figure 7): Human *Malassezia*-specific memory T cells display a strong Th17 signature. (**A-B**) $CCR6^+$ and $CCR6^-$ human memory $CD4^+$ T cells were sorted from the blood of atopic patients and non-atopic individuals and analyzed for type-17 (IL-17A, IL-22), type-1 (IFN-γ) and type-2 (IL-4) cytokine production by intracellular staining and flow cytometry after 5 days of co-culture with autologous monocytes that were pulsed with heat-killed *M. furfur*, *M. sympodialis*, *M. slooffiae* or *C. albicans*. Representative FACS plots (**A**) and summary graphs (**B**) with the percentages of cytokine-positive $CD4^+CCR6^+$ and $CD4^+CCR6^-$ T cells in non-atopic individuals (upper rows in **A**, grey bars in **B**) and atopic patients (lower rows in **A**, black bars in **B**). In **B**, each symbol represents one donor. Graphs show pooled data from three independent experiments. The mean + SEM of each group is indicated. Statistics were calculated using unpaired Student´s t-Test. *p<0.05, **p<0.01, ***p<0.001.

Table S1 (related to the Key Resource Table): Oligonucleotides used in this study

Figure S1:

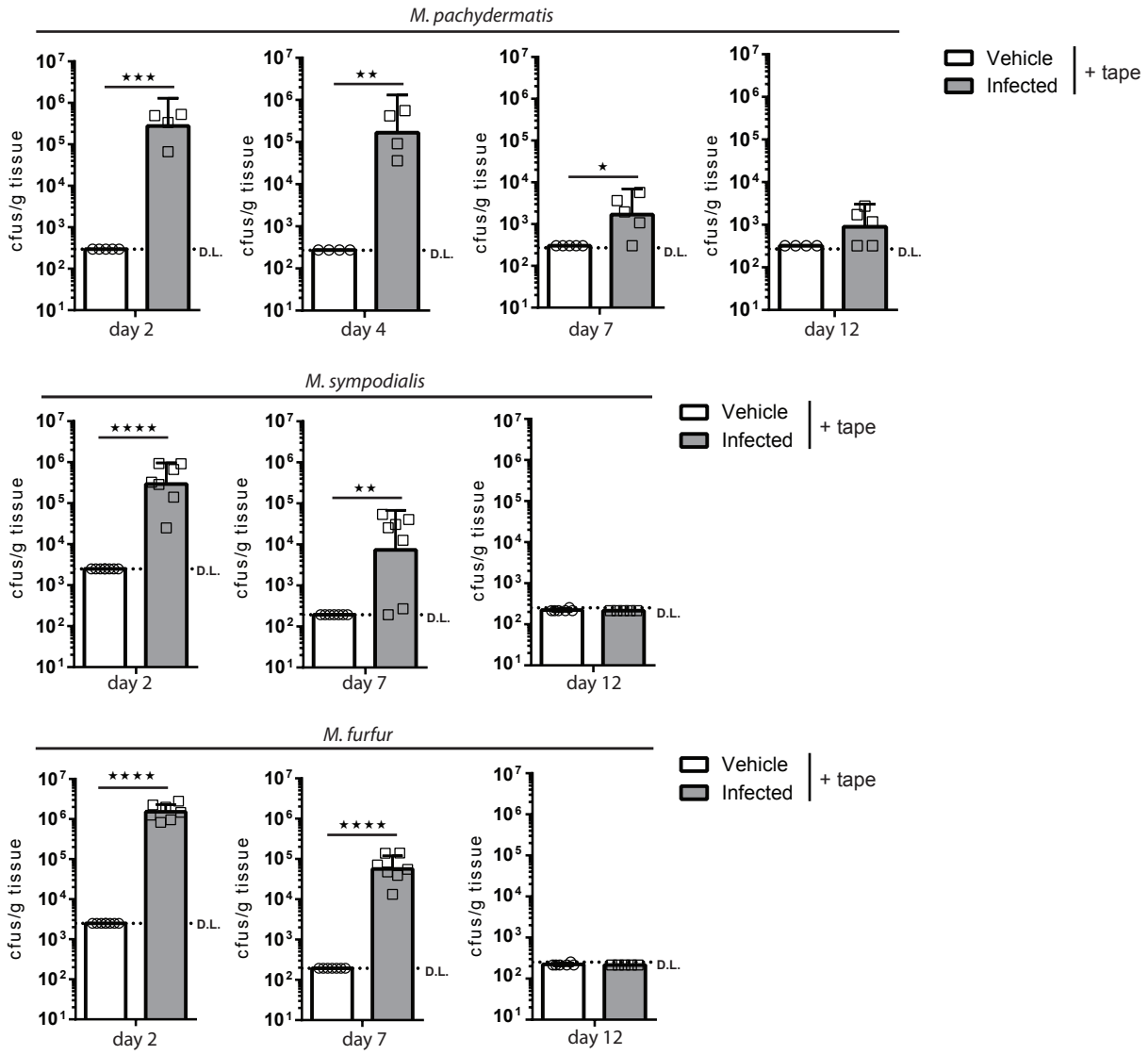

M. pachydermatis
M. sympodialis
M. furfur
Vehicle
Infected
+ tape
cfus/g tissue
D.L.
day 2
day 4
day 7
day 12

Figure S2:

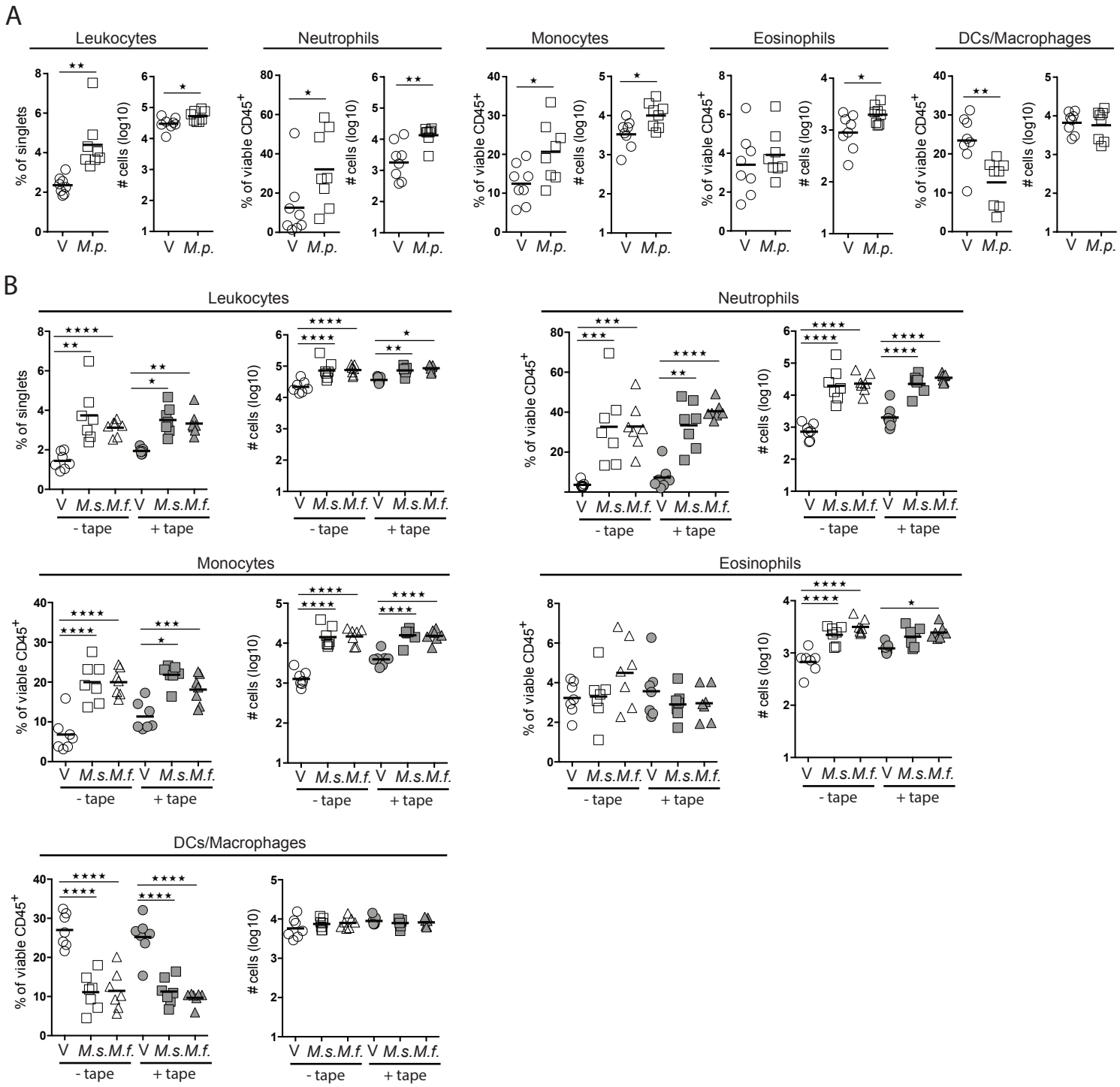

A
Leukocytes
Neutrophils
Monocytes
Eosinophils
DCs/Macrophages
% of singlets
% of viable CD45+
cells (log10)
V
M.p.
B
Leukocytes
Neutrophils
Monocytes
Eosinophils
DCs/Macrophages
% of singlets
% of viable CD45+
cells (log10)
V
M.s.M.f.
- tape
+ tape

Figure S3:

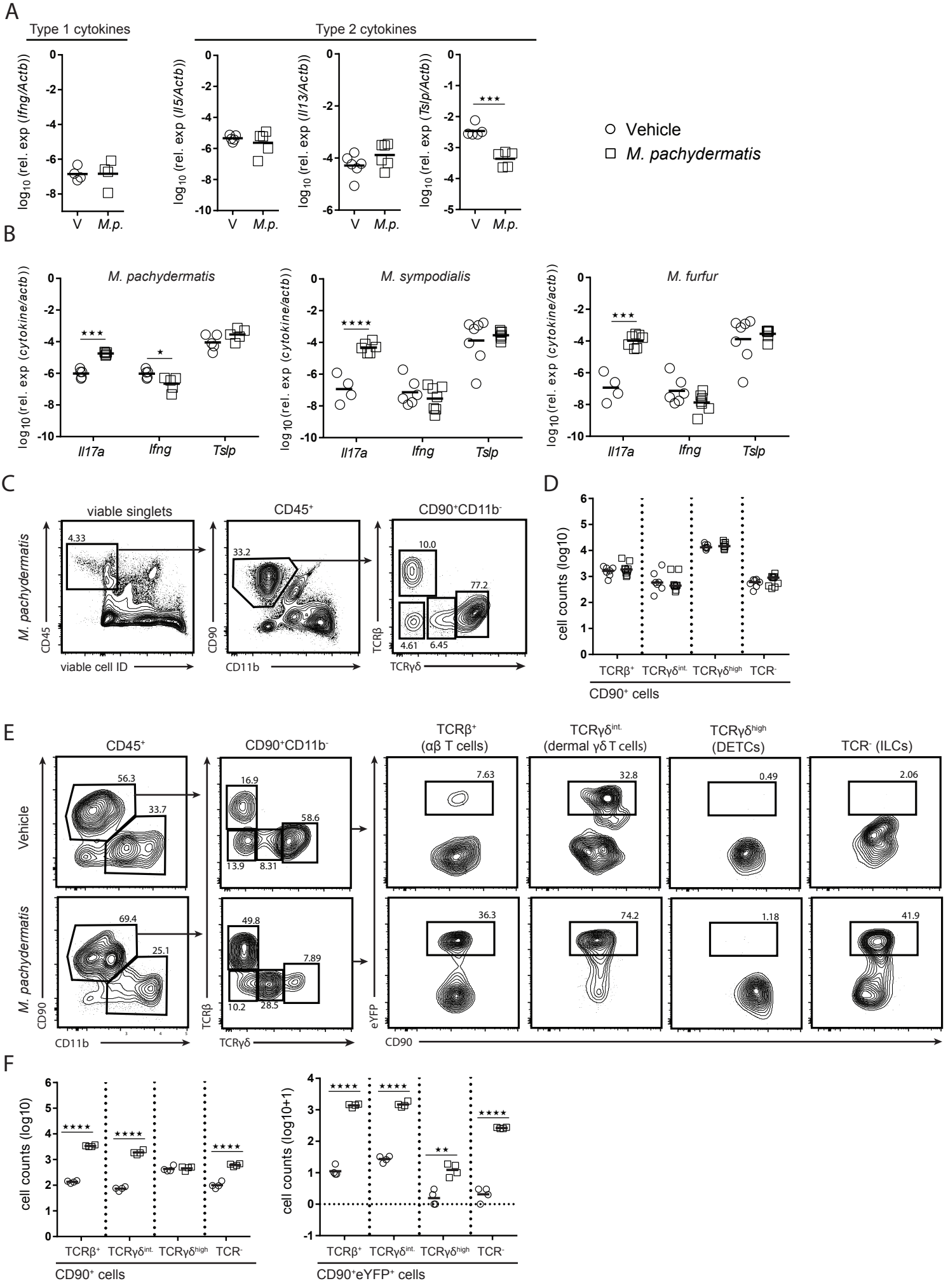
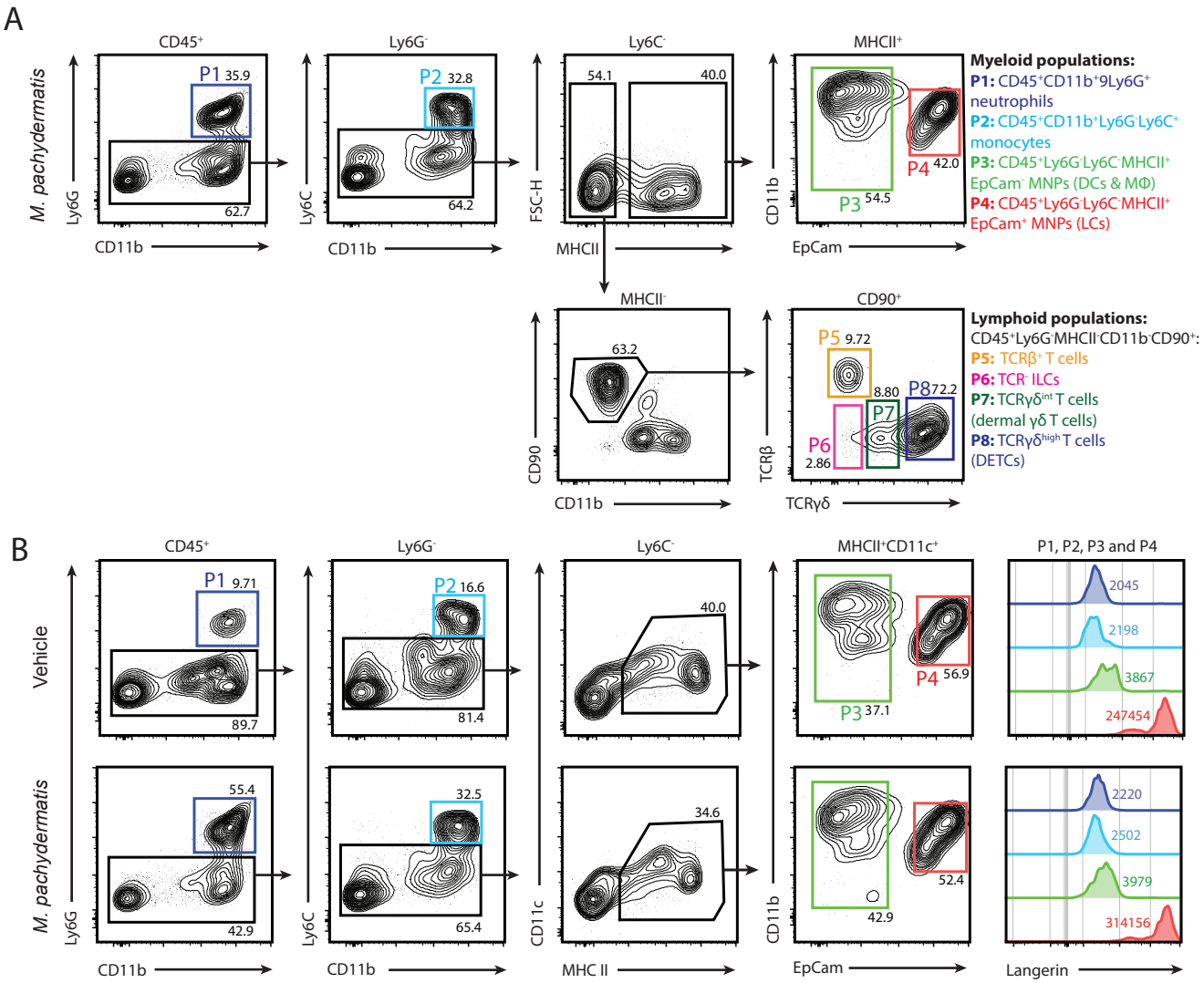

A
Type 1 cytokines
Type 2 cytokines
log10 (rel. exp (Ifng/Actb))
log10 (rel. exp (Il5/Actb))
log10 (rel. exp (Il13/Actb))
log10 (rel. exp (Tslp/Actb))
V
M.p.
Vehicle
M. pachydermatis
B
M. pachydermatis
M. sympodialis
M. furfur
log10 (rel. exp (cytokine/actb))
Il17a
Ifng
Tslp
C
viable singlets
CD45+
CD90+CD11b-
M. pachydermatis
CD45
viable cell ID
CD90
CD11b
TCRβ
TCRγδ
4.33
33.2
10.0
77.2
4.61
6.45
D
cell counts (log10)
TCRβ+
TCRγδint.
TCRγδhigh
TCR-
CD90+ cells
E
CD45+
CD90+CD11b-
TCRβ+ (αβ T cells)
TCRγδint. (dermal γδ T cells)
TCRγδhigh (DETCs)
TCR- (ILCs)
Vehicle
M. pachydermatis
56.3
33.7
16.9
58.6
13.9
8.31
7.63
32.8
0.49
2.06
69.4
25.1
49.8
7.89
10.2
28.5
36.3
74.2
1.18
41.9
CD90
CD11b
TCRβ
TCRγδ
eYFP
CD90
F
cell counts (log10)
cell counts (log10+1)
TCRβ+
TCRγδint.
TCRγδhigh
TCR-
CD90+ cells
CD90+eYFP+ cells

Figure S4:



P1: CD11b+Ly6G+ neutrophils, **P2**: Ly6G-Ly6C+CD11b+ monocytes, **P3**: MHCII+CD11c+EpCam- MNPs, **P4**: MHCII+CD11c+EpCam+ MNPs (LCs)

Figure S5:

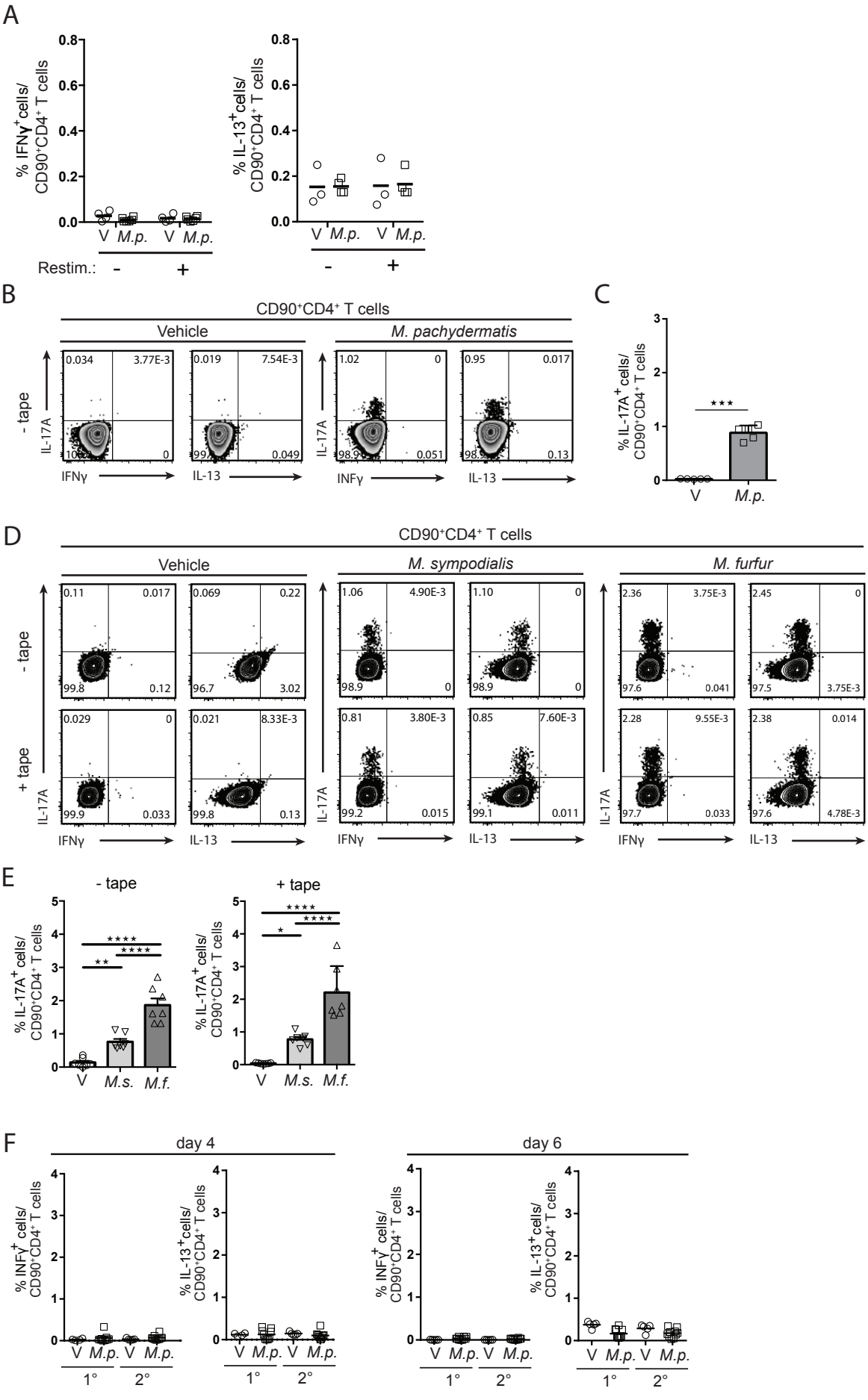

A
% IFNγ+cells/ CD90+CD4+ T cells
% IL-13+cells/ CD90+CD4+ T cells
V M.p. V M.p.
Restim.: - +
B
CD90+CD4+ T cells
Vehicle
M. pachydermatis
- tape
IL-17A
IFNγ
IL-13
0.034 3.77E-3 100 0
0.019 7.54E-3 99.9 0.049
1.02 0 98.9 0.051
0.95 0.017 98.8 0.13
C
% IL-17A+ cells/ CD90+CD4+ T cells
***
V M.p.
D
CD90+CD4+ T cells
Vehicle
M. sympodialis
M. furfur
- tape
+ tape
0.11 0.017 99.8 0.12
0.069 0.22 96.7 3.02
1.06 4.90E-3 98.9 0
1.10 0 98.9 0
2.36 3.75E-3 97.6 0.041
2.45 0 97.5 3.75E-3
0.029 0 99.9 0.033
0.021 8.33E-3 99.8 0.13
0.81 3.80E-3 99.2 0.015
0.85 7.60E-3 99.1 0.011
2.28 9.55E-3 97.7 0.033
2.38 0.014 97.6 4.78E-3
E
- tape
+ tape
% IL-17A+ cells/ CD90+CD4+ T cells
V M.s. M.f.
F
day 4
day 6
% INFγ+ cells/ CD90+CD4+ T cells
% IL-13+cells/ CD90+CD4+ T cells
V M.p. V M.p.
1° 2°

Figure S6:

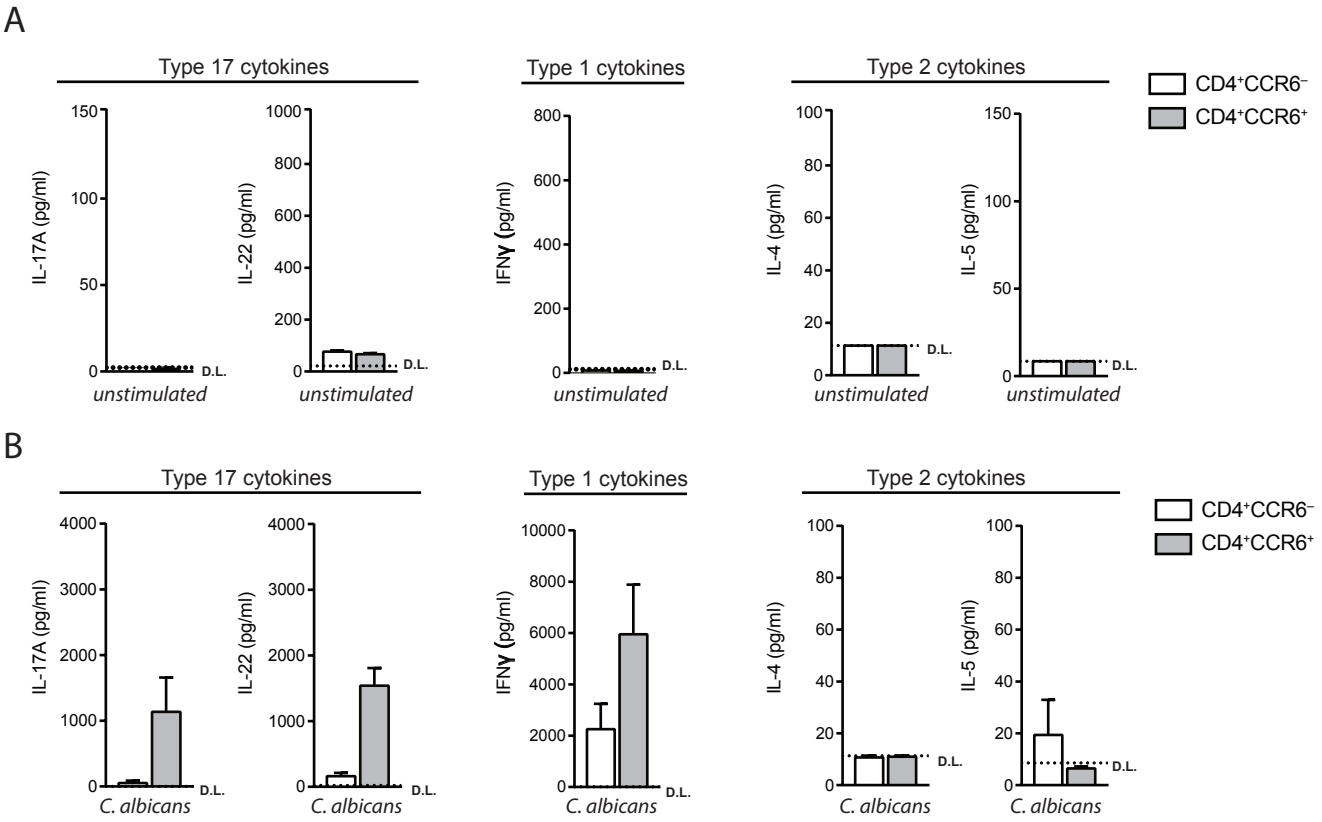
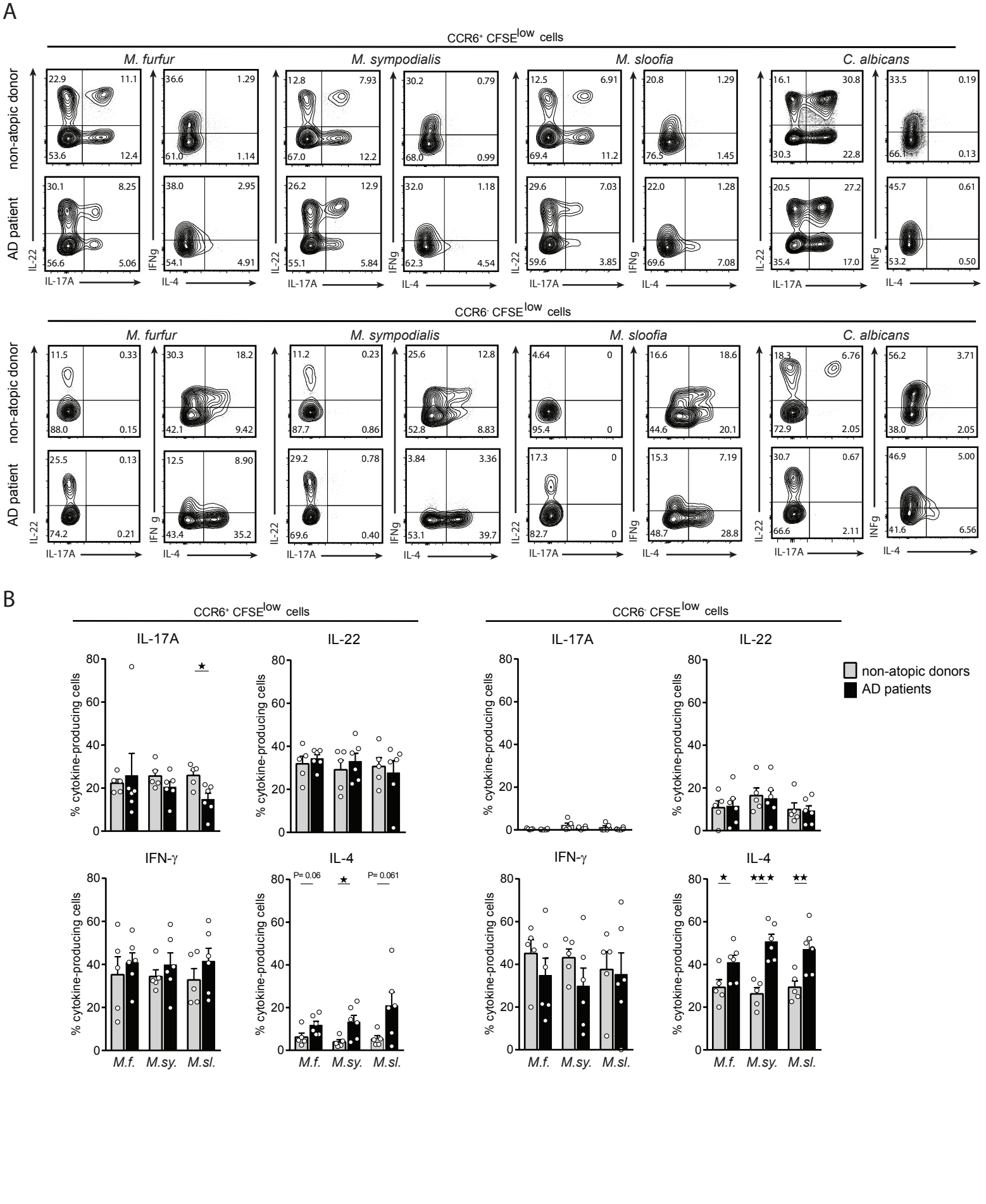

A
Type 17 cytokines
Type 1 cytokines
Type 2 cytokines
CD4+CCR6–
CD4+CCR6+
IL-17A (pg/ml)
IL-22 (pg/ml)
IFNγ (pg/ml)
IL-4 (pg/ml)
IL-5 (pg/ml)
D.L.
unstimulated
B
C. albicans

Figure S7:


A
CCR6+ CFSElow cells
M. furfur
M. sympodialis
M. sloofia
C. albicans
non-atopic donor
AD patient
IL-22
IL-17A
IFNg
IL-4
CCR6- CFSElow cells
B
CCR6+ CFSElow cells
CCR6- CFSElow cells
IL-17A
IL-22
IFN-γ
IL-4
% cytokine-producing cells
non-atopic donors
AD patients
P= 0.06
P= 0.061
M.f.
M.sy.
M.sl.

SUPPLEMENTAL TABLE S1: Oligonucleotides used in this study

Oligonucleotides	SOURCE	IDENTIFIER
Actb: fwd 5´-CCCTGAAGTACCCCATTGAAC-3´, rev 5´-CTTTTCACGGTTGGCCTTAG-3´	Microsynth	N/A
Il17a: fwd 5´- GCTCCAGAAGGCCCTCAGA-3´, rev 5´-AGCTTTCCCTCCGCATTGA-3´	Microsynth	(Overbergh et al., 2003)
Il6: fwd 5´-GAGGAT ACCACTCCCAACAGACC-3´, rev 5´-AAGTGCATCATCGTTGTTCATACA-3´	Microsynth	(Liao et al., 2009)
Il23p19: fwd 5´- CCAGCAGCTCTCTCGGAATC-3´, *Il23p19* rev 5´-TCATATGTCCCGCTGGTGC-3´	Microsynth	(Zelante et al., 2007)
Tslp: fwd 5´-TCTGGAGATTGCATGAAGGA-3´, rev 5´-AGAGAAGCCCTCAATGACCA-3´	Microsynth	N/A
Il22: fwd 5´-CATGCAGGAGGTGGTGCCTT-3´*, Il22* rev 5´-CAGACGCAAGCATTTCTCAG-3´	Microsynth	(Chung et al., 2006)
Infg: fwd 5´-GAACTGGCAAAAGGATGGTGA-3´, rev 5´-TGTGGGTTGTTGACCTCAAAC-3´	Microsynth	N/A
Il5: fwd 5´-TCACCGAGCTCTGTTGACAA-3´, rev 5´-CCACACTTCTCTTTTTGGCG-3´	Microsynth	N/A
Il13: fwd 5´-CCAGGTCCACACTCCATACC-3´, rev 5´-TGCCAAGATCTGTGTCTCTCC-3´	Microsynth	N/A
Gcsf: fwd 5´-CTTAAGTCCCTGGAGCAAGTG-3´, *r*ev 5´-GTGGCCCAGCAACACCAG-3´	Microsynth	N/A
Cxcl1: fwd 5´-CCGCTCGCTTCTCTGTG-3´, rev 5´-GCAGCTCATTGGCGATAG-3´	Microsynth	N/A
Cxcl2: fwd 5´-AGTGAACTGCGCTGTCAATGC-3´, rev 5´-GCAAACTTTTTGACCGCCCT-3´	Microsynth	N/A
Ccl2: fwd 5´-GGGATCATCTTGCTGGTGAA-3´, *Ccl2* rev 5´-AGGTCCCTGTCATGCTTCTG-3´	Microsynth	N/A
Ccl5: fwd 5´-CCCACTTCTTCTCTGGGTTG-3´, rev 5´-GTGCCCACGTCAAGGAGTAT-3´	Microsynth	N/A
Ccl11: fwd 5´-CTATGGCTTTCAGGGTGCAT-3´, *Ccl11* rev 5´-TCACTTCCTTCACCTCCCAG-3´	Microsynth	N/A
Defb3: fwd 5´-GTCTCCACC TGCAGCTTTTAG, *Defb3* rev 5´-ACTGCCAATCTGACGAGTGTT	Microsynth	N/A
Il1b: *Il1b* rev 5´-AGGCCACAGGTATTTTGTCG-3´; *Il17a* fwd 5´- GCTCCAGAAGGCCCTCAGA-3´	Microsynth	N/A
Ccl24: fwd 5´-TCTTATGGCCCTTCTTGGTG-3´, rev 5´-AATTCCAGAAAACCGAGTGG-3´	Microsynth	N/A